

**3-D SOIL STRUCTURE INTERACTION ANALYSES OF THREE
IDENTICAL BUILDINGS IN SAKARYA CITY AFTER 17 AUGUST 1999
KOCAELI EARTHQUAKE**

**A THESIS SUBMITTED TO
THE GRADUATE SCHOOL OF NATURAL AND APPLIED SCIENCES
OF
MIDDLE EAST TECHNICAL UNIVERSITY**

**BY
ORHAN ÜNAL**

**IN PARTIAL FULFILLMENT OF THE REQUIREMENTS FOR
THE DEGREE OF MASTER OF SCIENCE
IN
THE DEPARTMENT OF CIVIL ENGINEERING**

OCTOBER 2003

ABSTRACT

3-D SOIL STRUCTURE INTERACTION ANALYSES OF THREE IDENTICAL BUILDINGS IN SAKARYA CITY AFTER 17 AUGUST 1999 KOCAELI EARTHQUAKE

Ünal,Orhan

M.S., Department of Civil Engineering,
Supervisor: Assist. Prof. Dr Kemal Önder Çetin
October 2003, 116 Pages

The aim of this study is to analyze the soil structure interaction of three identical buildings on Şahinler Street of Sakarya city which had no damage to heavy damage after the Kocaeli (1999) earthquake. For the purpose of 3-D dynamic nonlinear analysis of the soil site and the overlying structures, Flac3D software was chosen as the numerical modeling framework. Soil properties were determined by using the results of available site investigation studies. A three dimensional mesh was created to represent the topographic and geometric constraints of the problem. Linearly elastic perfectly plastic constitutive model was implemented to model the soil behavior. The results of 3-D dynamic numerical analyses in the forms of acceleration, displacement, strain, stress and pore pressure were presented. The higher acceleration, strain

and stress levels calculated under the collapsed building can be attributed as the major cause of poor performance of the structure.

Keywords: Soil structure interaction analysis, Nonlinear analysis, Linearly elastic perfectly plastic constitutive models, acceleration, strain, stress.

ÖZ

17 AĞUSTOS 1999 KOCAELİ DEPREMİNDE SAKARYA ŞEHRİNDEKİ ÜÇ EŞ ÖZELLİKTEKİ BİNANIN 3 BOYUTLU YAPI ZEMİN ETKİLEŞİMİNİN ANALİZİ

Ünal, Orhan

Yüksek Lisans, İnşaat Mühendisliği Bölümü,
Danışman: Y. Doç. Dr Kemal Önder Çetin
Ekim 2003, 116 Pages

Bu çalışmanın amacı Kocaeli(1999) depremi sonrası Sakarya Şahinler Sokağındaki üç eş özellikteki yapıda gözlemlenen ve hasarsızdan ağır hasara doğru değişen performansı açıklamak üzere zemin yapı etkileşimini analiz etmektir. Bu amaçla bölgenin ve üzerinde bulunan binaların üç boyutlu dinamik, doğrusal olmayan analizi için bilgisayar programı olarak Flac3D seçilmiştir. Bölgeye uygun zemin özellikleri o bölgede yapılmış saha çalışmaları sonuçlarına göre belirlenmiştir. Problemin topografik ve geometrik sınırlarını temsil edecek üç boyutlu bilgisayar modeli oluşturulduktan sonra zemin davranışını temsil edecek uygun zemin davranış modeli olarak doğrusal elastik mükemmel plastik model seçilmiştir. Üç boyutlu dinamik analiz sonuçları ivme, deplasman, birim deformasyon, gerilme ve boşluk suyu basıncı şeklinde sunulmuştur.

Çöken bina temelinde hesaplanan yüksek ivme, birim deformasyon, gerilme deęerleri kabul edilemez yapısal performansın nedeni olarak sayılabilir.

Anahtar kelimeler: Yapı zemin etkileşimi, Doğrusal olmayan analiz, Zemin davranış modeli, İvme, Deplasman, Gerilme, Boşluk suyu basıncı.

to my mother

ACKNOWLEDGEMENTS

I would like to extend my sincere thanks to Assist. Prof. Dr. Kemal Önder Çetin for his supervision and support throughout the preparation of this thesis. I thank to my parents for their never ending support, encouragement, and patience. I also thank to Ms. Özlem Hakverdi for her deep understanding and moral support. I would also like to thank Ms. Berna Unutmaz for her valuable help and patience during my study.

TABLE OF CONTENTS

ABSTRACT.....	iii
ÖZ.....	v
ACKNOWLEDGMENTS.....	viii
TABLE OF CONTENTS.....	ix
LIST OF TABLES.....	xii
LIST OF FIGURES.....	xiii
LIST OF SYMBOLS.....	xvi

CHAPTER

1. Introduction

1.1 General.....	1
1.2 Research Statement.....	2
1.3 Scope	2

2. A Literature Survey On Numerical Analyses And Site Investigation Methods

2.1 Introduction.....	4
2.2 Static and Dynamic Analysis.....	4

2.2.1 Soil Structure Interaction.....	4
2.2.1.1 Direct Procedure.....	4
2.2.1.2 Substructure Procedure.....	6
2.2.1.3 Artificial Boundary conditions.....	10
2.2.2 Equivalent Linear and Nonlinear Methods.....	10
2.2.3 Numerical Methods.....	12
2.2.3.1 Finite Element Methods.....	12
2.2.3.2 Finite Difference Methods.....	14
2.3 Constitutive Models.....	16
2.3.1 Elastic Model.....	17
2.3.2 Mohr-Coulomb plasticity.....	17
2.3.3 Finn Model.....	20
2.4 SPT-CPT-Vs relationships.....	22
2.4.1 Standart Penetration Test(SPT).....	24
2.4.2 Cone Penetration Test (CPT).....	26
2.5 Liquefaction.....	28
2.5.1 Cyclic Stress Approach.....	28
2.5.2 Probabilistic Approach.....	29
3. Observed Structural Damage and Site Investigation Studies	
3.1 Damage to the Buildings after the earthquake.....	31
3.2 Site Profiles.....	34
3.3 Soil and Structural Properties.....	38
3.4 Characteristics of Adapazarı Strong Ground Motion Record.....	39
3.5 Properties of Finn Model Parameters.....	46
4. 3D- Mesh Generation of the 3 buildings in Adapazarı	
4.1 Damping phenomena	49
4.2 Input Ground Motion Characteristics.....	51
4.3 Preparation of Soil and Structural Mesh.....	55
4.3.1 Wave Transmission.....	56

4.3.2 Mesh Characteristics of the Site.....	50
5. Discussion of Numerical Analyses Result	
5.1 Introduction.....	60
5.1 The distribution of intensity of shaking under the buildings.....	60
5.2 Results of Displacement Analysis.....	61
5.4 The distribution of maximum stress, strain and pore pressures under the buildings.....	65
5.5 Liquefaction Triggering Assessment.....	70
6. SUMMARY AND CONCLUSION	
6.1 Summary.....	78
6.2 Conclusion.....	79
REFERENCES.....	81
APPENDIX.....	84
A. Details of Static Analysis	84
B. Detailed SPT-CPT data.....	90
C. Input Files.....	101

LIST OF TABLES

TABLE

3.1 Tabulated values of layer properties.....	37
3.2 Static and Dynamic Soil properties	42
3.3 Structural properties.....	43
3.4 Martin and Byrne constants.....	48
3.5 Constitutive models used in dynamic analysis.....	48
4.1 Shake 91 input soil profile data.....	52
4.2 Mesh properties.....	57

LIST OF FIGURES

FIGURE

2.1 FF system.....	5
2.2 Finite Element Mesh used in Direct analysis	6
2.3 Separation of Structure.....	7
2.4 FF diagram.....	7
2.5 Quadrilateral element	13
2.6 Failure envelope.....	18
2.7 Volumetric strain curves (Martin 1976).....	21
2.8 CPT-Based Soil Behaviour-Type chart.....	27
3.1 The photograph of the 3 buildings in Şahinler Street.....	32
3.2 The photograph of the building stated as C ₂ in Fig(3.1).....	32
3.3 General view of the Şahinler Street.....	33
3.4 K1 cross sectional view.....	35
3.5 K2 cross sectional view.....	36
3.6 Shear wave velocity profile	37
3.7 Cohesion vs Depth values.....	39
3.8 General 3D view of the site, estimated	44
3.9 Sakarya(1999) acceleration record.....	45
3.10 Arias intensity graph of Sakarya(1999) earthquake.....	46
3.11 Byrne's $\Delta\varepsilon_{vd}$ vs γ curves given the ε_{vd} constant.....	47
3.12 Martin's $\Delta\varepsilon_{vd}$ vs γ curves given the ε_{vd} constant.....	47
4.1 Modulus and Damping curve.....	50
4.2 Construction of the model input motion.....	51
4.3 Acceleration vs time data(up to 10Hz).....	53
4.4 Acceleration input ground motion.....	54
4.5 Velocity form of input ground motion.....	54

4.6 Displacement form of Input ground motion.....	54
4.7 Soil mesh under the building.....	55
4.8 Soil under the C1 building.....	58
4.9 Soil under the C2 building.....	58
4.10 Soil under the C3 building.....	58
4.11 K2 view of the three buildings.....	59
5.1 Schematic view of columns.....	61
5.2(a) Acceleration values of the building C1.....	62
5.2(b) Acceleration values of the building C2.....	62
5.2(c) Acceleration values of the building C3.....	62
5.3(a) Vertical displacements under C1.....	63
5.3(b) Vertical displacements under C2.....	63
5.3(c) Vertical displacements under C3.....	63
5.4(a) Horizontal displacements under C1.....	64
5.4(b) Horizontal displacements under C2.....	64
5.4(c) Horizontal displacements under C3.....	64
5.5(a) Max vertical stress under the building C1.....	66
5.5(b) Max vertical stress under the building C2.....	66
5.5(c) Max vertical stress under the building C3.....	66
5.6(a) Max shear stress under the building C1.....	67
5.6(b) Max shear stress under the building C2.....	67
5.6(c) Max shear stress under the building C3.....	67
5.7(a) Max shear strain under the building C1.....	68
5.7(b) Max shear strain under the building C2.....	68
5.7(c) Max shear strain under the building C3.....	68
5.8(a) Max pore pressure(kPa) under the building C1.....	69
5.8(b) Max pore pressure(kPa) under the building C2.....	69
5.8(c) Max pore pressure(kPa) under the building C3.....	69
5.9(a) Effective vertical stress vs depth at C ₁	72
5.9(b) Effective vertical stress vs depth at C ₂	72
5.9(c) Effective vertical stress vs depth at C ₃	72
5.10(a) Static shear stress vs depth at C ₁	73

5.10(b) Static shear stress vs depth at C ₂	73
5.10(c) Static shear stress vs depth at C ₃	73
5.11(a) α vs depth at C ₁	74
5.11(b) α vs depth at C ₂	74
5.11(c) α vs depth at C ₃	74
5.12(a) K _{α} vs depth at C ₁	75
5.12(b) K _{α} vs depth at C ₂	75
5.12(c) K _{α} vs depth at C ₃	75
5.13(a) Cyclic Stress Ratio vs depth at C ₁	76
5.13(b) Cyclic Stress Ratio vs depth at C ₂	76
5.13(c) Cyclic Stress Ratio vs depth at C ₂	76
5.14(a) Probability liquefaction vs depth at C ₁	77
5.14(b) Probability liquefaction vs depth at C ₂	77
5.14(c) Probability liquefaction vs depth at C ₃	77

LIST OF SYMBOLS

e	: Exponential
τ	: Shear stress
u^{\parallel}	: Acceleration
g	: Gravity
c	: Cohesion
ρ	: Density
V_s	: Shear wave velocity
ν	: Poisson's ratio
$[m_e]$: Element mass matrix
$[c_c]$: Element damping matrix
$[k_e]$: Element stiffness matrix
$\{Q(t)\}$: Element force vector
$\{u\}$: Global nodal point displacement vector
$[M]$: Global mass matrix
$[C]$: Global damping matrix
$[K]$: Global stiffness matrix
u_b	: Base motion
W_D	: Dissipated energy
A	: Area
γ_c, γ	: Strain

ϕ : Friction angle

ε_{vd} : Volumetric strain

$\Delta\varepsilon_{vd}$: Incremental volumetric strain

G : Shear Modulus

G_{max} : Maximum shear modulus

G_{sec} : Secant modulus

K : Bulk modulus

C1-4 : Martin constants

B1-2 : Byrne constants

λ : Wave length

f : Frequency

N : SPT penetration resistance

N_m : Measured penetration resistance

N_{60} : Corrected SPT N value

E_m : Actual hammer energy

E_{ff} : Theoretical free fall energy

C_N : Overburden correction factor

r_d : Stress reduction factor

a_{max} : Peak horizontal acceleration

CSR : Cyclic stress ratio

q_c : Tip resistance

f_s : Sleeve resistance

FR : Friction ratio

α_{1-2} : Constant for stress strain relation

I_a : Arias intensity

ω : Angular frequency

F_1^F : Force at the top surface in terms of frequency space

F_2^F : Force at the ground in terms of frequency space

U_c^F : Displacement at the top surface interms of freq. space

U_g^F : Displacement at the ground surface interms of freq.

C_p : Primary wave velocity

[S] : Impedance matrix

[N] : Matrix of Shape functions

[B] : Strain displacement matrix

[D] : Stress-strain matrix

|J| : Jacobian matrix

[η] : Matrix of damping terms

{R(t)} : Global nodal point force vector

f^s : Failure criterion

E_r : Tangent modulus

Δu : The increase in residual pore pressure

n_e : Porosity of sample

σ_{vo} : Total vertical overburden stress

szz : Axial stress in z direction

syx : Axial stress in y direction

syz : Shear stress in yz plane

CSR : Cyclic Stress ratio

FC : Fines Content

CHAPTER 1

INTRODUCTION

1.1 General

After the 17 August 1999 Kocaeli earthquake, different levels of structural damage was observed on the buildings of Adapazarı, Şahinler Street. In this study the earthquake damage to the three identical buildings C_1 , C_2 , C_3 as shown in Fig. (1.1), is investigated. Building C_1 performed very poorly and collapsed while the building C_2 next to it exhibited moderate structural damage, settled and translated significantly. Building C_3 performed quite well with no signs of translation and settlement. Dramatically different performances of these three identical buildings suggest the potential suspect of the problem as the foundation soils.



Fig 1.1 The photograph of the 3 buildings in Şahinler Street.

1.2 Research Statement

The goal of this study is to determine the effects of soil conditions on the observed structural damage of the overlying buildings during Kocaeli (1999) earthquake. For this purpose, series of numerical analysis were performed by carefully modeling;

- i) soil formation under the buildings
- ii) soil properties
- iii) properties of structural elements
- iv) structural elements
- v) earthquake shaking

to estimate;

- a) acceleration
- b) shear stresses and strains
- c) horizontal and vertical stresses
- d) horizontal and vertical displacements
- e) pore pressures

developed in the underlying soils which might have been identified as major parameters to explain the variability in the observed structural damage during the Kocaeli (1999) earthquake.

1.3 Scope

The literature survey, the previous studies and the methods about the dynamic and static analysis of the structures considering soil structure interaction are given in Chapter 2.

The general information about the soil and structure characteristics of Şahinler Street in Adapazarı are given in Chapter 3. The representation of premodified earthquake and its characteristics are also given in this chapter.

The steps of the analysis procedure, how the static and dynamic models are constructed and how the input ground motion, the material properties are selected are explained in Chapter 4.

Chapter 5 criticises the results of numerical analyses in the forms of depth figures.

Finally, a summary of the research findings, major conclusions and recommendations for future studies are presented in Chapter 6

CHAPTER 2

A LITERATURE SURVEY ON NUMERICAL ANALYSES AND SITE INVESTIGATION METHODS

2.1 Introduction

In this chapter, an overview of available methods and some important parameters for the evaluation of dynamic soil structure interaction problem is presented. Especially the parameters selected to be discussed in this chapter represent important factors that defines the soil behaviour of the site (Şahinler Street) in Adapazarı.

2.2 Static and Dynamic Analysis

2.2.1 Soil Structure Interaction

There are many numerical methods such as finite element, finite difference and boundary element methods for the analyses of soil structure interaction problems. These numerical methods can be used alone or together for the solution of the soil structure interaction problems.

Direct and substructuring procedures are the common ways of solving soil structure interaction problem by using finite element and boundary element methods.

2.2.1.1 The Direct Procedures

The direct procedures include two main steps, namely ;

- 1) site response analysis.
- 2) interaction analysis.

As an example, in site response analysis free field (FF) is considered. Given the displacement at the top surface (U_c), ground displacement (U_g) is calculated for a one layered soil.

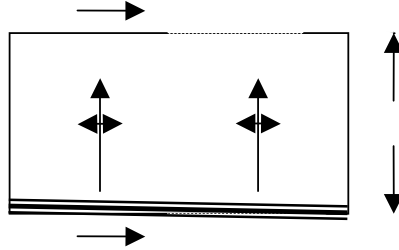


Fig 2.1 Free Field (FF) system

In frequency domain we can write free field system equations respectively;

$$\begin{bmatrix} F1^F \\ F2^F \end{bmatrix} = \frac{\rho \cdot \omega \cdot V_s}{\sin(\alpha \cdot d)} \cdot \begin{bmatrix} \cos(\alpha \cdot d) & -1 \\ -1 & \cos(\alpha \cdot d) \end{bmatrix} \cdot \begin{bmatrix} U_c^F \\ U_g^F \end{bmatrix} \quad (2.1)$$

where,

V_s : shear wave velocity

ρ : density of the soil

ω : angular frequency

$F1^F$: force at the top surface interms of frequency space

$F2^F$: force at the ground interms of frequency space

U_c^F : displacement at the top surface in terms of frequency space

U_g^F : displacement at the ground surface in terms of frequency space

α : ω/C_p

C_p : primary wave velocity

Since it is a FF system, $F1=F2=0$ thus we can write eq (2.1) as ;

$$U_g^F = \cos(\alpha d) U_c^F \quad (2.2)$$

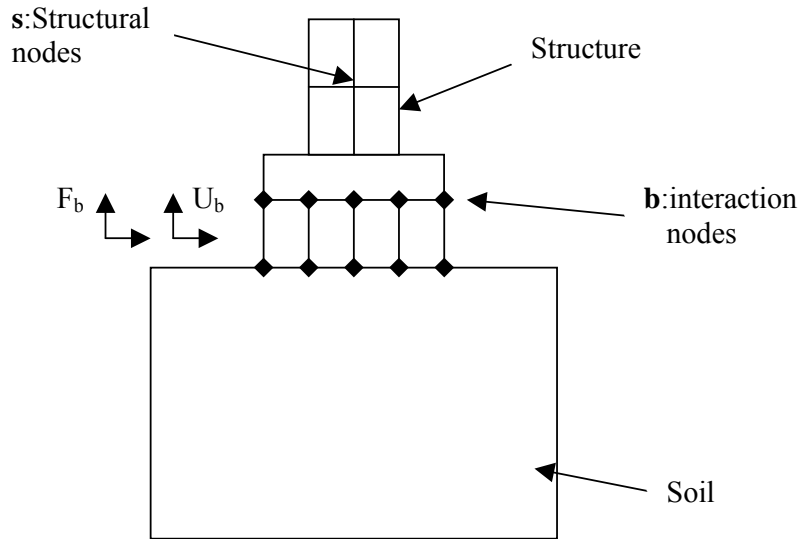


Fig 2.3 Separation of Structure

In Fig (2.3), U_b 's are the interaction displacements(ID) and F_b 's are the interaction forces (IF). In FF analysis soil is analyzed in the absence of IF's but the earthquake is taken into account.

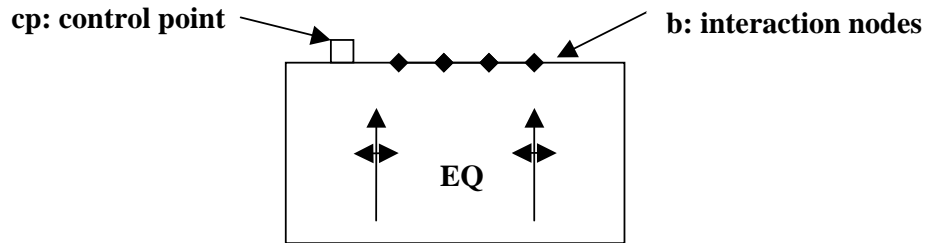


Fig 2.4 FF diagram

FF displacements of the (b) interaction points, U_b^f , can be given by U_c taken from the control point (cp) in the site. In impedance analysis soil layer is analyzed in the presence of IF's but in the absence of earthquake input. Impedance relation for the b points, can be written as;

$$[F_b^F] = [S] * U_b^F \quad (2.3)$$

where, [S] is the impedance matrix which may be found by unit load method. The Impedance relation can be modified in the presence of earthquake input. At this stage soil layer is considered in the presence of both the IF's and earthquake input.

$$[F_b^F] = [S] * (U_b^F - U_b^{fF}) \quad (2.4)$$

Equation (2.4) is the modified impedance relation. Finally the governing equations for the structure is written as;

$$\begin{bmatrix} \underline{K}_s & \underline{K}_{sb} \\ \underline{K}_{bs} & \underline{K}_b \end{bmatrix} \cdot \begin{bmatrix} \underline{U}_s^F \\ \underline{U}_b^F \end{bmatrix} = \begin{bmatrix} \underline{0} \\ -\underline{F}_b^F \end{bmatrix} \quad (2.5)$$

where \underline{K} is the stiffness matrix of the structure. Equation (2.5) can be rewritten by putting Eq. (2.4) into equation.

$$\begin{bmatrix} \underline{K}_s & \underline{K}_{sb} \\ \underline{K}_{bs} & \underline{K}_b + \underline{S} \end{bmatrix} \cdot \begin{bmatrix} \underline{U}_s^F \\ \underline{U}_b^F \end{bmatrix} = \begin{bmatrix} \underline{0} \\ -\underline{S}\underline{U}_b^F \end{bmatrix} \quad (2.6)$$

where \underline{S} gives the influence of soil layer on the response of structure. Using finite element or boundary element methods \underline{S} could be calculated. $\underline{S}\underline{U}_b^{fF}$ is the earthquake force expressed in terms of FF displacement. The equation (2.6) is solved in frequency space and by being transformed into time space \underline{U}_b , \underline{U}_s is found which are the b points displacements and the structural nodes displacements respectively.

The cases for the soil structure interaction can be extended by analyzing embedded structures and/or by using multilayered soils. For a detailed discussion of this, readers are referred to Dynamic Soil Structure Interaction Book by (John P. Wolf) .

Since all the techniques defined in this section are evaluated in frequency space, only equivalent linear models can be applicable for the calculations. The equivalent linear method is common in earthquake engineering for modelling wave transmission in layered sites and dynamic soil-structure interaction. There are also non-linear methods that use various constitutive models for defining the materials properly. Some insight into constitutive models and non-linear methods will be given in the following sections.

The soil-structure interaction problem was studied by considering the other effects such as the interaction between adjacent rigid surface foundations resting on a viscoelastic layered soil medium. Karabalis and Mohammadi (1998) have investigated the problem by analyzing the multi resonance occurrences, frequency shifting and altering of the peak amplitudes.

M.Pastor et al (1997) looked the soil dynamics problem from the undrained incompressible limit point of view. They stated that incompressibility may result in volumetric locking of the mesh with a loss of accuracy.

E.Şafak (2000) proposed an energy based analysis into the soil-structure response. In this study the energy flux to express the amount of energy transmitted, is equal to kinetic energy multiplied by the propagation velocity of the seismic waves. He treated the structure as the continuation of the multi layered soil and the propagating of energy flux in the layers is described in terms of up-going and down-going energy flux in each layer which allow calculation of the energy demand and energy dissipation in each layer. Also the site amplification can be determined easily.

2.2.1.3 Artificial Boundary Conditions

In static analysis, fixed or elastic boundaries can be realistically placed at some distance from the region of interest. In dynamic problems, however, such boundary conditions cause the reflection of outward propagating waves back into the model and do not allow the necessary energy radiation. Increased mesh dimensions can minimize the wave reflection problem, since material damping will absorb most of the energy in the waves reflected from distant boundaries. However this solution leads to a large computational burden. In numerical analysis the alternative is to use artificial (quiet) boundaries. The viscous boundary developed by Lysmer and Kuhlmayer (1969) is based on the use of independent dashpots in the normal and shear directions at the model boundaries representing the behaviour of far field. Experiments have shown that the method is completely effective at absorbing body waves approaching the boundary at angles of incidence greater than 30° .

This subject was studied in Lysmer and Kuhlmayer(1969) and John P. Wolf (1985) in details.

2.2.2 Equivalent Linear and Nonlinear Methods

The dynamic analysis can be classified into 2 as the equivalent linear method and the nonlinear method. In the equivalent –linear method a linear analysis is performed, with some initial values assumed for damping ratio and shear modulus in the various regions of the model. The maximum cyclic shear strain is recorded for each element and used to determine new values for damping and modulus, by reference to laboratory-derived curves that relate damping ratio and secant modulus to amplitude of cyclic shear strain. The new values of damping ratio and shear modulus are then used in a new numerical analysis of the model. The whole process is repeated several times, until there are no further changes in properties. It is said that converging points are representative of the response of the real site.

In contrast, only one run is done with a fully nonlinear method, since nonlinearity in the stress-strain law is followed directly by each element as the solution marches on in time. Provided that an appropriate law is used, the dependence of damping and apparent modulus on strain level are automatically modeled.

Both methods have their strengths and weaknesses. Equivalent linear method uses linear properties for each element that remain constant throughout the history of shaking and are estimated from the mean level of dynamic motion. The disadvantages of the method are that the method does not directly provide information on irreversible displacements and the permanent changes that accompany liquefaction. Also plastic yielding is modeled inappropriately and the interface and mixing phenomena that occur between different frequency components in a nonlinear material are missing from an equivalent linear analysis. On the other hand equivalent linear method takes much more liberties with physics, user friendly and accepts laboratory results from cyclic tests directly.

The nonlinear method other from equivalent linear method which is used by Flac3D (a computer program based on explicit finite difference scheme), correctly represents the physics but needs more parameter thus not user friendly. The method follows any prescribed nonlinear constitutive relation. If hysteretic-type model is used and no extra damping is specified, then the damping and tangent modulus are appropriate to the level of excitation at each point in time and space, since these parameters are embodied in the constitutive model. By default, if Rayleigh or local damping is used, the associated damping coefficients remain constant throughout shaking and the grid. Also using nonlinear material law makes interference and mixing of different frequency components occur naturally and irreversible displacements and other permanent changes are modeled

automatically. A proper plasticity formulation can be used and the use of different constitutive models may be studied easily.

Consequently a soil structure interaction problem can be taken into account from the nonlinear model point of view, that Flac3D does it so, thus a good model for dynamic soil structure interaction would capture the hysteresis curves and energy-absorbing characteristics of real soil.

2.2.3 Numerical Methods

Finite element, boundary element and finite difference methods are used in the solution of the complex mechanical problems for which analytical methods do not give a solution. Some of these numerical techniques (finite element and finite difference methods) will be explained in this section.

2.2.3.1 Finite Element Methods

The Finite element method treats a continuum as an assemblage of discrete elements whose boundaries are defined by nodal points. In finite element method it is assumed that the response of the continuum can be described by the response of the nodal points.

In Finite element method the problem of interest is first discretized by dividing it into elements. Then the displacement at any point within an element is expressed in terms of the nodal point displacements as the following $\{v\}^T = \{u, v\}$. For a quadrilateral element nodal point displacements can be given as $\{q^T\} = \{u_1, u_2, u_3, u_4, v_1, v_2, v_3, v_4\}$ as shown in Fig. (2.5) and displacements for any point in the element can be expressed in the following form.

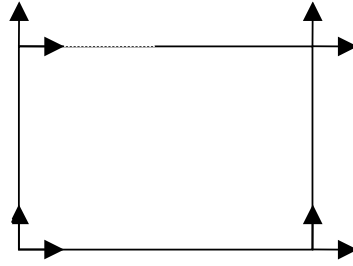


Fig. 2.5 Quadrilateral element

$$\{v\}=[N]\{q\} \quad (2.7)$$

where $[N]$ is a matrix of shape functions. The strain displacements matrix, $[B]$, allows the strains to be determined from the nodal point displacements

$$\{\varepsilon\}=[B]\{q\} \quad (2.8)$$

and the stress strain matrix $[D]$, relates stresses to strains:

$$\{\sigma\}=[D]\{\varepsilon\} \quad (2.9)$$

Defining a local coordinate system (s,t) and using the strain-displacement and stress-strain relationships, an element stiffness matrix can be written as

$$[k_e] = \int_{(-1)}^{(1)} \int_{(-1)}^{(1)} [B^T] \cdot [D] \cdot [B] \cdot |J| ds \cdot dt \quad (2.10)$$

where J is the jacobian matrix used in transformation of an arbitrary quadrilateral element to a gauss square.

A consistent element mass matrix can be written, assuming constant density within the element, as

$$[m_e] = \int_{(-1)}^{(1)} \int_{(-1)}^{(1)} [N^T] \cdot [N] \cdot |J| ds \cdot dt \quad (2.11)$$

Similarly a consistent damping matrix and the force vector for the element can be written respectively.

$$[c_e] = \rho \cdot \int_{(-1)}^{(1)} \int_{(-1)}^{(1)} [B^T] \cdot [\eta] \cdot [B] \cdot |J| ds \cdot dt \quad (2.12)$$

$$\{Q(t)\} = \int_{(-1)}^{(1)} \int_{(-1)}^{(1)} [N^T] \cdot \{W\} \cdot |J| ds \cdot dt + \int_{-1}^1 [N^T] \cdot \{T\} dS \quad (2.13)$$

where $[\eta]$ is a matrix of damping terms. $\{W\}$ is the vector of prescribed body forces and $\{T\}$ is a vector of external tractions that may be applied to some surface, S.

The equations of motion for the element can then be written as

$$[m_e]\{\ddot{q}\} + [c_e]\{\dot{q}\} + [k_e]\{q\} = \{Q(t)\} \quad (2.14)$$

Once the equations of motion for each element are obtained, they are combined in a way that satisfies compatibility of displacements to obtain the global equations of motion,

$$[M]\{\ddot{u}\} + [C]\{\dot{u}\} + [K]\{u\} = \{R(t)\} \quad (2.15)$$

where $[M]$ is the global mass matrix, $[C]$ the global damping matrix, $[K]$ the global stiffness matrix, $\{u\}$ is the global nodal point displacement vector and $\{R(t)\}$ the global nodal point force vector. For the case of loading induced by base motion, the global equation of motion is

$$[M]\{\ddot{u}\} + [C]\{\dot{u}\} + [K]\{u\} = - [M][1]\{\ddot{u}_b\} \quad (2.16)$$

where \ddot{u}_b is the base acceleration.

2.2.3.2 Finite Difference Methods

Mainly, the finite difference method is used to solve differential equations numerically. In finite difference approach, the methods can be classified according to their convergence criteria. For convergence,

explicit finite difference methods look for a conditional value. Implicit finite difference methods on the other hand are convergent in any condition. Explicit finite difference methods are faster when the incremental time, (Δt), is bigger. When Δt is small, the convergence rate drops dramatically. On the other hand explicit finite difference methods match the physics more accurately, thus most of the formulations used in the analysis of mechanical problems are explicit.

For a continuous media, the equation of motion is expressed as;

$$\sigma_{ij,i} + \rho \cdot b_i = \rho \cdot \frac{dv_i}{dt} \quad (2.17)$$

where ρ is the mass per unit volume of the medium, b_i is the body force per unit mass, and dv/dt is the material derivative of the velocity. Note that in the case of static equilibrium of the medium, the acceleration dv/dt is zero, and (2.17) reduce to the partial differential equations of equilibrium

$$\sigma_{ij,i} + \rho \cdot b_i = 0 \quad (2.19)$$

These equations can be defined by finite difference approach where first-order space and time derivatives of a variable are approximated by finite differences assuming linear variations of the variable over finite space and time intervals, respectively.

For an explicit finite difference approach the mesh element chosen can be solved of the form using central finite differences in that Nodal velocities are computed using the recurrence relation

$$v_i^{<l>} \left(t + \frac{\Delta t}{2} \right) = v_i^{<l>} \left(t - \frac{\Delta t}{2} \right) + \frac{\Delta t}{M^{<l>}} F_i^{<l>} \left(t, \{v_i^{<1>}, v_i^{<2>}, v_i^{<3>} \dots, v_i^{<p>}\}, k \right) \quad (2.19)$$

where the notation $\{ \}^{<l>}$ refers to the subset of nodal velocity values involved in the calculation at global node l , v the nodal velocity, M is the

modal mass and F is the out of balance force for the node. In turn the node location and the node displacements can be similarly updated using central difference approximation respectively.

$$x_i^{<l>}(t+\Delta t) = x_i^{<l>}(t) + \Delta t v_i^{<l>}(t + \frac{\Delta t}{2}) \quad (2.20)$$

$$u_i^{<l>}(t+\Delta t) = u_i^{<l>}(t) + \Delta t v_i^{<l>}(t + \frac{\Delta t}{2}) \quad (2.21)$$

The difference equations (2.19) will not provide valid answers unless the numerical scheme is stable. Some physical insight may be gained on this topic by viewing the idealized medium as an assembly of point masses (located at the nodes) connected by linear springs and dashpots, a conceptualization which may be made on the following grounds. The equations of motion for a mass-dashpot-spring system may be expressed, in matrix notation, as

$$[M]\{\ddot{u}\} + [C]\{\dot{u}\} + [K]\{u\} = \{P^*\} \quad (2.20)$$

which is the final form of dynamic equations as in the Eq.(2.15) obtained in the Finite element method, where P^* is the external force which can be written as $-[M][1]\{\ddot{u}_b\}$, \ddot{u}_b being the base acceleration when the case of loading induced by base motion occurs.

2.3 Constitutive Models

In the literature there are many constitutive models that define the material behaviour. Some of them are ;

- (1) null;
- (2) elastic, isotropic;
- (3) elastic, orthotropic;
- (4) elastic, transversely isotropic;
- (5) Drucker-Prager plasticity;
- (6) Mohr-Coulomb plasticity;

- (7) strain-hardening / softening Mohr-Coulomb plasticity;
- (8) ubiquitous-joint plasticity;
- (9) bilinear strain-hardening / softening ubiquitous-joint plasticity
- (10) modified Cam-clay plasticity; and.
- (11) Finn model for modelling pore pressure generation

In this section only the constitutive models (2),(6) and (11) will be discussed.

2.3.1 Elastic Model

Elastic model provides the simplest representation of material behaviour. This model exhibits linear stress-strain behaviour with no hysteresis on unloading.

In the elastic isotropic model, strain increments generate stress increments according to the linear and reversible law of Hooke;

$$\Delta\sigma_{ij} = 2 \cdot G \cdot \Delta\varepsilon_{ij} + \alpha_2 \cdot \Delta\varepsilon_{kk} \cdot \delta_{ij} \quad (2.21)$$

where the Einstein summation convention applies, δ_{ij} is the Kroenecker delta symbol, α_2 is a material constant related to the bulk modulus, K, and the shear modulus G. New stress values are then obtained from the relation

$$\sigma_{ij}^N = \sigma_{ij} + \Delta\sigma_{ij} \quad (2.22)$$

2.3.2 Mohr Coulomb Plasticity

In 1910, Mohr presented a theory for rupture in materials. According to this theory, failure along a plane in a material occurs by a critical combination of normal and shear stresses and not by normal or shear stress alone. The functional relation between normal and shear stress on the failure can be given by

$$s = f(\sigma) \quad (2.23)$$

where s is the shear stress at failure and σ is the normal stress on the failure plane. The failure envelope defined by Eq.(2.23) is a curved line, as shown in Fig (2.6). In 1776, Coulomb defined the function $f(\sigma)$ as

$$s = c + \sigma \tan \varphi \quad (2.24)$$

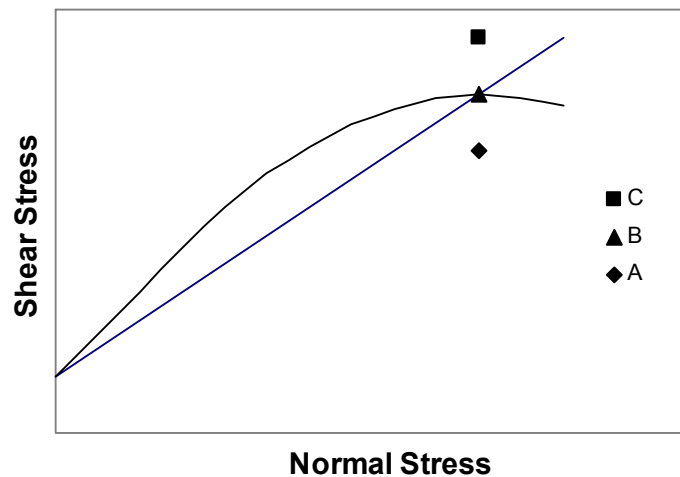


Fig 2.6 Failure envelope

where c is cohesion and φ is the angle of friction of the soil. Eq.(2.24) is generally referred to as the Mohr-Coulomb criteria. The significance of the failure envelope can be explained using Fig (2.6). If the normal and shear stresses on a plane in a soil mass are such that they plot as point A, shear failure will not occur along that plane. Shear failure along a plane will occur if the stresses plot as point B, which falls on the failure envelope. A state of stress plotting as point C cannot exist, since this falls above the failure envelope.

In saturated soils, the stress carried by the soil solids is the effective stress and so Eq.(2.24) must be modified:

$$s = c + (\sigma - u) \tan \phi = c + \sigma' \tan \phi \quad (2.25)$$

where u is the pore pressure and σ' is the effective stress on the plane. The term ϕ is also referred to as the drained friction angle. For sand, inorganic silts and normally consolidated clays, $c \approx 0$. The value of c is greater than zero for over consolidated clays and sands.

Using this Mohr-Coulomb criterion, Mohr-Coulomb constitutive model can be constructed where the failure envelope for this model corresponds to Mohr-Coulomb criterion (shear yield function) with cutoff (tension yield function). The position of stress point on this envelope is controlled by a non-associated rule for shear failure and an associated rule for tension failure.

The Mohr-Coulomb criterion can be expressed in terms of the principal stresses $\sigma_1, \sigma_2, \sigma_3$, which are the three components of the generalized stress vector for this model. The components of the corresponding generalized strain vector are the principal strains $\varepsilon_1, \varepsilon_2, \varepsilon_3$. The incremental expression of Hooke's law in terms of the generalized stress and stress increments has the form

$$\Delta\sigma_1 = \alpha_1 \cdot \Delta\varepsilon_1^e + \alpha_2 \cdot (\Delta\varepsilon_2^e + \Delta\varepsilon_3^e) \quad (2.26)$$

$$\Delta\sigma_2 = \alpha_1 \cdot \Delta\varepsilon_2^e + \alpha_2 \cdot (\Delta\varepsilon_1^e + \Delta\varepsilon_3^e)$$

$$\Delta\sigma_3 = \alpha_1 \cdot \Delta\varepsilon_3^e + \alpha_2 \cdot (\Delta\varepsilon_2^e + \Delta\varepsilon_1^e)$$

where α_1 and α_2 are material constants defined in terms of the shear modulus, G , and bulk modulus, K , as

$$\alpha_1 = K + 4/3 * G \quad (2.27)$$

$$\alpha_2 = K - 2/3 * G \quad (2.28)$$

The criterion may be represented in the plane (σ_1, σ_3) . Defining the failure criterion as

$$f^s = \sigma_1 - \sigma_3 N_\phi + 2c(N_\phi)^{1/2} \quad (2.29)$$

where ϕ is the friction angle, and N_ϕ can be defined as

$$N\phi = \frac{1 + \sin \phi}{1 - \sin \phi} \quad (2.30)$$

This basic model can produce curves of apparent damping and modulus versus cyclic strain that resemble results from laboratory tests.

2.3.3 Finn Model

According to Martin (1976) it is the grain rearrangement rather than grain volume change that takes place, thus the volume of the void space decreases under constant confining stress. If the voids are filled with fluid, then the pressure of the fluid increases and the effective stress acting on the grain matrix decreases. Consequently it is the transfer of externally applied pressure from grains to fluid that accounts for the fluid-pressure increase.

Martin (1976) states that pore pressure build up is a secondary effect. The primary effect is the irrecoverable volume contraction of the matrix of grains when a sample is taken through a complete strain cycle when the confining stress is held constant. Martin et al (1975) also notes that the relation between irrecoverable volume-strain and cyclic shear-strain amplitude is independent of confining stress.

Martin (1976) starts the formulation by stating the volumetric compatibility at the end of the load cycle as,

change in volume of voids=net change in volume of soil structure.

$$\frac{\Delta u \cdot n_e}{k_w} = \Delta \varepsilon_{vd} - \frac{\Delta u}{E_r} \quad (2.31)$$

where Δu is the increase in residual pore pressure for the cycle, k_w is bulk modulus of water, n_e is porosity of sample, E_r is tangent modulus of the one-dimensional unloading curve at a point corresponding to the initial vertical effective stress, $\Delta \varepsilon_{vd}$ is reduction in volume of sand structure due to slip deformation, $\Delta u / E_r$ is increase in volume of sand structure due to

recoverable volumetric strain, and $\Delta u_{n_e}/k_w$ = change of volume of voids. For saturated samples $k_w = 2 \times 10^6$ kPa whereas E_r is generally in the order of 10^5 kPa.

Since the water is incompressible then under conditions of zero volume change Equation (2.31) reduces to

$$\Delta u = E_r \cdot \Delta \varepsilon_{vd} \quad (2.32)$$

Finally Martin et al (1976) supply the Eq. (2.33) that relates the increment of volume decrease ($\Delta \varepsilon_{vd}$) to the cyclic shear strain amplitude (γ), where γ is presumed to be the engineering shear strain.

$$\Delta \varepsilon_{vd} = D1 \cdot (\gamma - D2 \cdot \varepsilon_{vd}) + \frac{D3 \cdot \varepsilon_{vd}^2}{\gamma + D4 \cdot \varepsilon_{vd}} \quad (2.33)$$

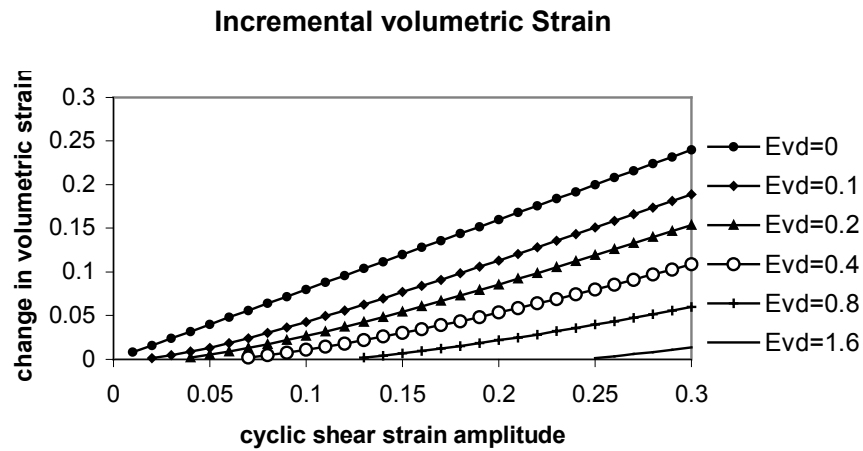


Fig 2.7 (Martin 1976) volumetric strain curves for the sand with $D1=0.8$, $D2=0.79$, $D3=0.45$ and $D4=0.73$.

Eq. (2.33) involves the accumulated irrecoverable volume strain ε_{vd} in such a way that the change in volume strain decreases as volumetric strain increases. Presumably, $\Delta \varepsilon_{vd}$ should be zero if γ is zero; this implies that the constants are related as follows: $D1 \cdot D2 \cdot D4 = C3$.

An alternative and simple formula is proposed by Byrne (1991) for the determination of $\Delta \varepsilon_{vd}$

$$\frac{\Delta \varepsilon_{vd}}{\gamma} = B1 \cdot \exp(-B2 \cdot (\frac{\varepsilon_{vd}}{\gamma})) \quad (2.34)$$

where in many cases $B2=0.4/B1$. So Eq(2.34) involves only one independent constant. According to (Byrne 1991) the only independent variable can be determined by;

$$B1 = 8.7 \cdot (N_1)_{60}^{-1.25} \quad (2.35)$$

Finally these pore pressure models can be inserted into the standard Mohr-Coulomb plasticity model. Actually Finn model is the build-in constitutive model constructed in the way explained above.

2.4 SPT-CPT-Vs relationships

The behaviour of soils subjected to dynamic loading is governed by dynamic soil properties. The measurement of dynamic soil properties is a critical task in the solution of geotechnical earthquake engineering problems. A wide variety of field and laboratory techniques are available for the measurement of dynamic soil properties, each with different advantages and limitations with respect to different problems. Many are oriented toward measurement of low-strain properties and many others toward large strain.

Low strain field tests are;

1) Seismic Reflection Test which allows the wave propagation velocity and thickness of the layers.

2) Seismic Refraction Test which involves measurement of the travel times of p-s waves .

3) Suspension Logging Test which allows measurement of wave propagation velocities in a single, uncased bore hole, but only for the high frequencies of the waves.

4) Rayleigh wave Test which is useful for determining the near surface shear wave velocity.

5) Seismic Cross-Hole Test which also allows measuring wave propagation velocities along horizontal paths with using two or more boreholes.

6) Seismic Down-Hole(Up-Hole) Tests which allow measuring the travel times of p-s waves from the energy source to the receiver which can be performed in a single borehole.

7) Seismic Cone Test which is very similar to the Down-Hole Test.

High-Strain field tests are;

1) Standard Penetration Test

2) Cone Penetration Test:

3) Dilatometer Test

4) Pressuremeter Test which is the only in situ test capable of measuring stress-strain, as well as strength behaviour.

Laboratory tests on the other hand are usually performed on relatively small specimens that are assumed to be a representative of a larger body of soil. Only limited number of laboratory tests are able to determine the properties of soils at low strain levels. These are;

1) Resonant Column Test,

2) Ultrasonic Pulse Test,

3) Piezoelectric Bender Element Test.

At higher shear strain amplitudes, soils generally exhibit volume change tendencies. Under drained loading conditions, these tendencies are allowed to manifest themselves in the form of volumetric strain, but under undrained conditions they result in changes in pore pressure. Some of the large-strain laboratory tests are;

1) Cyclic Triaxial Test

2) Cyclic Direct Simple Shear Test

3) Cyclic Torsional Shear Test

Soil properties that influence wave propagation and other low-strain phenomena include stiffness, damping, Poisson's ratio and density. Of

these, stiffness and damping are the most important parameters at low strains. At high levels of strain, the influence of the rate and number of cycles of loading on shear strength may also be important. Volume change characteristics are also important at high strain levels.

The tests should be performed with due recognition of the available uncertainty. Sources of the uncertainty include the inherent variability of soils, induced anisotropy, drilling and sampling disturbance, limitations of field and laboratory testing equipment, testing errors and interpretation errors. Thus careful attention should be needed for the minimization of uncertainty.

Also the selection of testing techniques for measurement of dynamic soil properties requires careful consideration and understanding of the specific problem at hand.

In the following section only Standard Penetration and Cone Penetration Tests will be discussed because the data gathered from the soil site in (Şahinler Street) Adapazarı are of type SPT, CPT and Vs.

2.4.1 Standard Penetration Test (SPT)

The standard penetration test is by far the oldest and the most commonly used in situ test in geotechnical engineering. In the SPT, a standard split barrel sampler is driven into the soil at the bottom of a bore hole by repeated blows (30 to 40 blows per minute) of a 63.6 kg hammer released from a height of 76 cm. The sampler is usually driven 46 cm. The number of blows required to achieve the last 30 cm of penetration is taken as the standard penetration resistance, N. The N value is a function of the soil type, confining pressure, and soil density, but is also influenced by the test equipment and procedures.

It has become common to normalize the N value to an overburden pressure (100 kPa) and to correct it to an energy ratio of 60% according to Eq. (2.36);

$$(N_1)_{60} = N_m \cdot C_N \cdot \frac{E_m}{0.6 \cdot E_{ff}} \quad (2.36)$$

where N_m is the measured penetration resistance, C_N , an overburden correction factor, E_m the actual hammer energy, and E_{ff} the theoretical free-fall energy.

In many countries, the SPT has been also the most commonly used in situ test for characterization of liquefaction resistance. The Cone Penetration test (CPT), shear wave velocity measurements (V_s) and the Becker penetration test (BPT) are the other tests that have gained common usage for evaluation of liquefaction resistance.

The SPT N value is one of the tools that can be used to estimate shear modulus G . Defining the $G_{sec} = \tau_c / \gamma_c$ and $G_{max} = \rho V_s^2$, where τ_c , γ_c are the shear stress and shear strain amplitudes respectively, ρ is the soil density and V_s is the shear wave velocity, the modulus ratio (G_{sec} / G_{max}) varies with cyclic strain amplitude and other parameters. The variation of the modulus ratio with shear strain is described graphically by a modulus reduction curve which gives the information about the soil stiffness. For the cases where the V_s is not available, G_{max} for sand, can be estimated by using the following equations proposed by Seed et al. (1986)

$$G_{max} = 20000 \cdot (N_1)_{60}^{0.333} \cdot (\sigma'_m)^{0.5} \quad (2.37)$$

where σ'_m is the mean principle effective stress (lb/ft^2). On the other hand, Imai and Tonouchi (1982) proposed the following equation

$$G_{max} = 325 \cdot (N_1)_{60}^{0.68} \quad (2.38)$$

where G_{max} expressed in (kip/ft^2).

2.4.2 Cone Penetration Test (CPT)

In recent years, use of the cone penetration test (CPT) in geotechnical engineering practice has increased sharply. The CPT involves the steady penetration of a standart cone penetrometer into the ground. The standard cone penetrometer has a conical tip of 10 cm^2 area and 60° apex angle immediately below a cylindrical friction sleeve of 150 cm^2 surface area. The penetrometer is pushed into the ground at a constant rate of 2 cm/sec . The tip and friction sleeve are each connected to load cells that measure the tip resistance, q_c , and sleeve resistance, f_s ,

during penetration. The friction ratio $FR=f_s/q_c$ is also a useful parameter. It is high in cohesive soils and low in cohesionless soils. Using these cone resistance and friction ratio CPT-Based Soil Behaviour-Type chart can be obtained as proposed by Robertson (1990) in Fig 2.8.

The CPT can be performed rapidly and relatively inexpensively. It provides a continuous profile of penetration resistance that can detect the presence of thin layers that are easily missed in SPT testing. However, the CPT cannot be used at sites with very stiff and very dense soils without damaging the probe or rods. The presence of gravel -size particles may also limit the use of the CPT.

The CPT has gained common usage for evaluation of liquefaction resistance. CSR vs q_{c1} charts give important relation to liquefaction as in the SPT tests.

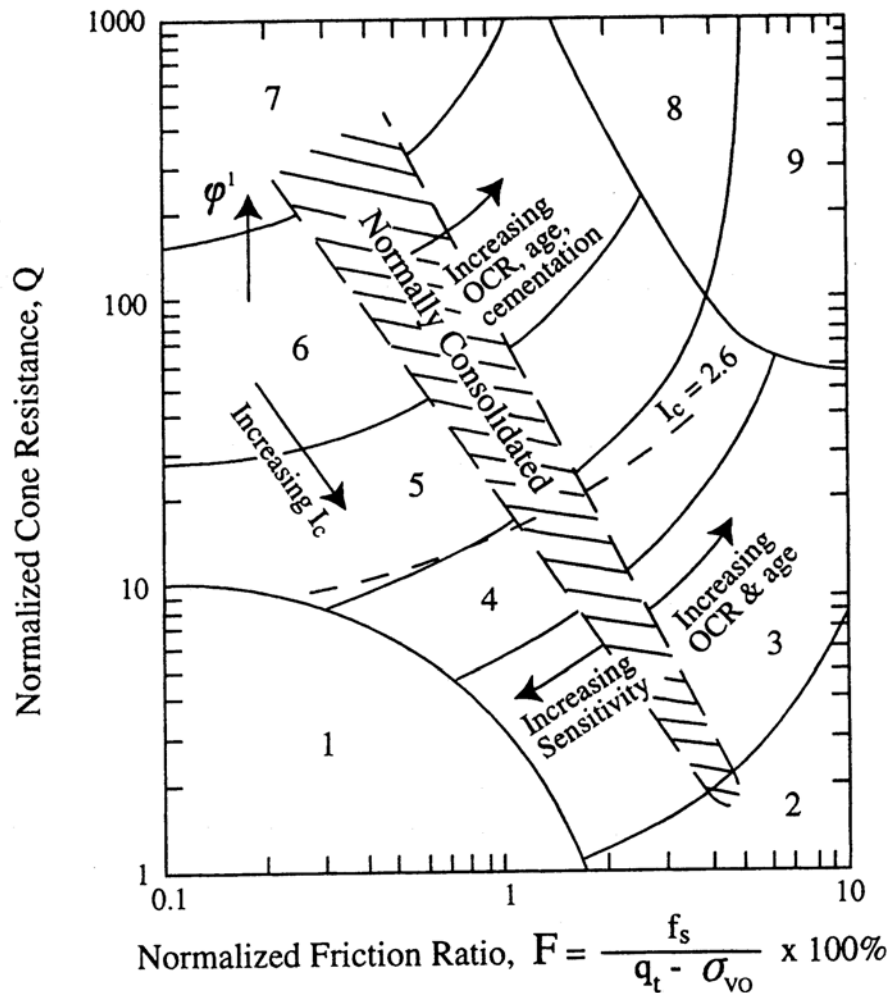
There exist G_{max} relations for CPT- q_c value as in the SPT- N_{60} value. For the cases where the V_s is not available, G_{max} , can be estimated by using the following equations

$$G_{max} = 1634 \cdot (q_c)^{0.25} \cdot (\sigma'_v)^{0.375} \quad (2.39)$$

where σ'_v is the vertical effective stress (kPa). Eq(2.39) is proposed by Rix and Stokoe (1991) for sand.

$$G_{max} = 406 \cdot (q_c)^{0.695} \cdot e^{-1.130} \quad (2.40)$$

For clay, Mayne and Rix (1993) proposed the Eq. (2.40) where G_{max} is expressed in (kPa) and e is the exponential.



- | | |
|--|-------------------------------------|
| 1. Sensitive, fine grained | 6. Sands - clean sand to silty sand |
| 2. Organic soils - peats | 7. Gravelly sand to dense sand |
| 3. Clays - silty clay to clay | 8. Very stiff sand to clayey sand* |
| 4. Silt mixtures - clayey silt to silty clay | 9. Very stiff, fine grained* |
| 5. Sand mixtures - silty sand to sandy silt | |
- *Heavily overconsolidated or cemented

Fig 2.8 CPT-Based Soil Behaviour-Type chart

2.5 Liquefaction

The term liquefaction is used to define the phenomena that involve deformations caused by monotonic, transient, or repeated disturbance of saturated soils under undrained conditions. The generation of excess pore

pressure under undrained loading conditions is a hallmark of all liquefaction phenomena.

A number of approaches to evaluation of liquefaction have developed over the years. In this section only Cyclic Stress approach and Probabilistic approach will be discussed.

2.5.1 Cyclic Stress Approach

The level of excess pore pressure required to initiate liquefaction is related to the amplitude and duration of earthquake-induced cyclic loading. The cyclic stress approach is based on the assumption that excess pore pressure generation is fundamentally related to the cyclic shear stresses, hence seismic loading is expressed in terms of cyclic shear stresses as in the Eq(2.41).

$$\tau_{cyc} = 0.65 * \tau_{max} \quad (2.41)$$

where τ_{max} is the maximum shear stress .

Cyclic shear stress is frequently normalized by the initial effective overburden pressure to produce a cyclic stress ratio (CSR) as in Eq(2.42).

$$CSR = \frac{\tau_{cyc}}{\sigma'_{v0}} \quad (2.42)$$

Defining the maximum shear stress as,

$$\tau_{max} = \left(\frac{a_{max}}{g}\right) \cdot (\sigma_{v0}) \cdot r_d \quad (2.43)$$

the cyclic stress ratio in Eq(2.42) can also be written as in Eq(2.44):

$$CSR = 0.65 \cdot \left(\frac{a_{max}}{g}\right) \cdot \left(\frac{\sigma_{v0}}{\sigma'^*_{v0}}\right) \cdot r_d \quad (2.44)$$

where a_{max} is peak horizontal acceleration at the ground surface, g is the acceleration of gravity, σ_{v0} and σ'^*_{v0} are total and effective vertical overburden stresses, respectively and r_d is the stress reduction coefficient. Finally, CSR versus $(N_1)_{60}$ plot can be produced drawing the liquefaction susceptible boundary curves considering the clean-sand base curve, influence of fines content, and moment magnitude of the earthquake. This

is the methodology that has become a standard of practice in many countries for evaluating liquefaction resistance of soil Seed and Idriss (1971).

Especially the determination of the C_N in Eq.(2.36), r_d in Eq.(2.43), influence of fines content, are the main concepts that are discussed in literature. Youd et al (2001) gave important documentation about the discussion of evaluation of liquefaction resistance of soils and their parameters stated above.

Laboratory tests show that the cyclic shear stress required to trigger liquefaction increases at high effective confining pressures. Seed (1983) proposed that the effects of initial shear stress and high effective confining pressures be accounted for by modifying the cyclic stress ratio as follows:

$$(CSR_{field})_{\alpha,\sigma} = (CSR_{field})_{\alpha=0,\sigma} \cdot K_{\alpha} \cdot K_{\sigma} \quad (2.45)$$

where $\alpha = \tau_{h,static} / \sigma_{vo}$ and K_{α} and K_{σ} are correction factors for initial shear stress and effective overburden pressure, respectively.

2.5.2 Probabilistic Approach

There are many potential sources of uncertainty in both loading and resistance aspects of liquefaction problems, and probabilistic approaches have been developed to deal with them. In this section only the method of Çetin et al. (2000) will be discussed.

Çetin et al. (2000) defines the CSR as the function of $N_{1,60}$, M_w , σ_v' , FC and P_L in the formula given in Eq(2.46).

$$CSR(N_{1,60}, M_w, \sigma_v', FC, P_L) = \exp \left[\frac{N_{1,60} \cdot (1 + 0.004 \cdot FC) - 29.53 \cdot \ln(M_w) - 3.70 \cdot \ln(\sigma_v') + 0.05 \cdot FC + 44.97 + 2.70 \cdot \Phi^{-1}(P_L)}{13.32} \right] \quad (2.46)$$

where M_w is the earthquake magnitude, FC is the fines content, σ_v' is the vertical effective stress and P_L is the probability of liquefaction.

The use of the formula is that when the CSR, FC, M_w , σ_v' and $N_{1,60}$ are known, the probability of liquefaction can be predicted. This property will be used in this thesis.

CHAPTER 3

OBSERVED STRUCTURAL DAMAGE AND SITE INVESTIGATION STUDIES

3.1 Damage to the Buildings after the Earthquake

After the 17 August 1999 Kocaeli earthquake, different levels of structural damage was observed on the buildings of Adapazarı, Şahinler Street. In this study the earthquake damage to the three identical buildings C_1 , C_2 , C_3 as shown in Fig. (3.1), is investigated. Building C_1 performed very poorly and collapsed after it translated significantly while the building C_2 next to it exhibited moderate structural damage, thus settled (17 cm. at its western side) and translated significantly (60 cm. on average). Building C_3 performed quite well with no signs of translation and settlement. Dramatically different performances of these three identical buildings suggest the potential suspect of the problem as the foundation soils. Within the confines of this thesis, answer to this question will be looked for. The figures (3.1) and (3.2) give important information about the damage level of the street.

Fig (3.3) shows the general plan view of Şahinler Street. Also the settlement and translation values of the buildings C_1 , C_2 , C_3 can be seen from Fig (3.3). The site was mapped by PEER and METU teams immediately after the earthquake. Series of site investigation studies were carried out at the site including SPT, CPT and seismic CPT.



Fig 3.1 The photograph of the 3 buildings in Şahinler Street.



Fig 3.2 The photograph of the building stated as C₂ in Fig(3.1)

ISTIKLAL DISTRICT
N40.7

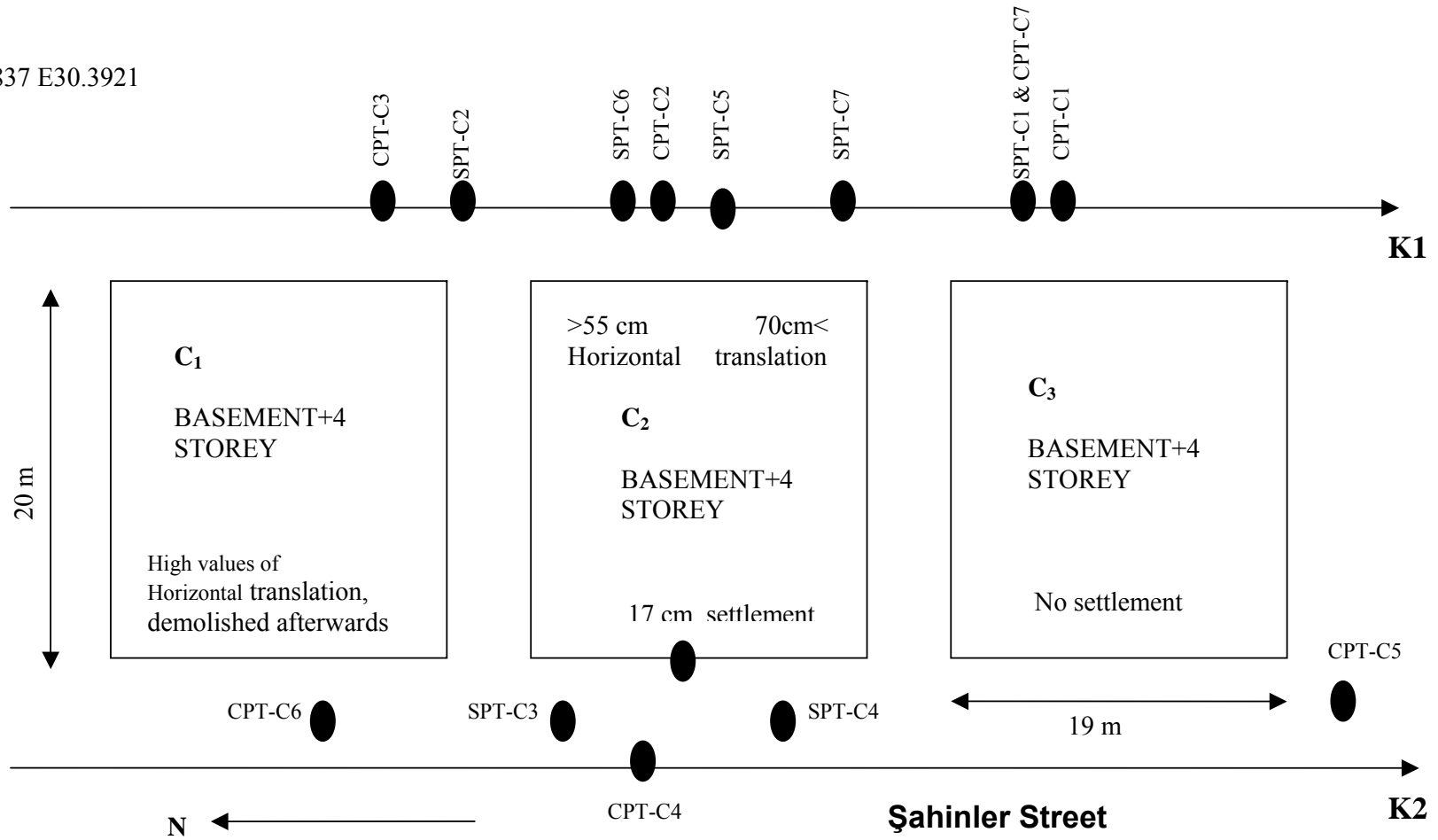


Fig 3.3 General Schematic view of the Şahinler Street

3.2 Site Investigation Studies

The investigation of Şahinler street starts with the construction of 2D cross sectional (K1, K2) views of the site as shown in Fig (3.3). K1 and K2 can be seen in Fig (3.4) and Fig (3.5) respectively. The cross sections K1 and K2 compose of SPT, CPT profiles with the estimated soil layers from these site investigation studies.

It can be seen from the Fig (3.4) and Fig (3.5) that there are basically 4 different soil layers. The top layer composed of mainly silty-clay. SPT N values for this layer range from 1 to 8. A second layer of silty-sand layer is underlying the top silty clay layer whose SPT N values range from 20 to 40. The third layer is clay and silt. The SPT N values in this layer are between 6 and 21. The layer at the bottom was relatively stiffer and dense, thus for the runtime simplicity it was not modeled in the analysis of the problem.

CPT data was obtained from <http://peer.berkeley.edu> and are given in Appendix B.

Shear wave velocity (V_s) profiles reported by PEER group was used in the analysis as shown in Fig (3.6). The information about the Poisson's ratios and soil densities of the site are summarized in Table (3.1)

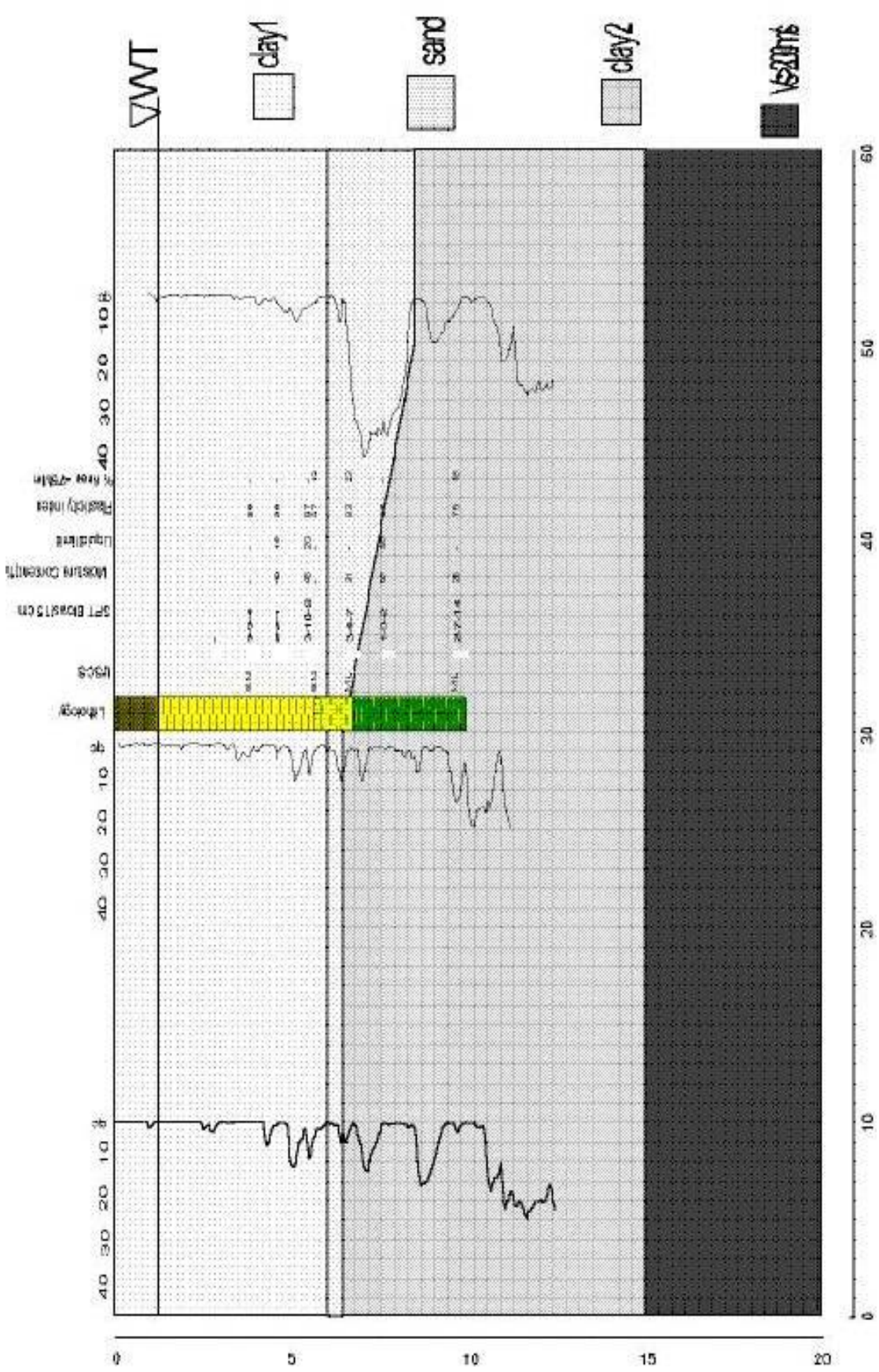


Fig 3.5 K2 cross sectional view

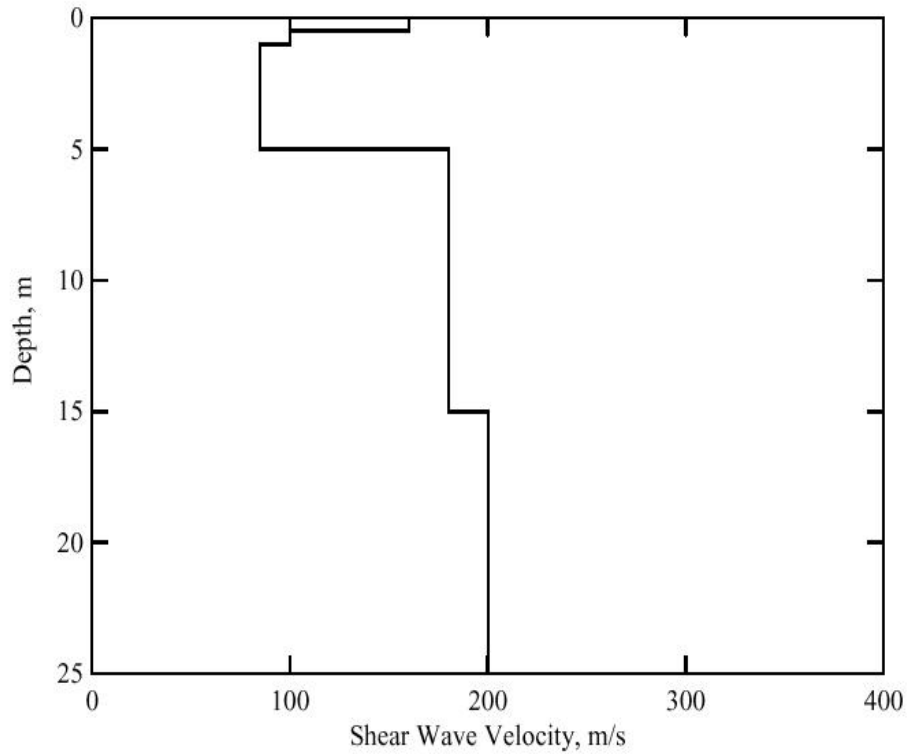


Fig. 3.6 Shear wave velocity profile determined from forward modeling of Site C North Centerline.

Table 3.1 Tabulated values of layer properties determined from forward modeling of Site C South Centerline

Depth to Top of Layer, m	Layer Thickness, m	Shear Wave Velocity, m/s	Assumed Values		
			P-Wave Velocity, m/s	Poisson's Ratio	Mass Density, g/cc
0	1.0	95	177.7	0.3	1.92
1.0	3.0	100	1500	0.4978	2.0
4.0	10.0	155	1500	0.4946	2.0
14.0	11.0	225	1500	0.4885	2.0

3.3 Soil and Structural Engineering Properties

The dynamic analyses of the 3 buildings in Şahinler Street was performed by computer program Flac3D (Fast Lagrangian analysis of continua). The constitutive models used for the analysis are the Finn Model, Mohr Coulomb plasticity model and Elastic Model. Finn Model requires a series of parameters namely,

- 1) Maximum Shear Modulus, G_{max}
- 2) Bulk Modulus, K
- 3) Cohesion, c
- 4) Friction angle, ϕ
- 5) Tension
- 6) C_1, C_2, C_3 and C_4 constants for pore pressure calculations.

Mohr Coulomb plasticity model uses the parameters of Finn model except the C_1, C_2, C_3 and C_4 constants. On the other hand, Elastic Model only uses

- 1) Maximum Shear Modulus, G_{max}
- 2) Bulk Modulus, K

Maximum Shear Modulus G_{max} is calculated using the Eq. (3.1).

$$G_{max} = \rho * V_s^2 \quad (3.1)$$

where ρ is the soil density, and V_s is the shear wave velocity. The related data for ρ and V_s were obtained by using the Fig(3.6) and Table (3.1).

In Table (3.1) Poissons's ratio as a function of soil depth is given. Using the values for poisson's ratios, the bulk modulus as a function of Youngs modulus can be calculated using the equation (3.2). In Table (3.1) Poisson ratios, ν are around 0.5 which indicates that the site is undrained and incompressible during the earthquake.

$$K = \frac{E}{3 \cdot (1 - 2 \cdot \nu)} \quad (3.2)$$

where E is the Young's modulus. Knowing G and ν , E can be calculated easily by using the Eq. (3.3) .

$$E = G \cdot 2(1 + \nu) \quad (3.3)$$

Computation of cohesion values is a critical task. For the purpose of determining the cohesion, the Eq(3.4) is used.

$$\tau = \frac{q_c - \sigma_v}{N_k} \quad (3.4)$$

where q_c is the soil resistance obtained from CPT, σ_v is the total stress for the soil site, N_k is a factor to be determined. For the case of Şahinler Street $N_k=15$ is used for the determination of undrained shear strength, τ .

For undrained cases cohesion is equal to τ , thus the estimated τ values were used as cohesion, c . Fig(3.7) is the graph of cohesion values of the whole site as a function of depth. The places of CPT-c1, c2, c3, c4, c5 and c6 are given in Fig(3.3).

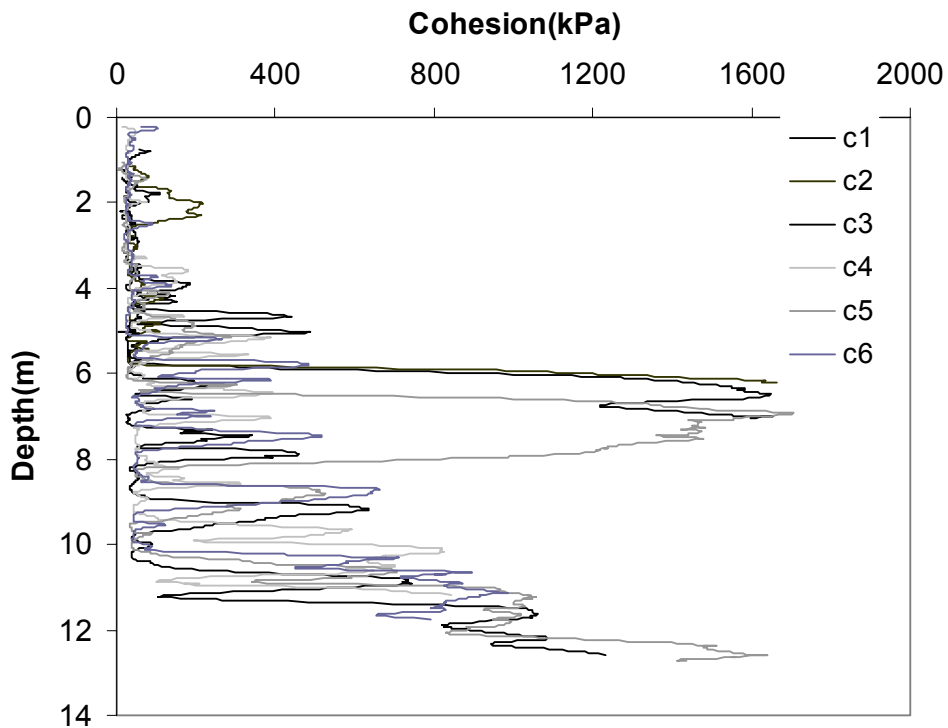


Fig 3.7 Cohesion vs Depth values using the CPT -c1,c2,c3,c4,c5,c6 q_c values.

Since the values of cohesion increase dramatically at depths larger than 5m, it is possible to use elastic model instead of Finn model for which only G , K are required for the analysis. Thus observing the anomalies in

the deeper portions of the soil, which may be due to errors in the measurements, the use of basic Elastic Model is also preferred since the drastic fluctuations at 5-10 m. depths make the determination of the further parameters difficult. Such an approach also decreases runtime requirement for computational analysis.

The friction angle is determined by using the Eq(3.5).

$$\frac{\nu}{1-\nu} = 1 - \sin \phi \quad (3.5)$$

where ν is the Poisson's ratio which can be taken from Table(3.1).

Since the computer program Flac3D version 2.0 does not support the simple Byrne formula, the constants C1, C2, C3 and C4 are derived using Byrne curves as explained in Chapter 4.

The soil parameters related to soil properties are summarized in Table (3.2).

The parameters of static analysis and the dynamic analysis are given in Table (3.2). The aim of static analysis is to model stress conditions before the earthquake and ensure the static equilibrium which is needed in Flac3D analysis for the sake of accuracy. The static analysis is done using Elastic model for all the soil layers. The reason for using elastic model is to shorten runtime. Static analysis has minor importance in the whole analysis of the dynamic problem.

As seen in Table(3.2) the Bulk Moduli values for static cases are lower than the values for dynamic case. In constructing Table (3.2), drained case for the static analysis and undrained case for the dynamic analysis are used. Note that Poisson's ratio has high value for dynamic case than for the static case.

The raft foundations of the buildings are modeled as elastic materials. The parameters for the foundation are also given in Table (3.2).

In our analysis, elastic model is used in static and dynamic analysis for each soil layer except the top layer. Mohr Coulomb plasticity model together with the Finn model is used for the top layer during dynamic analysis.

		Stiffness Parameters				Strength Parameters		
	Soil	K(kPa)	E(kPa)	G(kPa)	Vs(m/s)	ϕ	μ	C(kPa)
Static Drained	Silty Clay	7.6e4	5.5e4	1.5e4	100		0.38	
	Silty Sand	1.26e5	1.66e5	6.5e4	180		0.28	
	Clay	9.2e4	1e5	3e4	130		0.31	
Dynamic Undrained	Silty Clay	5e5	6e4	1.5e4	100	15	0.48	50
	Silty Sand	3.2e6	1.9e5	6.5e4	180		0.49	
	Clay	9e5	1.2e5	3e5	130		0.49	
	Stiff	1e5		1e5	230			

Table 3.2 Static and Dynamic Soil Properties for the site in Adapazarı

The structural properties are estimated by modeling the buildings C₁, C₂, C₃ as framed structures such that in each floor there are 4 column elements and 4 beam elements. For each buildings there are 4 stories with each story height, 3 m. Length and width of the structures are 20 m. and a stiff material under the structure is defined to simulate the mat behaviour. Each floor weight of 4000 kN is distributed equally to 4 beams. Also the beams and columns are designed to represent a 4 story building with its natural period. The other properties of concrete, beams and columns are given in Table (3.3).

Table 3.3 Structural properties

Concrete beam properties	Building Properties
E=25 E6 kPa	Natural Period=0.4 sec
F=50 kN (load on a single beam)	Column Length=3m.
Inertia x=0.083	Beam Length=12 m.
Inertia y=0.083	Mat foundation
Inertia r=0.166	
Crossectional area :1m ²	

Fig 3.8 shows 3-D view of the modeled site .

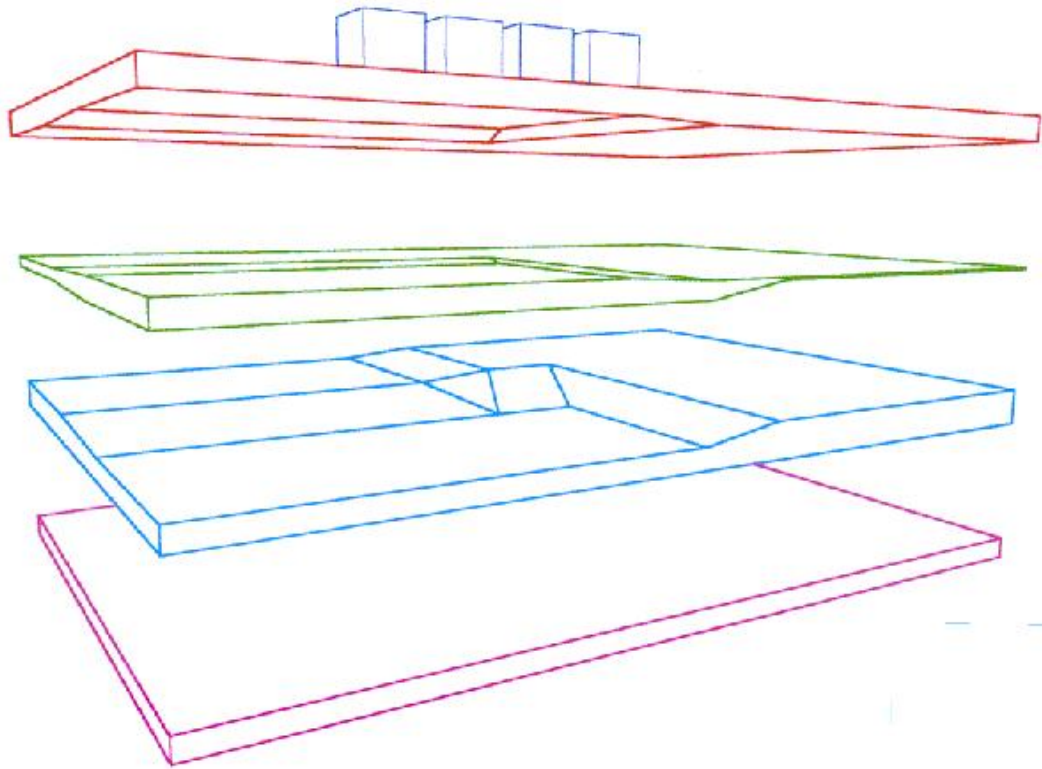
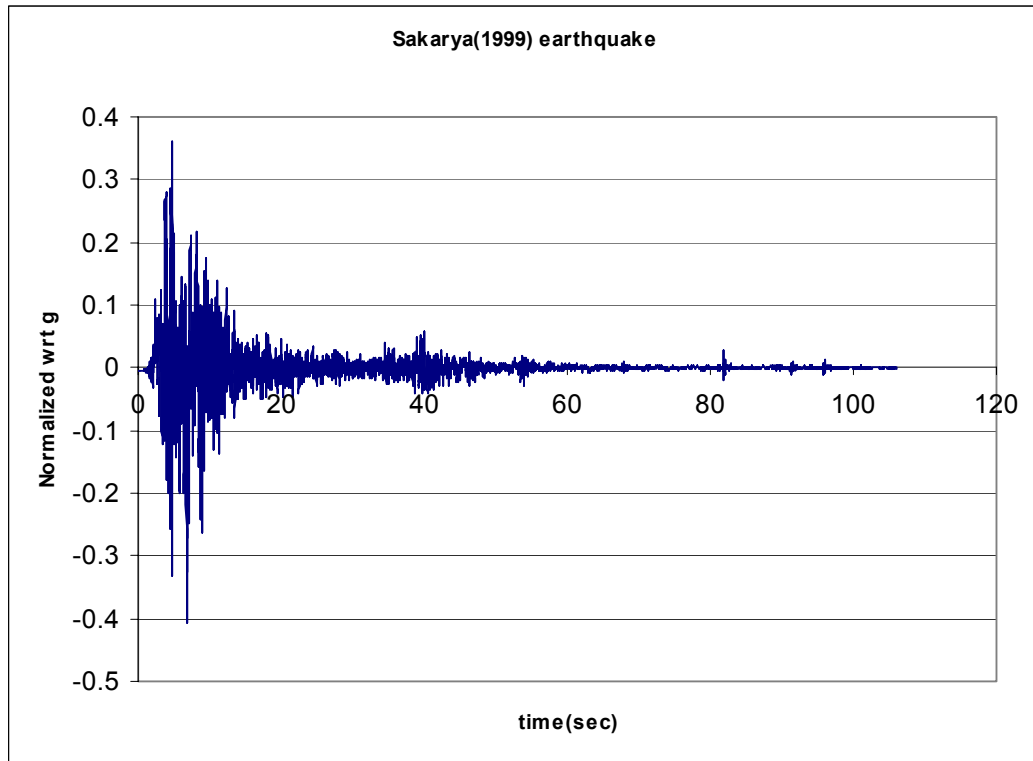


Fig 3.8 General 3D view of the site (estimated)

3.4 Characteristics of Adapazarı Strong Ground Motion Record

The strong ground motion station is located with Bayındırlık complex on a rock/stiff soil site in Adapazarı. The acceleration characteristics of the record are given in Fig (3.9).



Fig(3.9) Sakarya(1999) acceleration record.

The duration of Sakarya(1999) earthquake was approximately 120 sec. which was very long for the analysis from run time point of view. Due to the runtime limitations, energy based approximation was implemented on Sakarya (1999) earthquake record which aims to eliminate the parts that don't contribute to the cumulative energy significantly.

The Arias Intensity relationship stated in Eq(3.6) was used to estimate energy accumulation characteristics of Sakarya record. The final curve was drawn in Fig (3.10).

$$I_a = \frac{\pi}{2 \cdot g} \cdot \int_0^{\infty} [a(t)]^2 \cdot dt \quad (3.6)$$

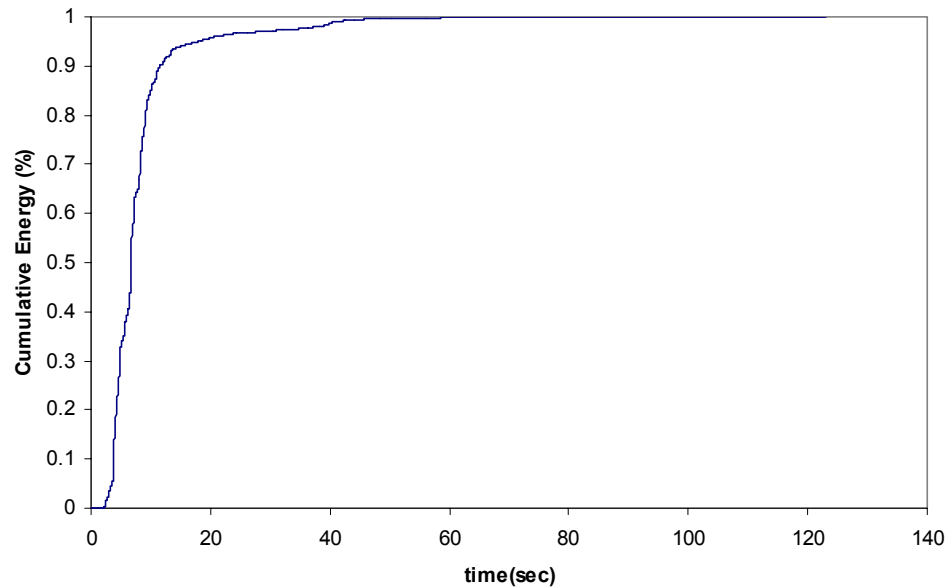


Fig 3.10 Arias Intensity graph of Sakarya(1999) earthquake.

It is observed from the Fig(3.10) that 91% of the seismic energy of the Sakarya (1999) record arrived between the period (2-13 sec). To eliminate long run times only first eleven seconds of the Sakarya record will be used for the analyses.

The response spectrum and power spectrum given in Appendix A also show the important characteristics of the Sakarya(1999) earthquake .

3.5 Properties of Finn Model Parameters

The basic theory of the Finn Model was introduced in Chapter 2. In this section the parameters related to the site in Adapazarı are obtained. Recall that Martin's formula needs the determination of the 4 constants D1, D2, D3, and D4; on the other hand Byrne needs only 2 constants B1 and B2.

For the determination of D1, D2, D3 and D4 first the Byrne constants are constructed for the $N_{60} = 5$, which is representative for the top layer of our site in Adapazarı. After the construction of Byrne curves, D1, D2, D3, D4 constants of Martin's formula are found by comparing the estimated

Martin's curves using the Byrne's curves. Fig (4.12) and (4.13) are the Byrne and Martin curves respectively.

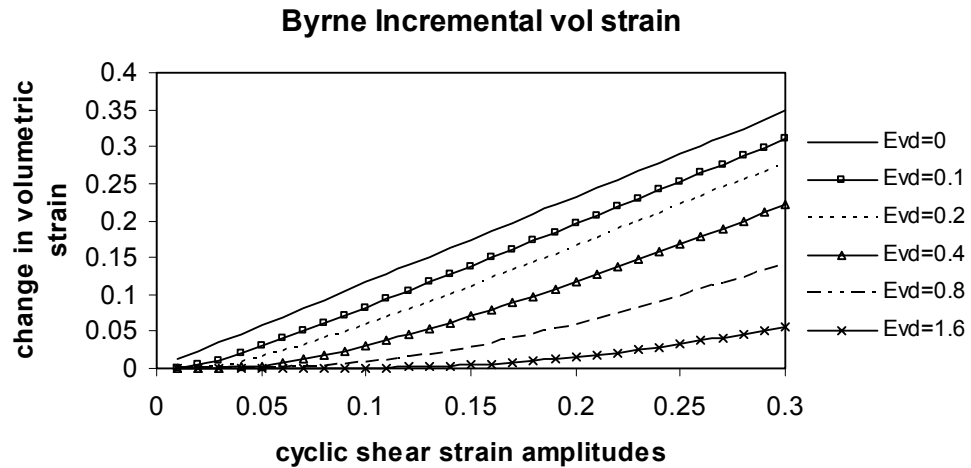


Fig 3.11 Byrne $\Delta\varepsilon_{vd}$ vs γ curves given the ε_{vd} is constant.

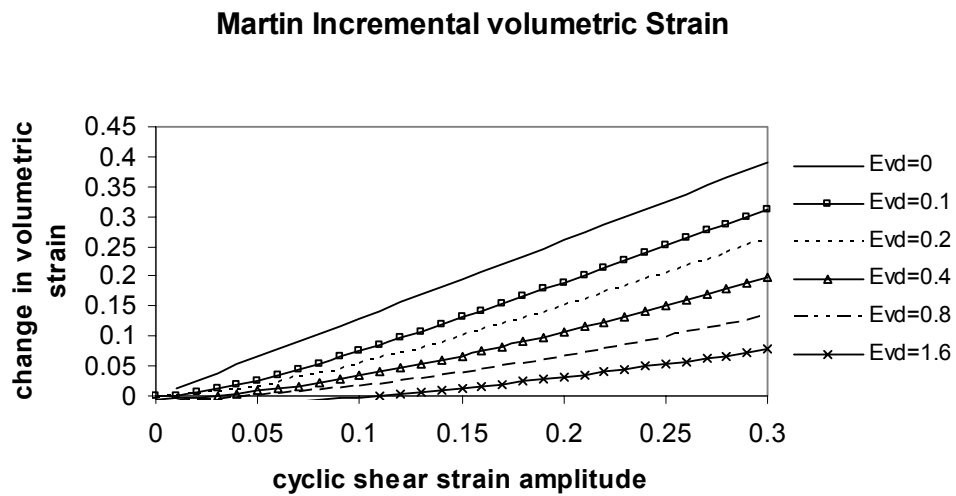


Fig 3.12 Martin $\Delta\varepsilon_{vd}$ vs γ curves given the ε_{vd} is constant.

It can be seen from the graphs that for a cyclic shear strain, γ , change in volumetric strain, ($\Delta\varepsilon_{vd}$), decreases with the increasing

cumulative volumetric strain, (ϵ_{vd}), as stated in Martin (1976). The Byrne and Martin constants are summarized in Table (4.2).

Table 3.4 Martin and Byrne constants

Martin Constants		Byrne Constants	
D1	1.3	B1	1.16
D2	0.75	B2	0.34
D3	0.77		
D4	0.8	N ₆₀	5

Finally, the resultant constitutive models are applied to the soil layers for the dynamic analysis.

Table 3.5 Constitutive models used in dynamic analysis

Soil Layers	Model
Silty Clay	<i>Mohr-Finn</i>
Silty Sand	<i>elastic</i>
Clay	<i>elastic</i>

CHAPTER 4

3D- MESH GENERATION OF THE 3 BUILDINGS IN ADAPAZARI

4.1 Damping phenomena

The dynamic analyses for the purpose of seismic response assessment of 3 buildings in Adapazari were performed by the computer program Flac3D. Flac3D is based on the explicit finite difference scheme and solves the full equations of motion using lumped grid point masses derived from the real density of surrounding zones. The Flac3D formulation can also be coupled to the structural element model thus permitting analysis of dynamic soil-structure interaction using nonlinear method.

For the case of 3 buildings in Adapazari, the standard Mohr-Coulomb plasticity model can produce curves of apparent damping and modulus versus cyclic strain. The formulation is given below.

Below the yield, the secant shear modulus G is equal to G_0 (constant shear modulus). Given the cyclic shear strain, γ , and the constant yield stress, τ_m , secant modulus is

$$G = \frac{\tau_m}{\gamma} \quad (4.1)$$

The maximum stored energy, W , during the cycle is

$$W = \frac{\tau_m \cdot \gamma}{2} \quad (4.2)$$

and the dissipated energy is

$$\Delta W = 4 \cdot \tau_m \cdot (\gamma - \gamma_m) \quad (4.3)$$

where $\gamma_m = \tau_m / G_0$.

Denoting the damping ratio D and noting that $4\pi D \approx \Delta W / W$ for small D , Eq(4.4) can be written by using the Eq(4.2) and (4.3).

$$D = \frac{2 \cdot (\gamma - \gamma_m)}{\pi \cdot \gamma} \quad (4.4)$$

The normalized modulus (G/G_0) and damping ratio, D , versus normalized cyclic strain, γ/γ_m , can be plotted as shown in Fig (4.1).

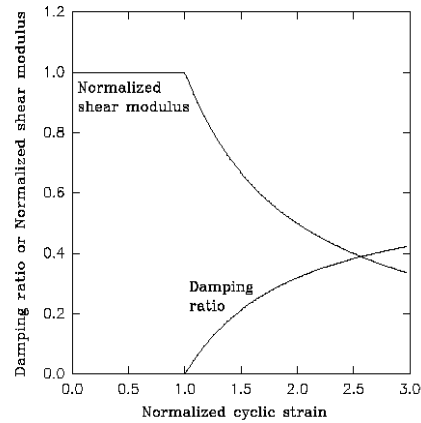


Fig 4.1 Modulus and damping ratio versus cyclic strain for elastic/plastic model

Thus, if the constitutive model used in the analysis contains an adequate representation of the hysteresis that occurs in real material, then no additional damping would be necessary.

The discussion now will go on with the construction of Input Ground Motion specific to the site.

4.2 Input Ground Motion Characteristics

The determination of the model input ground motion representing the real site motion was a critical task for our analyses. For the appropriate use of the rock record of Sakarya(1999) earthquake in the case of 3 buildings in Şahinler street, the record needed to be modified to take into account the soil site-specific effects. To do so, the Sakarya(1999) record was assigned as outcrop on the bedrock to the computer program Shake91 and the output was taken within the top of the clay layer of Shake91 model. Fig (4.2) summarizes the soil profile and some selected parameters used for Shake 91 runs.

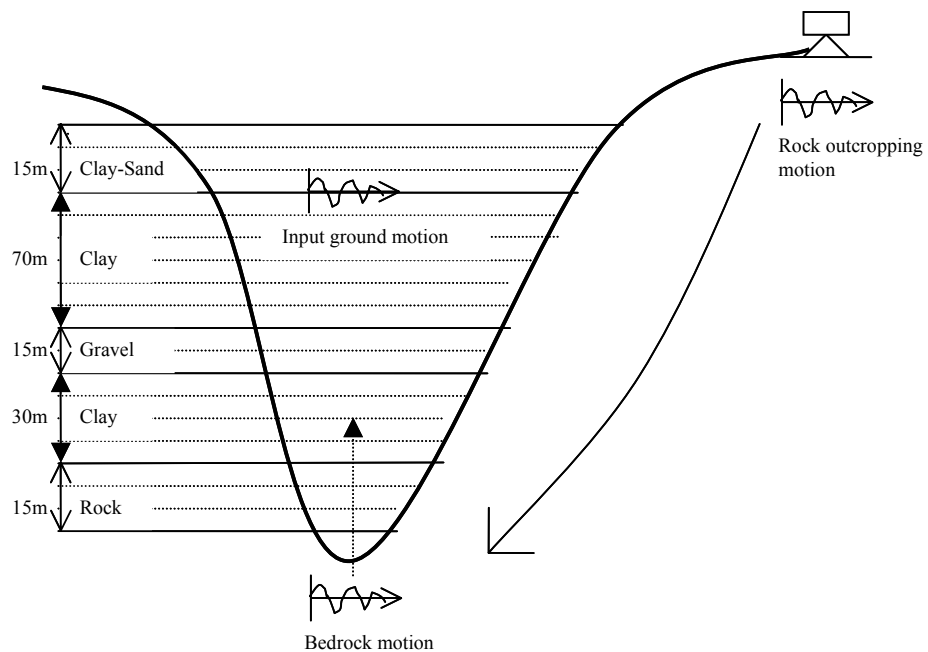


Fig 4.2 Construction of the model input motion.

The Shake91 model consisted of 17 layers, with basically 5 soil type, starting with the surface and ending at 150m depth. The model was constructed so that while going to the deeper portions of the site the shear

wave velocities were gradually increased and also appropriate modulus and damping curves were applied to the soil layers. The Shake91 input can be found in Appendix C. A summary of soil profiles and parameters is presented in Table (4.1).

Table 4.1 Shake 91 input soil profile data

Layer NO.	Type	Thickness(m)	Depth(m)	G(kPa)	Vs(m/s)
1	clay	4.5	2.25	6.704	100
2	sand	4.5	6.75	22.556	183.333
3	clay	4.5	11.25	11.926	133.333
4	clay	15	21	26.859	200
5	clay	15	36	41.959	250
6	clay	15	51	60.422	300
7	clay	15	66	74.582	333.333
8	clay	15	81	90.246	366.667
9	gravel	3	90	224.937	566.667
10	gravel	6	94.5	446.449	798.333
11	gravel	6	100.5	446.449	798.333
12	clay	6	106.5	215.560	566.667
13	clay	9	114	141.646	459.333
14	clay	15	126	141.646	459.333
15	clay	9	138	141.646	459.333
16	rock	4.92	144.96	311.341	666.667
17	Base	Base	Base	729.699	1000

Shake91 acceleration vs. depth data output taken at a depth of 15m. is presented in Fig (4.3).

Shake91 Output

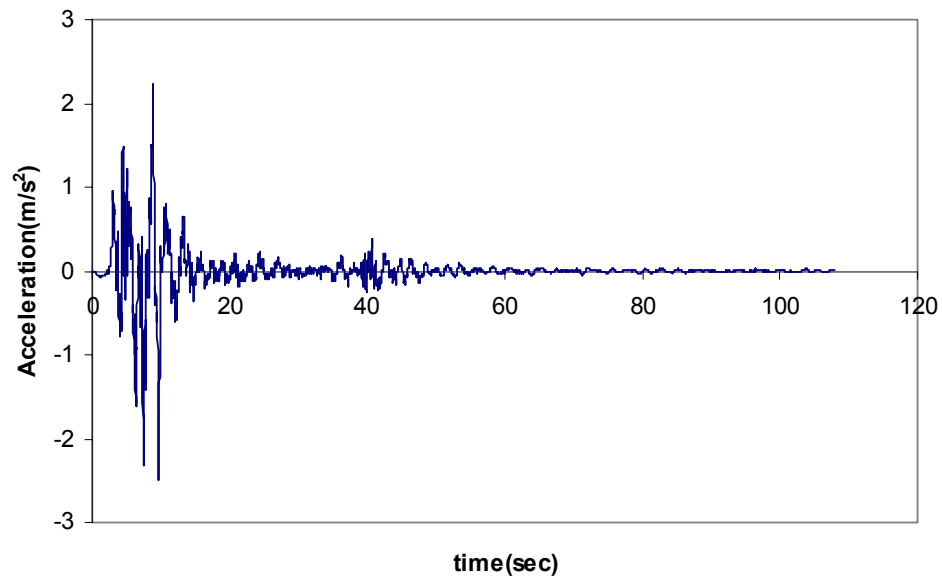


Fig 4.3 Acceleration vs time data taken at a depth of 15m after 10Hz and higher frequency components filtered. ($a_{\max} = 0.25g$)

The output taken from the Shake91 would be used as the input ground motion in the case of 3 buildings in Adapazarı but due to the runtime and mesh inefficiencies, the high frequency (10 Hz and higher) components were filtered out and only the acceleration record between 2.28 to 13.01 seconds was taken into account based on the Arias Intensity discussion (see Chp3). The final input ground motion was obtained as shown in Figures 4.4 to 4.6. Details of “why high frequency components were filtered” will be discussed in section 4.3.

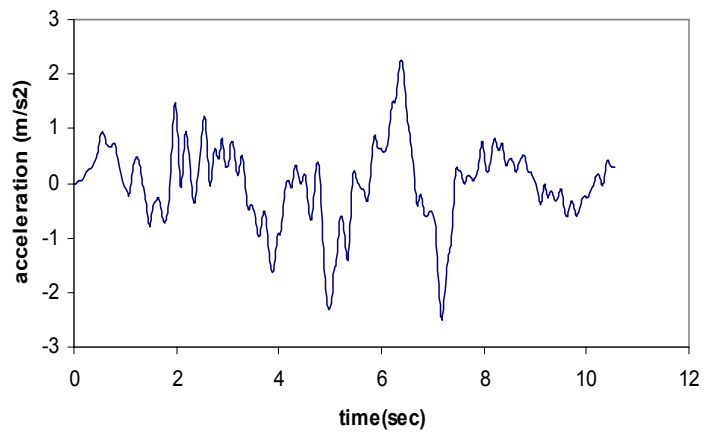


Fig 4.4 Acceleration Input ground motion

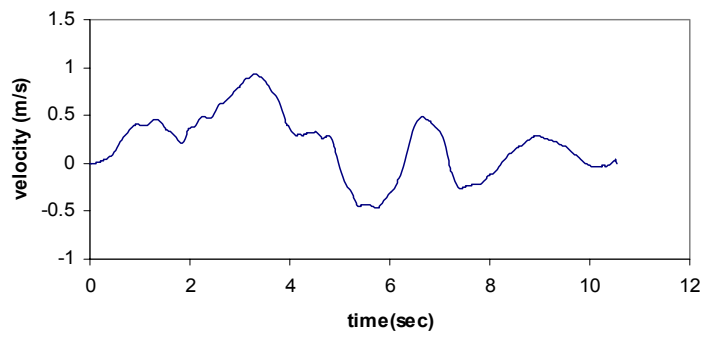


Fig 4.5 Velocity form of Input ground motion

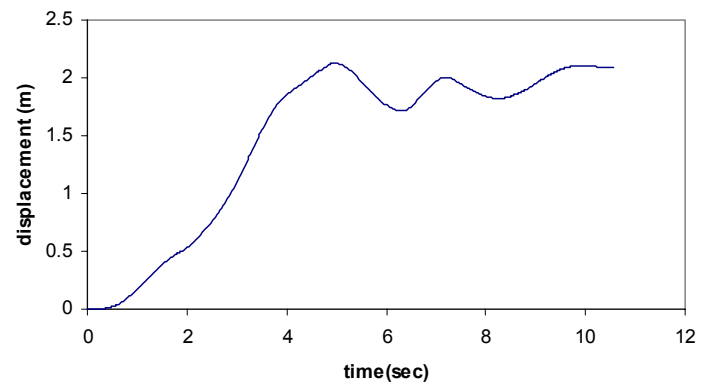


Fig 4.6 displacement form of Input ground motion

4.3 Preparation of Soil and Structural Mesh

Preparation of the soil mesh is an important step in this study. Tens of mesh models were tried to get consistent results. The results forced us to use uniform mesh for dynamic simulations. In Fig(4.6), the final mesh configuration of the soil is given.

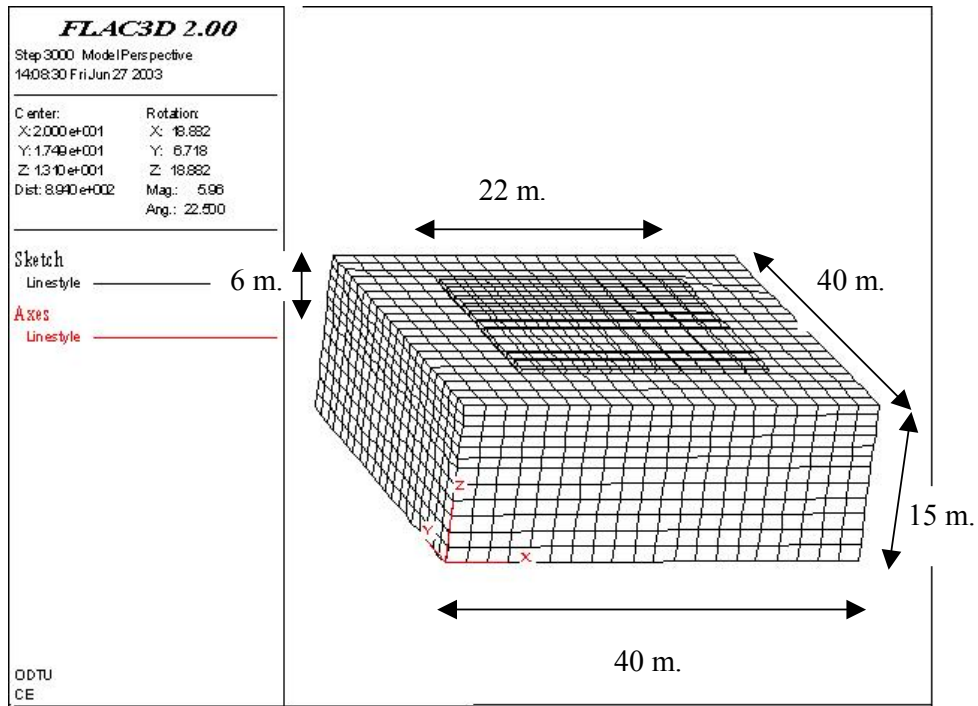


Fig 4.7 Soil Mesh under the building

The site dimensions for each building are (40m×40m×15m) and (20×20×12) mesh points are used. The mesh generation of z axes is important since the input motion waves propagate on that axes. By considering the estimated V_s of the soil layers, top 6m of the soil is modeled by using 1m mesh elements, while the rest was modeled with 2m mesh element in z axes. The discussion of implementing different element sizes in the mesh generation will be explained in the following pages.

4.3.1 Wave transmission

Numerical distortion of the propagating wave can occur in dynamic analysis as a result of poor modeling. Both the frequency content of the input wave and the wave speed characteristics of the system affect the numerical accuracy of the wave transmission. It was shown that for accurate representation of wave transmission through a model, the spatial element size, (Δl), must be smaller than approximately one-tenth to one-eighth of the wavelength associated with the highest frequency of the component of the input wave. (Lysmer et al. (1969))

$$\Delta l \leq \frac{\lambda}{10} \quad (4.5)$$

where λ is the wavelength associated with the highest frequency component that contains appreciable energy .

The equation which relates λ to the frequency component is given below.

$$f = \frac{V_s}{\lambda} \quad (4.6)$$

where V_s is the shear wave velocity in the soil.

By combining the Eq(4.5) and (4.6), Eq(4.7) can be written.

$$f = \frac{V_s}{10 \cdot \Delta l} \quad (4.7)$$

For the soil site in Adapazarı, the largest element dimension for the model can be estimated by using Eq(4.7) Recall that V_s for the top layer is equal to 100m/sec. The input motion used for the analysis has the maximum frequency component, f , 10Hz. Then maximum Δl must be 1m for the top soil layer to allow waves propagate accurately in the vertical direction. In fact 1m mesh element is used while constructing the model. For modeling the effects of earthquake shaking with frequencies higher than 10 Hz, the use of smaller elements for the accurate wave propagation is needed. The optimum mesh size for the deeper soil layers can be calculated in a similar way.

4.3.2 Mesh Characteristics of the Site

This section continues with the construction of 3D modeling in Flac3D. Since Flac3D is 3 dimensional explicit finite difference program, 3D model of the Adapazarı site can be constructed on Flac3D considering the 2D crossections presented in Chapter3. The figures (4.8), (4.9) and (4.10) show the estimated soil layers.

The soil layers with the red color represent the soil type of clay, silty clay to clayey silt, green color represents the silty sand to sandy silt and the blue color at the bottom represent the clay and silts. The yellow one at the top is the stiff soil layer which represents the foundation whose dimensions are (22m×22m×0.5m).

Table 4.2 is the summary of the mesh properties for each building.

Table 4.2 Mesh Properties

Site Properties
Mesh Length=40m.
Mesh Width=40m.
Mesh Heigth=15m.
Water Table=1.4m
3 layers and a mat foundation

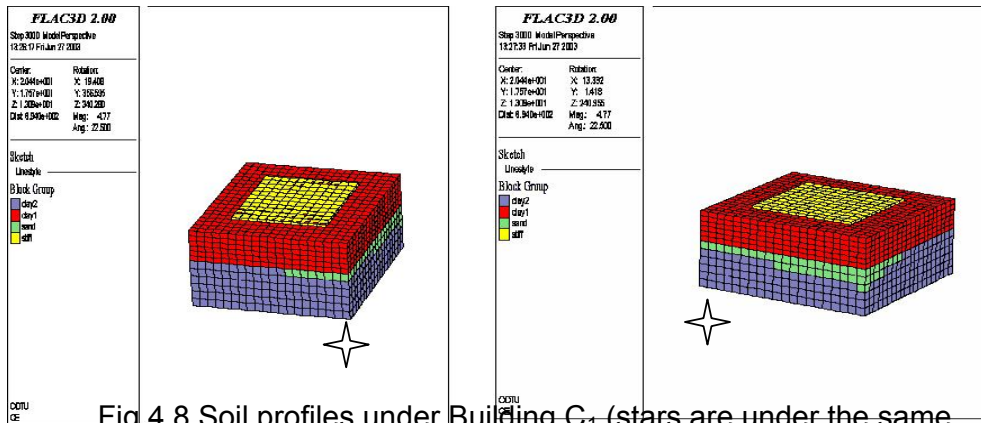


Fig 4.8 Soil profiles under Building C₁ (stars are under the same point i.e: mesh is rotated)

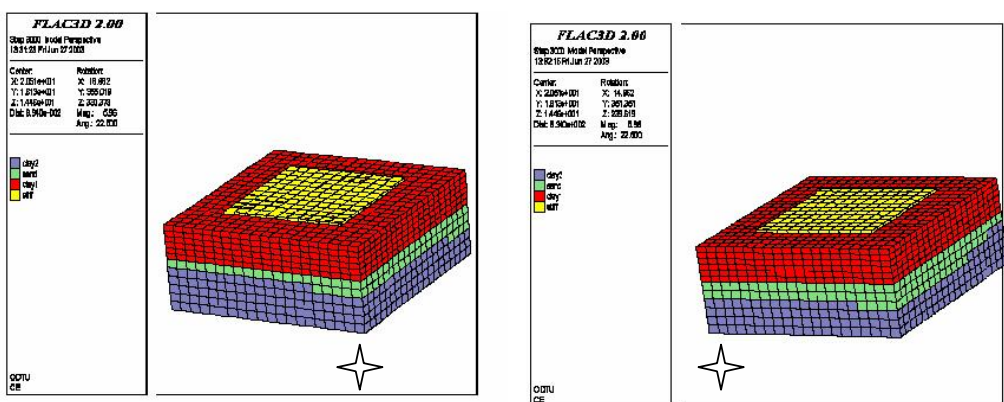


Fig 4.9 Soil profiles under Building C₂ (stars are under the same point. i.e: mesh is rotated)

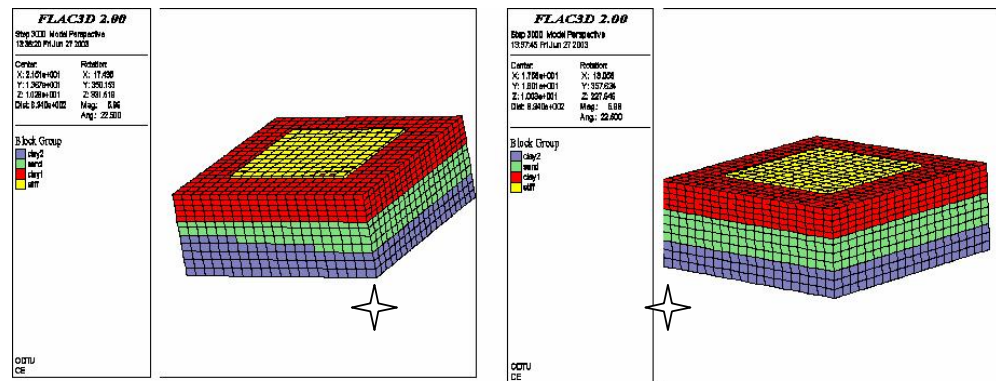


Fig 4.10 Soil profiles under Building C₃ (stars are under the same point. i.e: mesh is rotated)

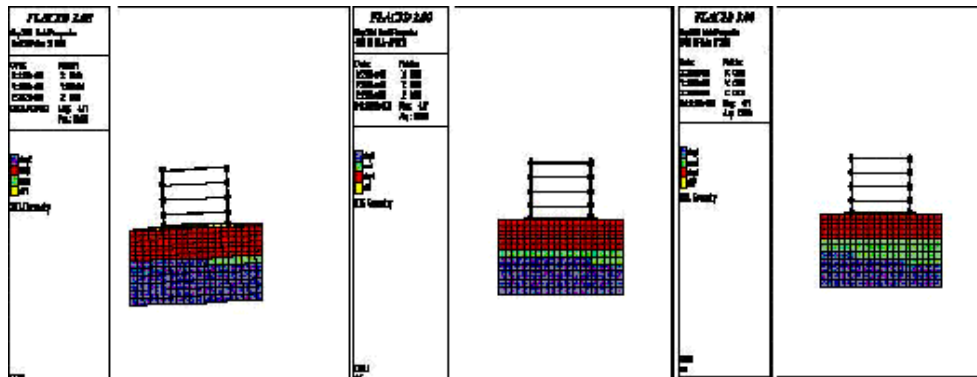


Fig 4.11 Cross Sectional view of the 3 buildings, C₁ on the left, C₂ at the middle, C₃ on the right

CHAPTER 5

DISCUSSION OF NUMERICAL ANALYSES RESULTS

5.1 Introduction

After having performed the static analysis to achieve the static force equilibrium in the site, our analyses continued with the dynamic studies using the Mohr-Coulomb and Finn constitutive models representing the soil behaviour properly. In this chapter, the results of 3-D dynamic numerical analyses in the forms of i) acceleration, ii) displacement, iii) strain, iv) stress and v) pore pressure will be presented.

5.2 The distribution of shaking intensity under the buildings

The distribution of maximum acceleration values were estimated under each building. Points 2,3,4 and 5 in Figure 5.1 are located under building columns whereas point 1 is the free field control point which is not subject to the shaking of the buildings. Planview of 5 points are shown in Figure 5.1.

The variation of maximum acceleration with depth at these 5 points are shown in Figures 5.2(a) through 5.2(c).

As shown on these figures, the collapsed building C_1 was shaken by a greater maximum acceleration ($\sim 0.30g$) than no damage building C_3 ($\sim 0.25g$). The main reason for the C_1 building shaken by higher acceleration values is that the silty clay soil layer that amplified the acceleration is thicker under building C_1 compared to building C_3 . Relatively stiffer soil layer under the building C_3 is significantly thicker. This has a great influence on deamplifying the acceleration of the site under C_3 .

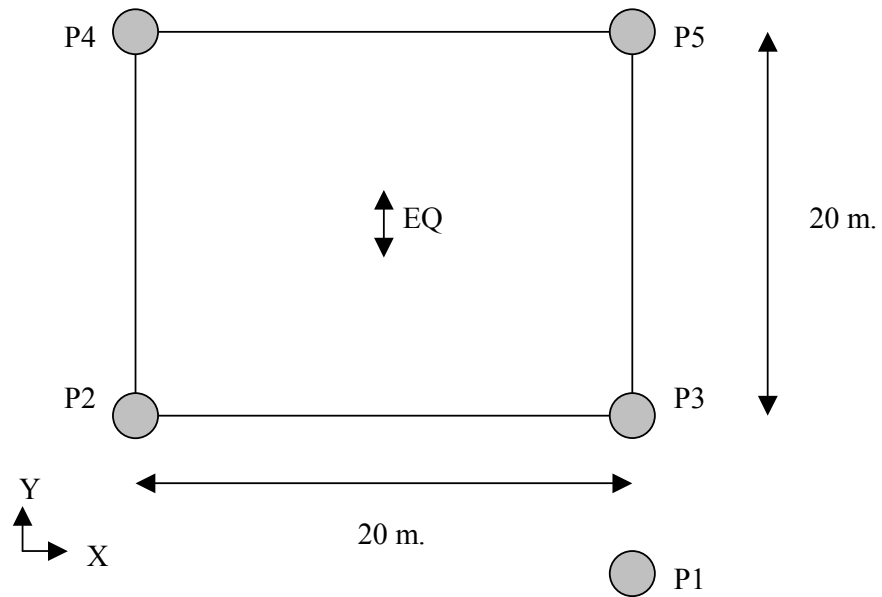


Fig 5.1 Schematic view of P2,3,4,5 under the columns and P1 at the free field.

5.3 Results of displacement analysis

Both vertical and horizontal displacements were estimated as parts of the numerical analyses.

Figures 5.3(a), through 5.3(c) show maximum vertical displacements estimated during earthquake shaking. Positive vertical (z) displacements indicate upward (against gravity) displacement whereas the negative (z) displacements are downward (settlement) values. It can be seen on Figures 5.3(a), through 5.3(c) that a relative displacement of approximately 5, 4 cm and 3 cm were calculated for the Buildings C_1 , C_2 and C_3 respectively. At the free field, 6 cm upward movement was estimated.

Maximum horizontal displacements shown in Figures 5.4(a) through 5.4(c) can also give information about the translation of the buildings. The

horizontal displacements for the Buildings C₁, C₂ and C₃ are estimated as 4cm, 2cm and 1cm respectively.

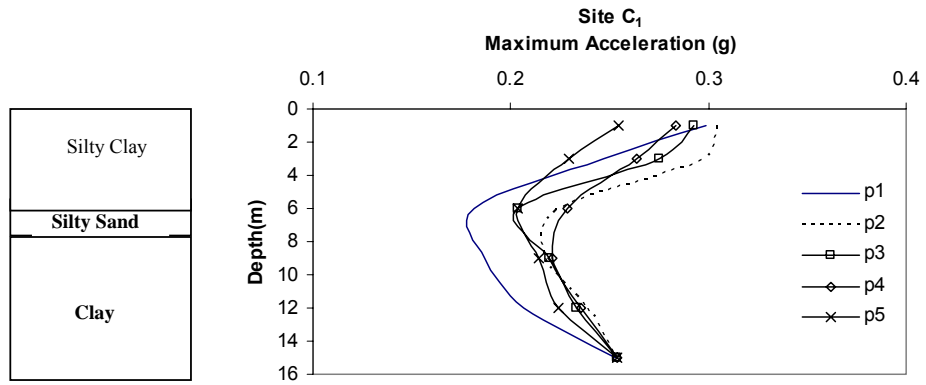
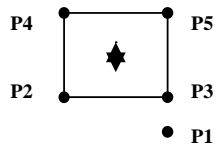


Fig 5.2(a) Maximum Acceleration vs depth at Building C₁

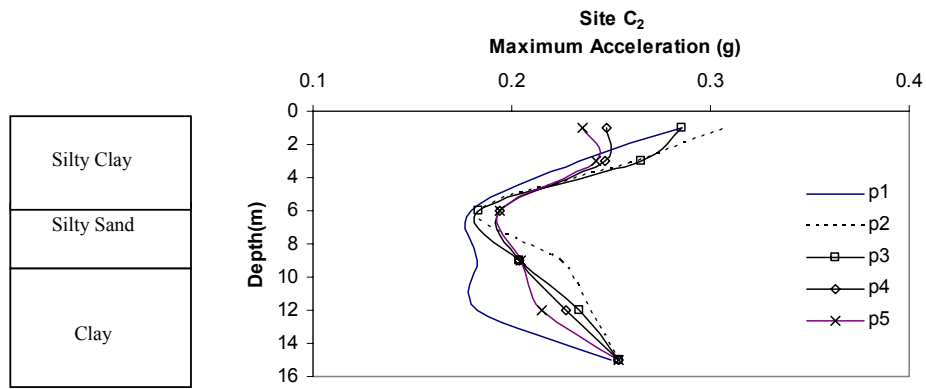


Fig 5.2(b) Maximum Acceleration vs depth at Building C₂

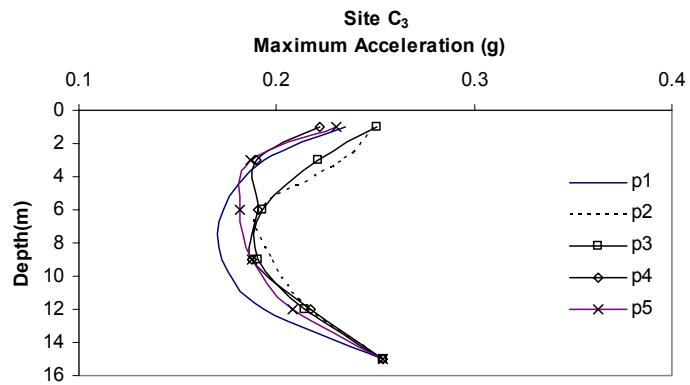
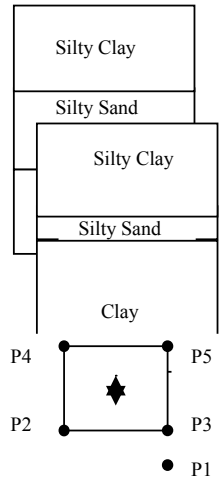


Fig 5.2(c) Maximum Acceleration vs depth at Building C₃

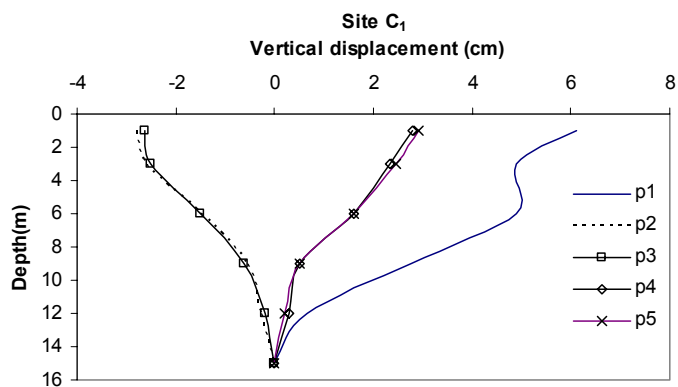


Fig 5.3(a) Maximum Vertical displacement vs depth at Building C₁

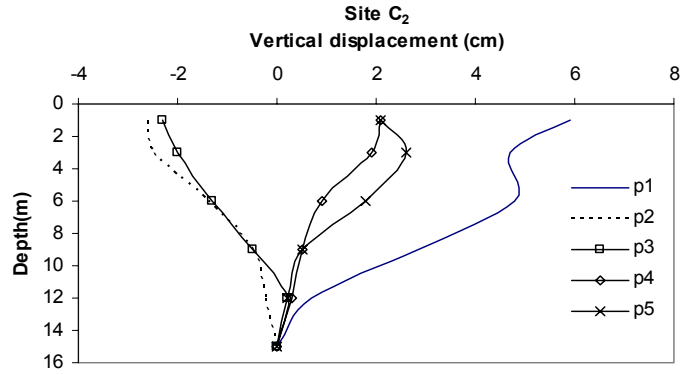


Fig 5.3(b) Maximum Vertical displacement vs depth at Building C₂

Silty Clay
Silty Sand
Clay

Silty Clay
Silty Sand
Clay

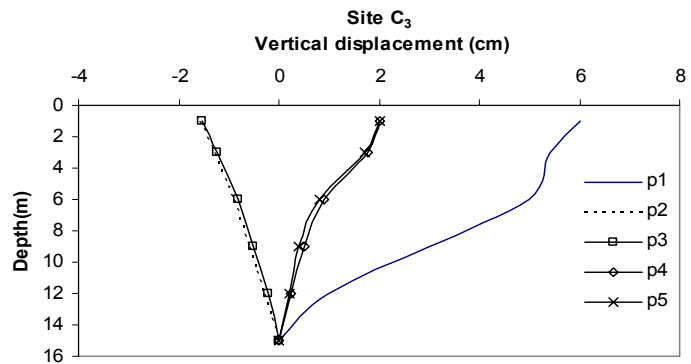


Fig 5.3(c)

Maximum Vertical displacement vs depth at Building C₃

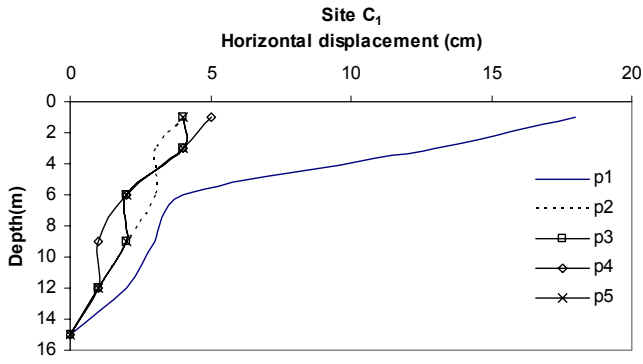
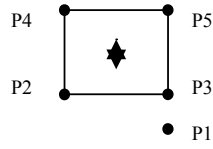


Fig5.4(a) Maximum Horizontal displacement vs depth at C₁

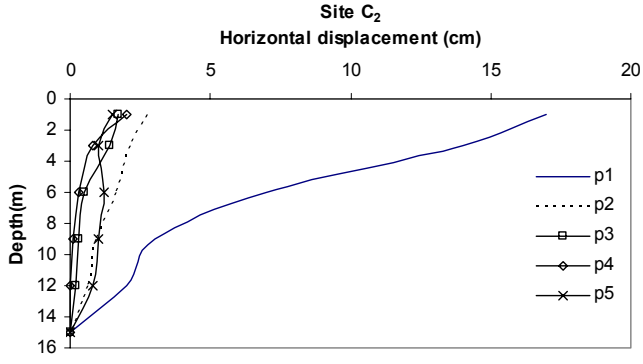


Fig5.4(b) Maximum Horizontal displacement vs depth at C₂

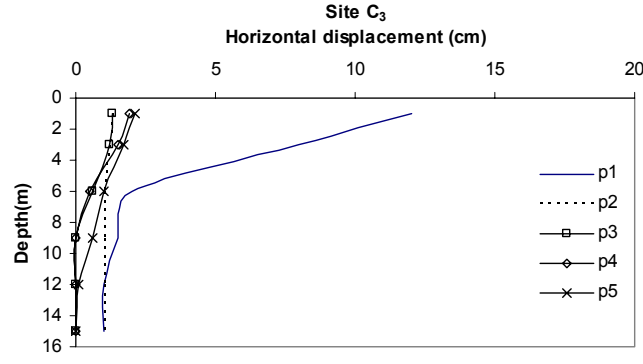


Fig 5.4(c) Maximum Horizontal displacement vs depth at C₃

5.4 The distribution of maximum stress, strain and pore pressures under the buildings

Vertical and shear stresses as well as strain and pore pressure distributions under each building will be discussed next.

As shown in Figures 5.5(a) through 5.5(c), there is a linear increase as expected in the vertical stress, σ_{zz} , with depth for the 3 buildings. Vertical stress is 100kPa at the foundation level and increases to 400 kPa at about 16 m. depth.

Similarly as shown in Figures 5.6(a) through 5.6(c), the shear stresses, (τ), are estimated as in the range of 100-130 kPa at 16 m. depth and 40-60 at the foundation level.

The analysis of shear strain histories presented in Figures 5.7(a) through 5.7(c) show that there is plastic yielding at various depths which increased horizontal displacements. As a similar observation it can be stated that shear strains are higher for the building C_1 ($\gamma \sim 3\%$) to buildings C_2 and C_3 ($\gamma \sim 2.5\%$). Especially the shear strain values for the building C_3 , which performed satisfactorily during earthquake are smaller than the ones under building C_1 .

As shown in Figures 5.8(a) through 5.8(c) there is a gradual increase in pore pressure with depth for each of the 3 buildings. The maximum pore pressure values are higher under the buildings than that in the free field. Higher pore pressure values are believed to be due to soil structure interaction. The values of pore pressure starts with 110kPa at 2m depth and ends with 180kPa at 4.5m depth. These high pore pressures indicate a potential liquefaction problem which will be analyzed next.

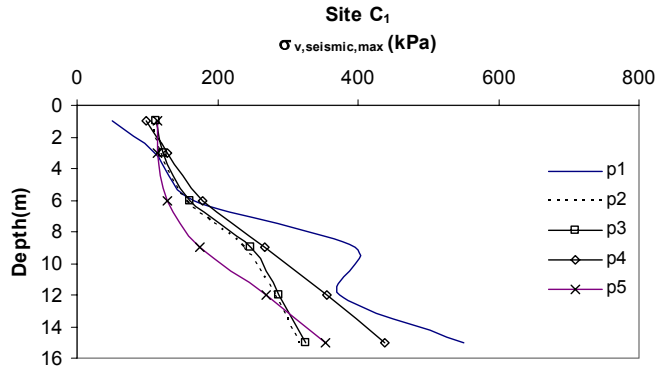
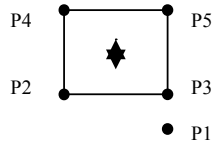


Fig 5.5(a) Maximum vertical stress vs depth at C₁

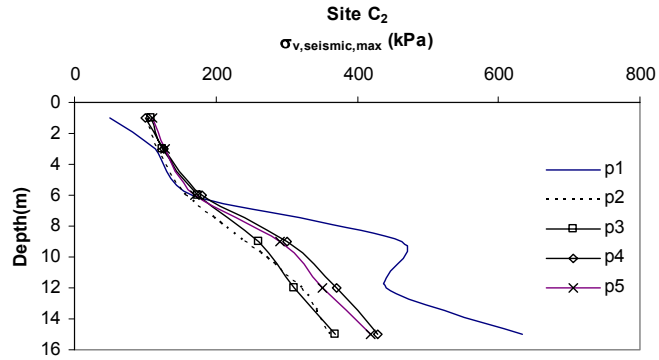


Fig 5.5(b) Maximum vertical stress vs depth at C₂

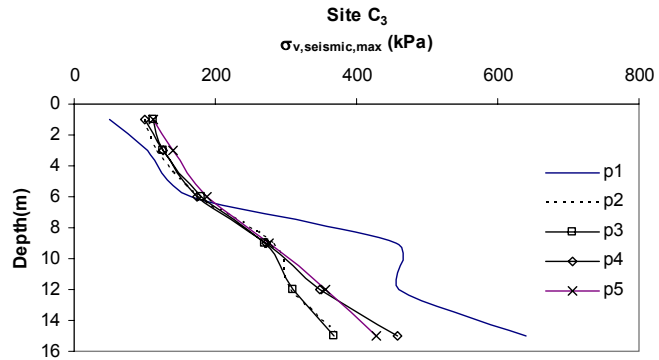


Fig 5.5(c) Maximum vertical stress vs depth at C₃

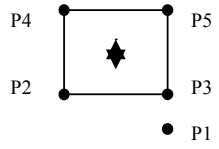
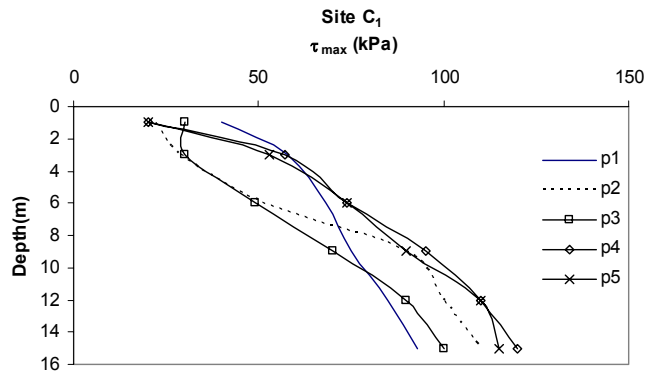


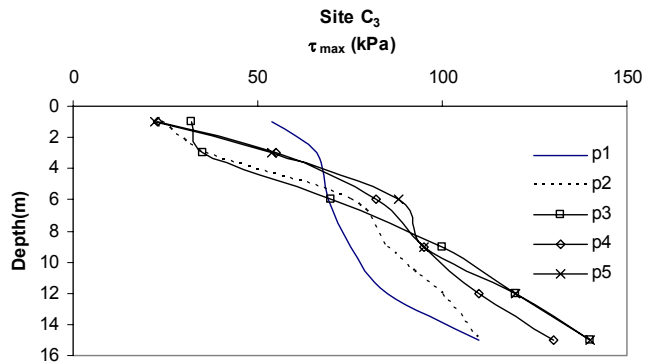
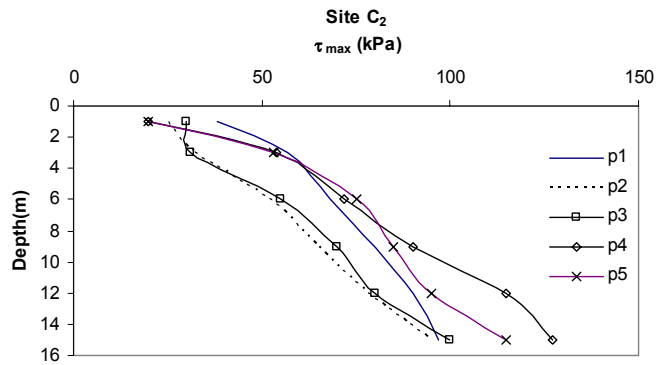
Fig 5.6(a)



Maximum shear stress vs depth at C₁



Fig 5.6(b)
 Maximum shear stress vs depth at C₂



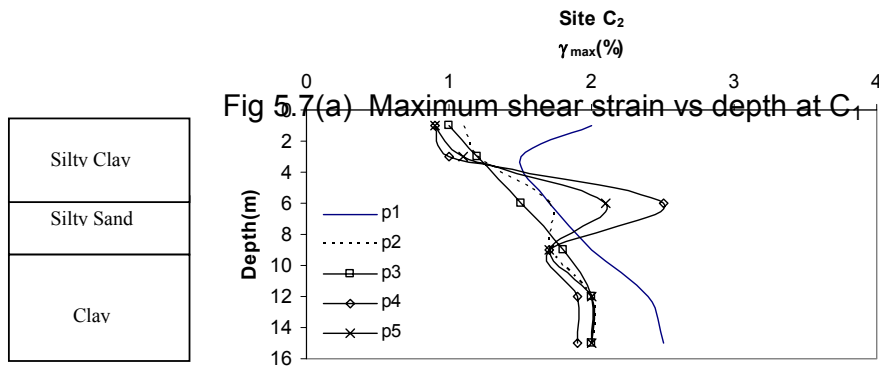
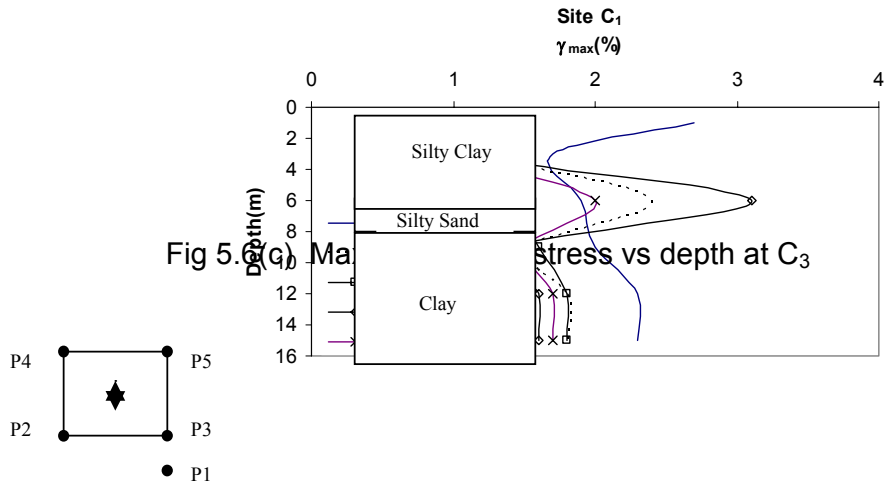


Fig 5.7(b)

Maximum shear strain vs depth at C₂

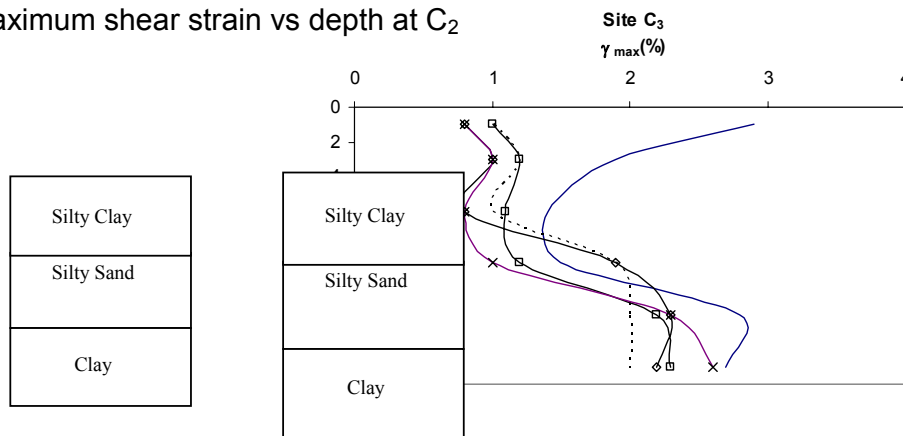


Fig 5.7(c) Maximum shear strain vs depth at C₃

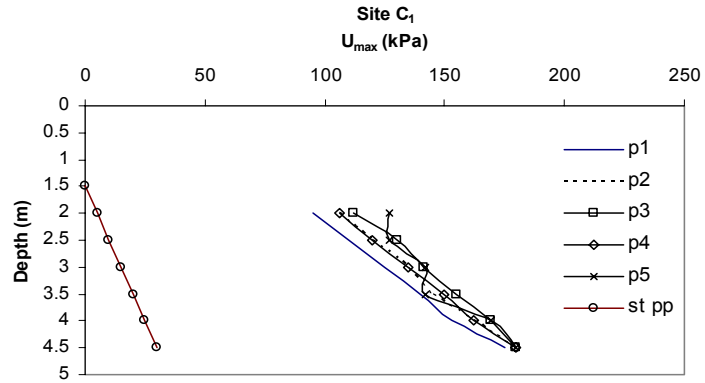
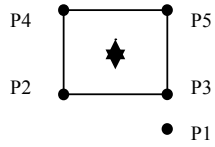


Fig5.8(a) Maximum pore pressure(kPa) vs depth at C₁

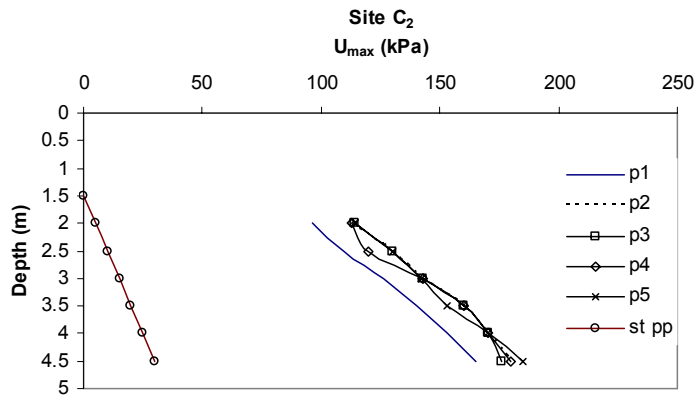


Fig 5.8(b) Maximum pore pressure(kPa) vs depth at C₂

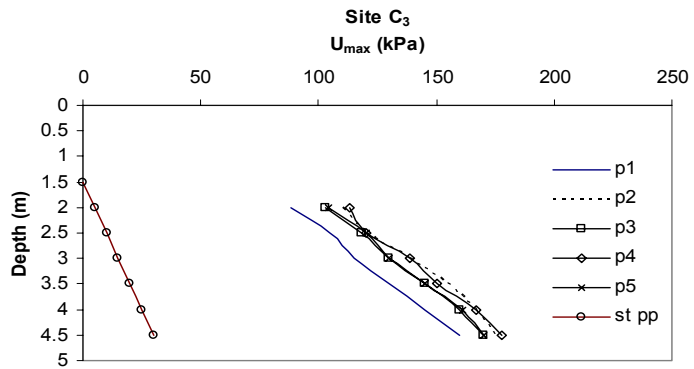


Fig 5.8(c) Maximum pore pressure(kPa) vs depth at C₃

5.5 Liquefaction Triggering Assessment

“Simplified Procedure” as suggested by Seed and Idriss (1971) was implemented for the purpose of estimating normalized shear stresses (CSR) developed within soil profiles during shaking. CSR as defined by Seed and Idriss (1971) was estimated as given in Eqn (5.1).

$$CSR_{\alpha} = 0.65 \cdot \frac{\tau_{\max}}{\sigma'_v} \quad (5.1)$$

where τ_{\max} is the maximum shear stress developed during shaking and σ'_v is the vertical effective stress.

Vertical effective stresses were calculated as part of the static analyses and the results were shown in Figures 5.9(a) through 5.9(c).

τ_{\max} values were estimated as part of the dynamic analyses and were presented in Figures 5.6(a) through 5.6(c).

For the purpose of assessing liquefaction initiation risk, CSR_{α} should be corrected for initial shear stresses present under buildings before the earthquake shaking. The correction is known as K_{α} and applied to CSR_{α} as given in Eqn (5.2).

$$(CSR)_{\alpha=0} = (CSR)_{\alpha} \cdot K_{\alpha} \quad (5.2)$$

where K_{α} is the correction factor and is a function of α defined as the ratio of initial shear stresses to vertical effective stresses.

Initial (static) shear stresses present under buildings before shaking is presented in Figures 5.10(a) through 5.10(c). Similarly α values are presented in Figures 5.11(a) through 5.11(c). K_{α} correction as shown in Figure 5.11 is applied to CSR_{α} and $CSR_{\alpha=0}$ is estimated. The CSR values for the Building C_1 is 0.1 to 0.3. On the other hand these values change in between 0.1 and 0.4 for the Buildings C_2 and C_3 . The higher CSR values are due to the intermediate Silty Sand layer which is thicker under the buildings C_2 and C_3 . That layer has taken higher shear stresses during the earthquake which may be due to the fact that it is much more stiffer than the other two layers at the top and at the bottom. The CSR values in the

free field for the three buildings are slightly lower than the CSR values under the buildings.

By applying the probability of liquefaction formula recommended by Çetin et al (2000), liquefaction triggering probabilities were estimated as shown in Figures 5.14(a) through 5.14(c). The soft soil under the three Buildings have a tendency to liquefy. On the other hand P_L values decrease through the stiffer soil. The related figures show that the Liquefaction potential is higher under the collapsed Building C_1 than under the Buildings C_2 and C_3 which may be due to the fact that the soft soil under the building C_1 is thicker than the one under the Building C_2 and C_3 .

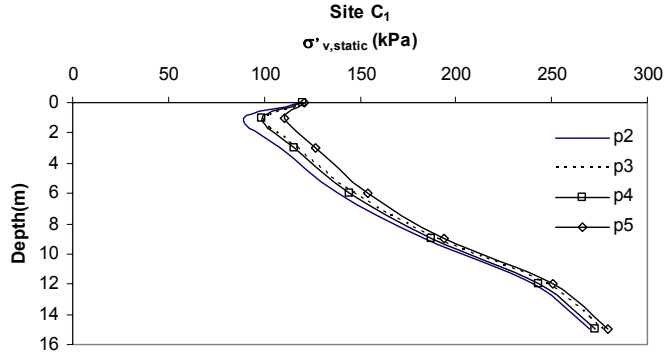
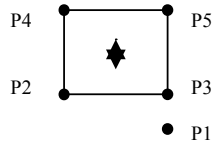


Fig 5.9(a) Vertical Effective stress vs depth at C₁

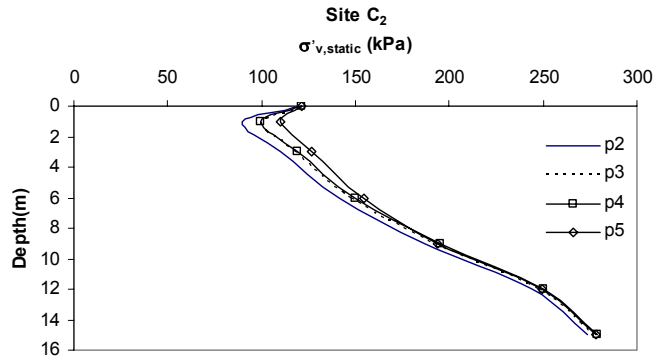


Fig 5.9(b) Vertical Effective stress vs depth at C₂

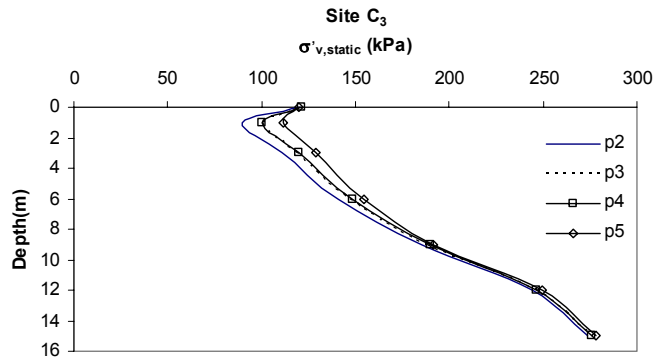


Fig 5.9(c) Vertical Effective stress vs depth at C₃

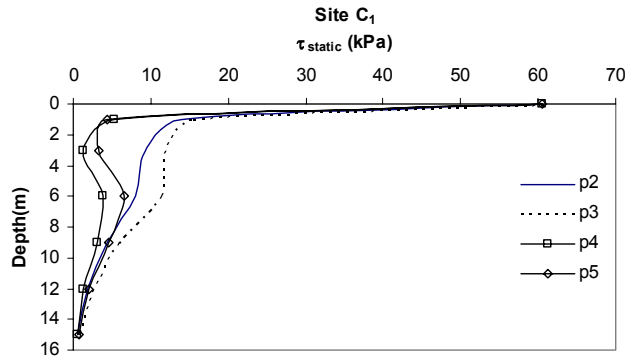
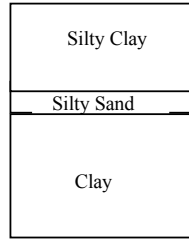
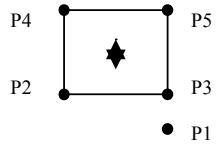


Fig 5.10(a) Static shear stress vs depth at C₁

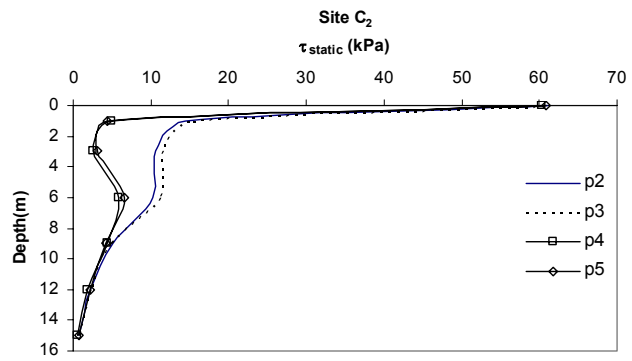


Fig 5.10(b) Static shear stress vs depth at C₂

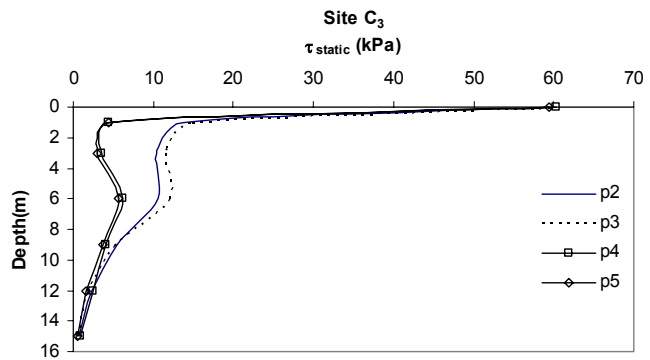


Fig 5.10(c) Static shear stress vs depth at C₃

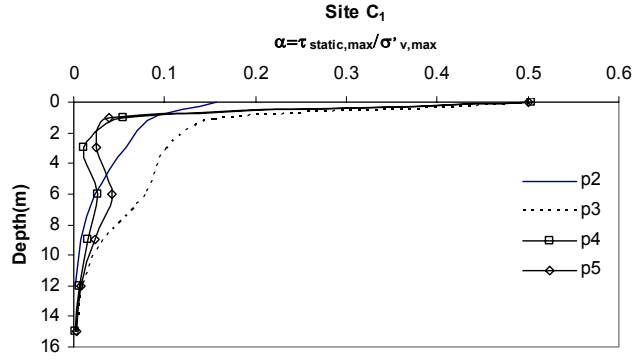
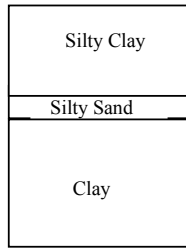
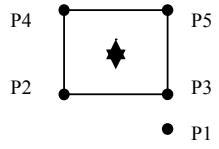


Fig 5.11(a) α vs depth at C₁

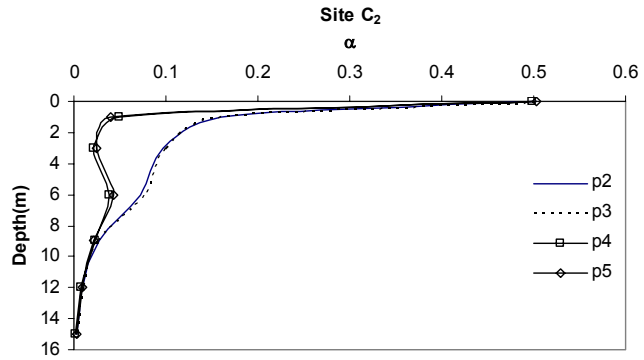


Fig 5.11(b) α vs depth at C₂

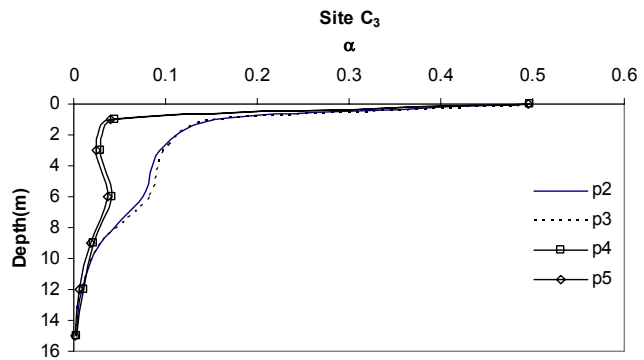


Fig 5.11(c) α vs depth at C₃

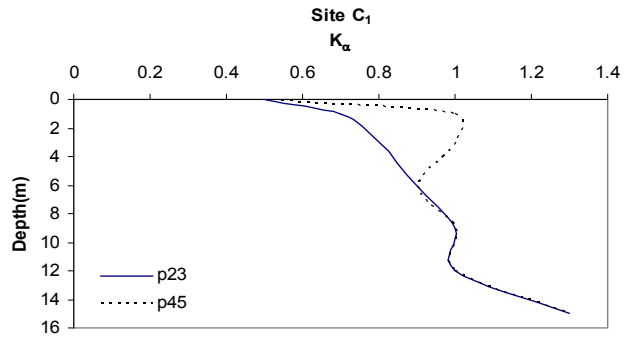
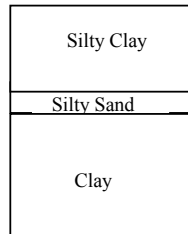
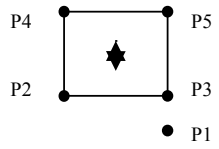


Fig 5.12(a) K_α vs depth at C₁

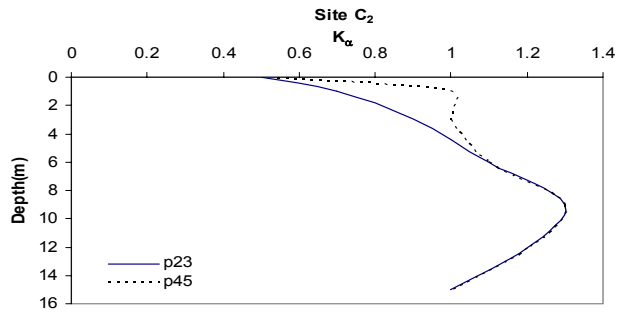


Fig 5.12(b) K_α vs depth at C₂

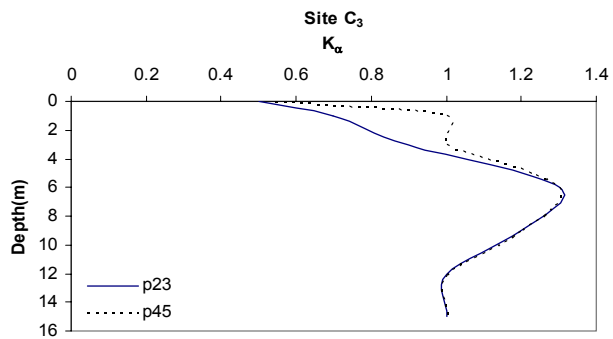


Fig 5.12(c) K_α vs depth at C₃

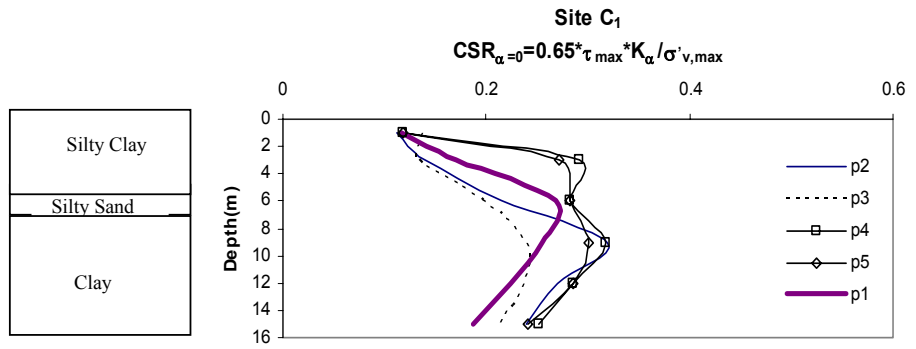
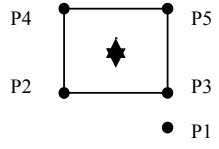


Fig 5.13(a) Cyclic Stress Ratio vs depth at C₁

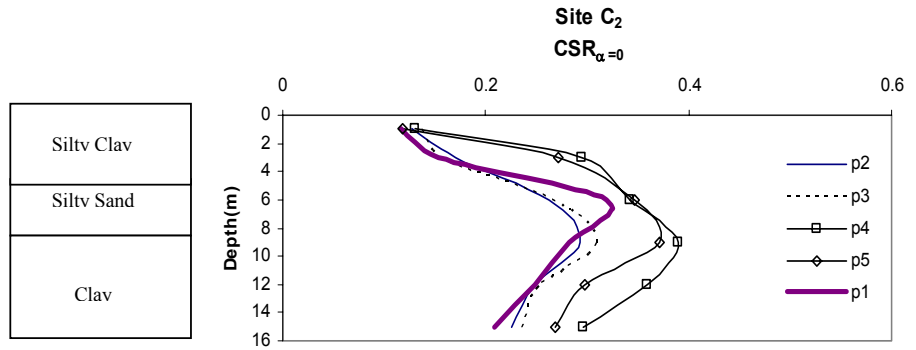


Fig 5.13(b) Cyclic Stress Ratio vs depth at C₂

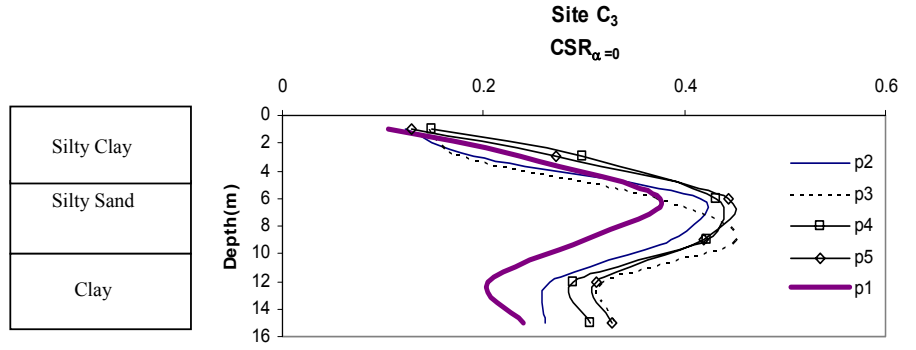


Fig 5.13(c) Cyclic Stress Ratio vs depth at C₃

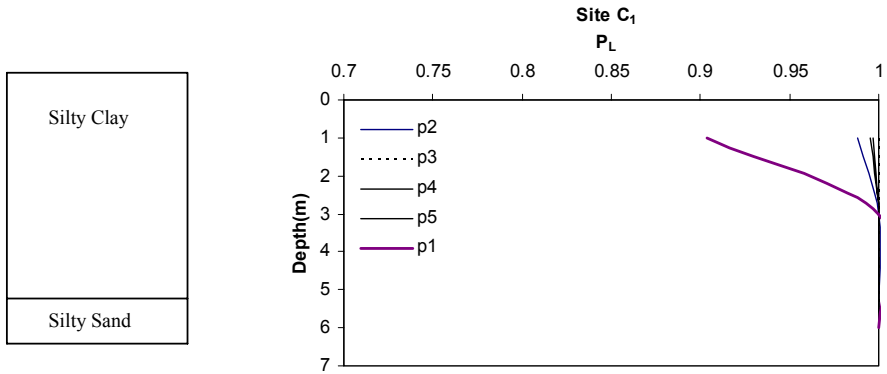
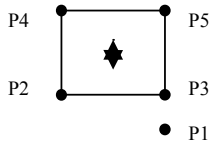


Fig 5.14(a) Probability of liquefaction vs depth at C₁

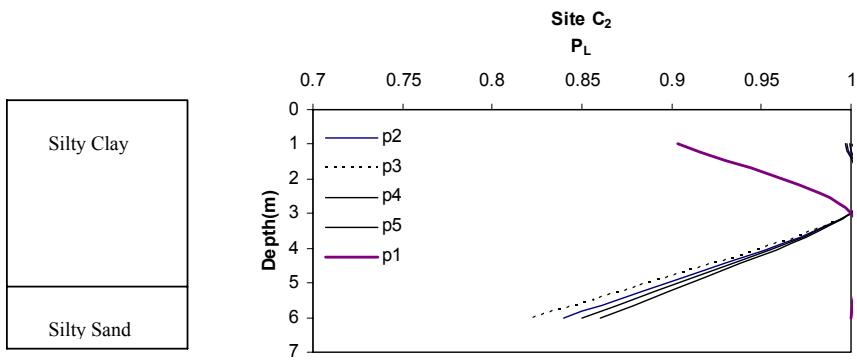


Fig 5.14(b) Probability of liquefaction vs depth at C₂

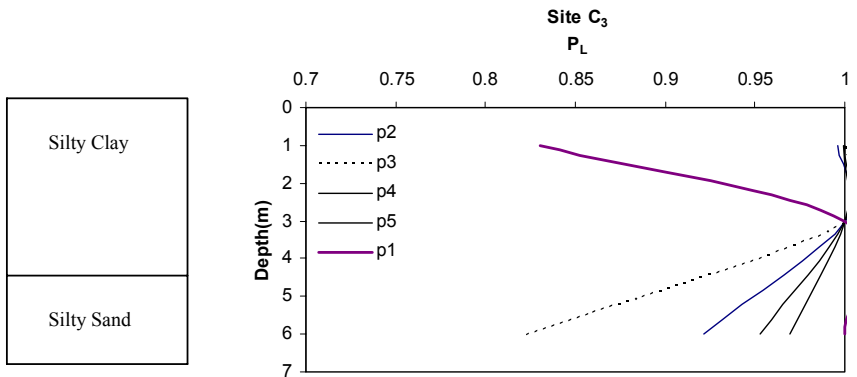


Fig 5.14(c) Probability of liquefaction vs depth at C₃

CHAPTER 6

SUMMARY AND CONCLUSION

6.1 Summary

The soil structure interaction at three neighbouring sites in Sakarya was analyzed to see the effects of foundation soils on the identical buildings. 2-D cross-sections of the site of estimated soil layers were constructed based on available SPT, CPT and Vs data. After determining the soil properties of these layers and the structural properties of the buildings, 3-D mesh models of the site were constructed.

First static analyses were performed. In static analysis, all the soil layers were considered to be elastic. The aim of performing static analysis was to obtain static force equilibrium which would be used in the dynamic analysis.

Secondly input ground motion was constructed. A site response analysis for 150 m. deep soil profile (representative soil profile at the site) was performed by Shake91. After obtaining the proper input ground motion and filtering for high frequency waves, the final input ground motion was obtained.

Finally the dynamic analysis was performed. Finn model parameters for the dynamic analysis were determined. Viscous boundary conditions were applied and the 3D dynamic nonlinear analysis of the site was done by using the computer program Flac3D.

The site of interest consisted of 3 buildings located on Şahinler street, for the sake of reducing run times the analyses were performed separately for each of the 3 buildings. When the Mohr-Coulomb failure criterion was implemented the run time for Flac3D dynamic analysis was

approximately 1.15 hours on a P-4 computer. Run time exceeded 3 hours when the Finn model was chosen to evaluate additionally the pore pressures.

6.2 Conclusion

As a result of our studies, following observations were made which could potentially explain different levels of structural damage at three identical neighbouring residential buildings in Sakarya.

i) Collapsed building C₁ was estimated to be shaken by a maximum acceleration of 0.30 g whereas moderately damaged and no damage buildings were estimated to be shaken by a maximum accelerations of 0.26 g and 0.24 g respectively. These different intensities of shaking could be potentially explained by the variation of the thickness of soft soil layer from 6.5 m. under C₁ to 4.5 m. under C₃.

ii) The maximum strains (~3%) for building C₁ during the earthquake were found to be higher than that of buildings C₂ (~2.5 %) and C₃ (~2 %). It is believed that high shear strain values may negatively affect the building performance during earthquake.

iii) A relative vertical displacement of approximately 5 cm, 4 cm. and 3 cm. are estimated for the Buildings C₁, C₂ and C₃ respectively. The horizontal displacements for the Buildings C₁, C₂ and C₃ are estimated as 4 cm, 2 cm and 1 cm respectively. The maximum displacement values for non settled building C₃ are smaller than that of the buildings C₁ and C₂ which were highly translated and settled during the earthquake. Even though calculated translational and vertical displacements are much smaller than in-situ values, they are believed to be a good indication of structural performance.

iv) Although the pore pressure values are similar for the 3 buildings, it can be concluded that the building C₁ is the one that was most affected due to the soil stiffness loss (liquefaction).

v) Since the exact degree of incompressibility can not be estimated, some accuracy losses occur in the computer models.

As a conclusion, results of these studies revealed that there could be major changes in foundation soil profiles which in turn may affect the structural performance dramatically. This conclusion supports the importance of soil site investigations before the design of overlying structures.

REFERENCES

- Aksar,D.Ü.,(2001),”A Study on Response of Güldürcek Dam during 6, June 2000 Çankırı Earthquake” M.S. Thesis, Middle East Technical University, Ankara ,Turkey.
- Clough, R.W, Penzien J.. (1993), “Dynamics of Structures”, McGraw-Hill, Taipei,Taiwan.
- Çetin, K. O., Seed, R. B., Der Kiureghian, A., Tokimatsu, K., Harder, L.F., and Kayen, R.E.(2000)”SPT-Based Probabilistic and Deterministic Assessment Of Seismic Soil Liquefaction Initiation Hazard”, Research Report No. 2000/05, Pacific Earthquake Engineering Research Center.
- Finn, W.L., Byrne, M.P. ,Martin, G.R.(1976)”Seismic Response and Liquefaction of Sands” Journal of the Geotechnical Engineering Division ,ASCE, vol 102,No. GT8, August.
- Itasca Consulting Group, (2002) “Flac3D manual”, Minneapolis, USA.
- Imai, T., Tonouchi, K. (1982)”Correlation of N-value with s-wave velocity and shear modulus” Proceedings, 2nd European Symposium on Penetration Testing, Amsterdam. pp. 57-72.
- Karabalis, D.L. ,Mohammadi, M. (1998)”3-D Dynamic Foundation-Soil-Foundation Interaction on a Layered Soil. ” Soil dynamics and Earthquake engineering, 17.pp. 139-152.

- Kavruk, F.M., (2003), "Seismic Behavior of Embankment Dams" M.S. Thesis, Middle East Technical University, Ankara, Turkey.
- Kramer, S. L. (1996), "Geotechnical Earthquake Engineering", Prentice Hall, Upper Saddle River, New Jersey
- Kuhlmeyer, R.L., Lysmer, J. (1973) "Finite Element Method Accuracy for Wave Propagation Problems." J. Soil Mech. & Foundations, Div. ASCE, 99(SM5), 421-427 (May).
- Lysmer, J., Kuhlmeyer, R.L. (1969) "Finite Dynamic Model for infinite Media" J. Eng. Mech., 95(EM4), 859-877
- Martin, G.R., Finn, W.L. (1975) "Fundamentals of Liquefaction under Cyclic Loading" Journal of the Geotechnical Engineering Division, ASCE, vol 101, No. GT5, May.
- Mayne, P.W., Rix, G.J. (1993) " G_{max} - q_c relationships for clay" Geotechnical Testing Journal, ASTM, vol 16, No. 1, pp. 54-60.
- Pastor, M., Meredo, F.J.A. (1997) "Stabilized Finite Elements for Harmonic Soil Dynamics Problems near the Undrained Incompressible Limit" Soil dynamics and Earthquake engineering, 16, pp. 161-171.
- Rix, G.J., Stokoe, K. H. (1991), "Correlation of initial tangent modulus and cone penetration resistance." Calibration Chamber Testing. International Symposium on Calibration Chamber Testing. A.B. Huang, ed., Elsevier Publishing. New York, pp. 351-362.
- Robertson, P. K., Fear, C. E. (1997), "Earthquake Geotechnical Engineering", Ishihara (editor), Balkema, Rotterdam, pp. 1253-1289.

Schnabel,P.B., Lysmer, J., Seed, H.B.(1972-1991) "SHAKE: A computer program for Earthquake Response Analysis of Horizontally Layered Sites," University of California ,Berkeley,

Seed, H.B., Idriss, I.M.(1971) "Simplified procedure for evaluating soil liquefaction potential" Journal of the Soil Mechanics and Foundations Division ,ASCE, vol 107,No. SM9, pp.1249-1274

Seed, H.B., Wong, R.T., Idriss, I.M., Tokimatsu, K. (1986)"Moduli and damping factors for dynamic analyses of cohesionless soils" Journal of the Geotechnical Engineering Division, ASCE, vol 112, No. 11, pp.1016-1032

Seed, H.B. ,Lysmer, J.(1975)"Soil Structure Interaction Analyses for Seismic Response " Journal of the Geotechnical Engineering Division ,ASCE, vol 101,No. GT5, May.

Şafak,E. (2000)" Characterization of seismic hazard and structural response by energy flux" Soil dynamics and Earthquake engineering, 20.pp. 39-43.

Wolf, J.P. (1985) "Dynamic Soil-Structure Interaction" New Jersey, Prentice Hall,

Youd, T.L., Idriss, I.M., Andrus, R.D. et all (2001)"Liquefaction Resistance of Soils: Summary Report from the 1996 NCEER and 1998 NCEER/NSF Workshops on Evaluation of Liquefaction Resistance of Soils." Journal of Geotechnical and Geoenvironmental Engineering, Vol 127, No.10, October.

Appendix A

In this section , the vertical stress and the vertical displacement results of the static analysis will be given. Also the FFT, response spectrum of the (Sakarya 1999) rock record can be found in this section. The final figure is the FFT of the input ground motion used in dynamic analysis

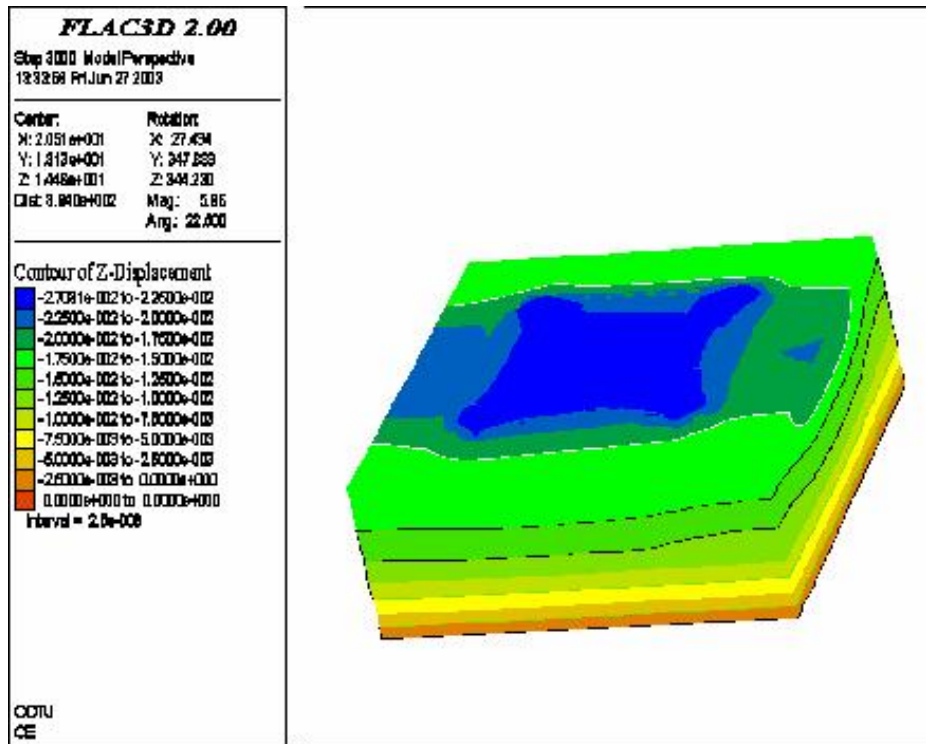


Fig A3 Vertical displacement(m) of the building C2

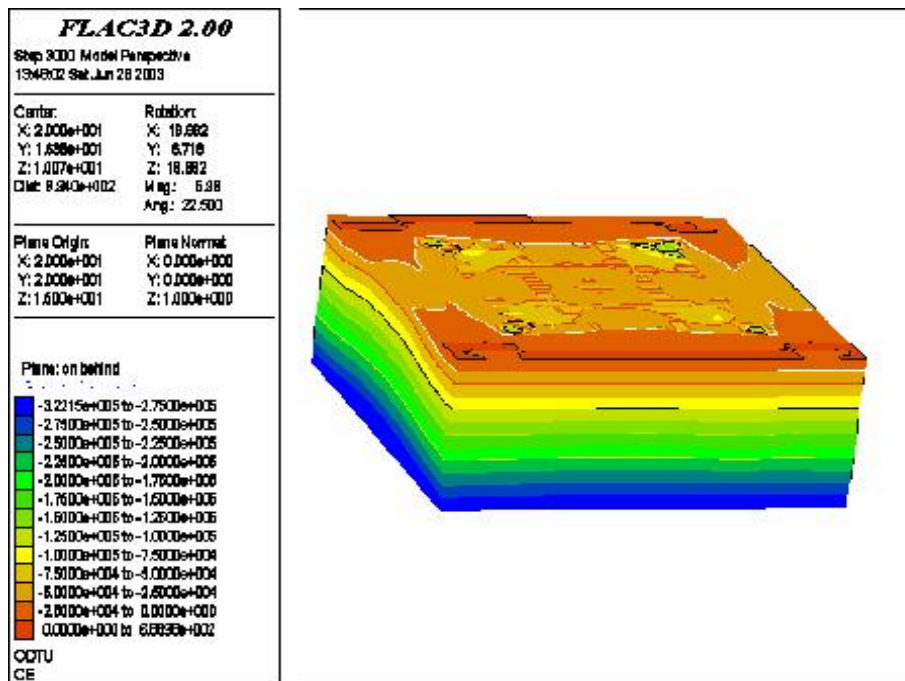


Fig A4 Vertical stress(Pa) of the building C2

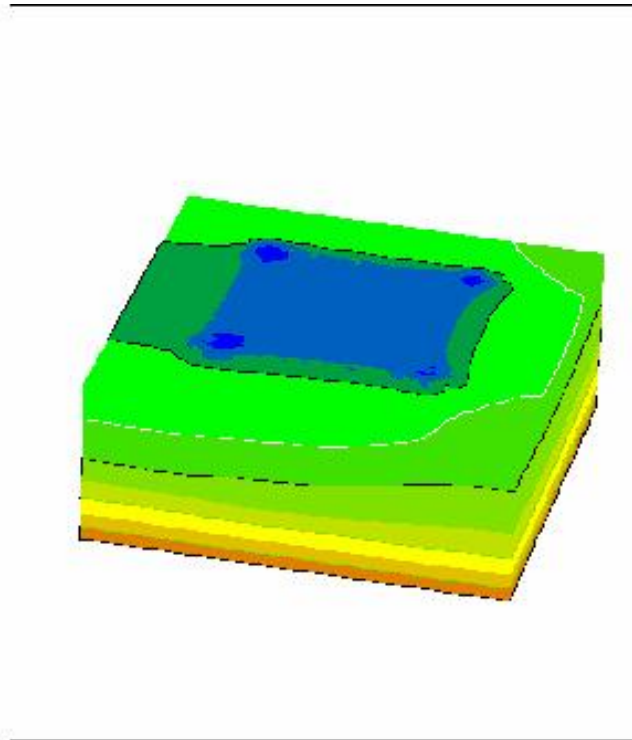
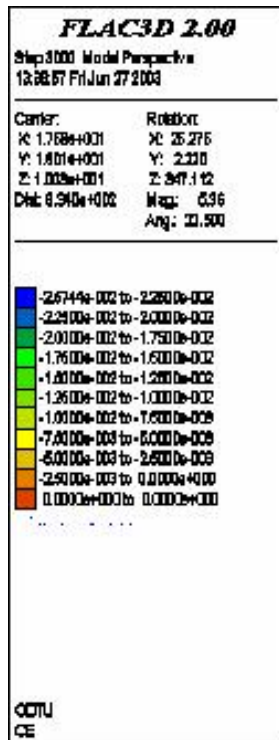


Fig A5 Vertical displacement(m) of the building C3

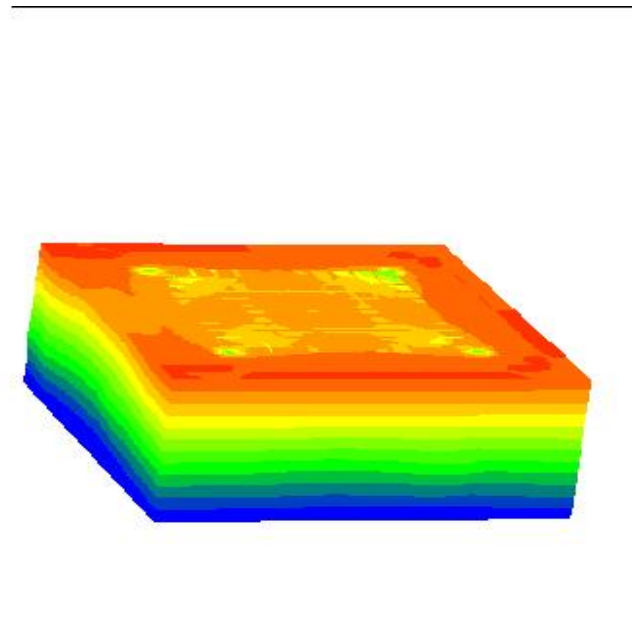
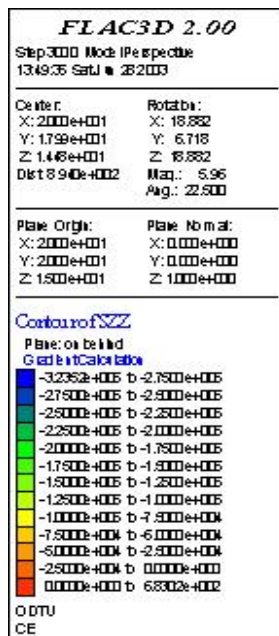


Fig A6 Vertical stress(Pa) of the building C3

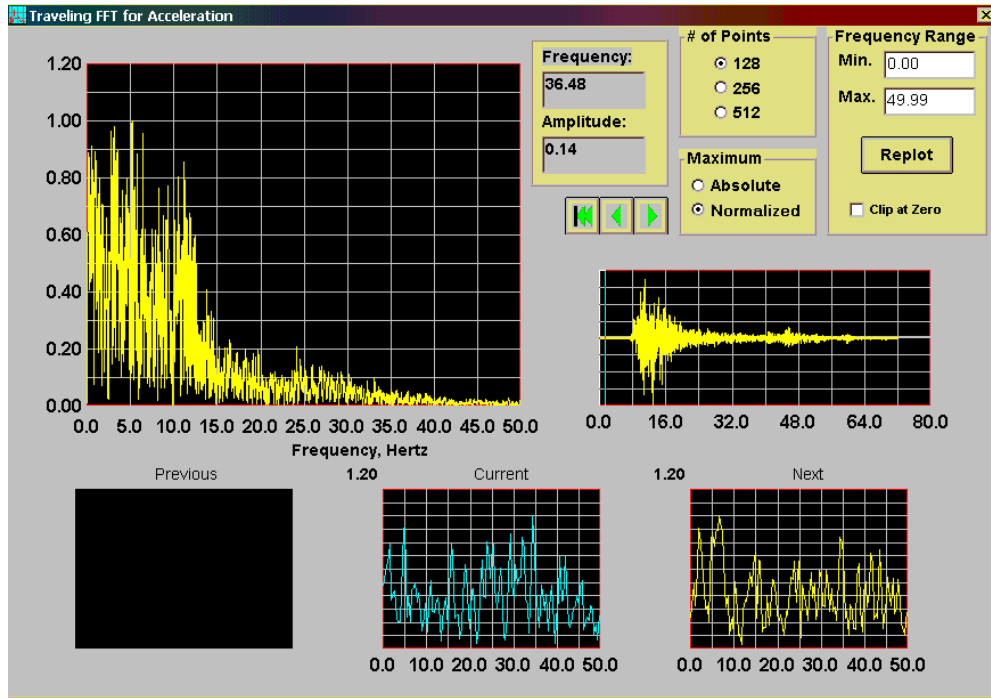


Fig A7 FFT of the original (Sakarya 1999) rock record.

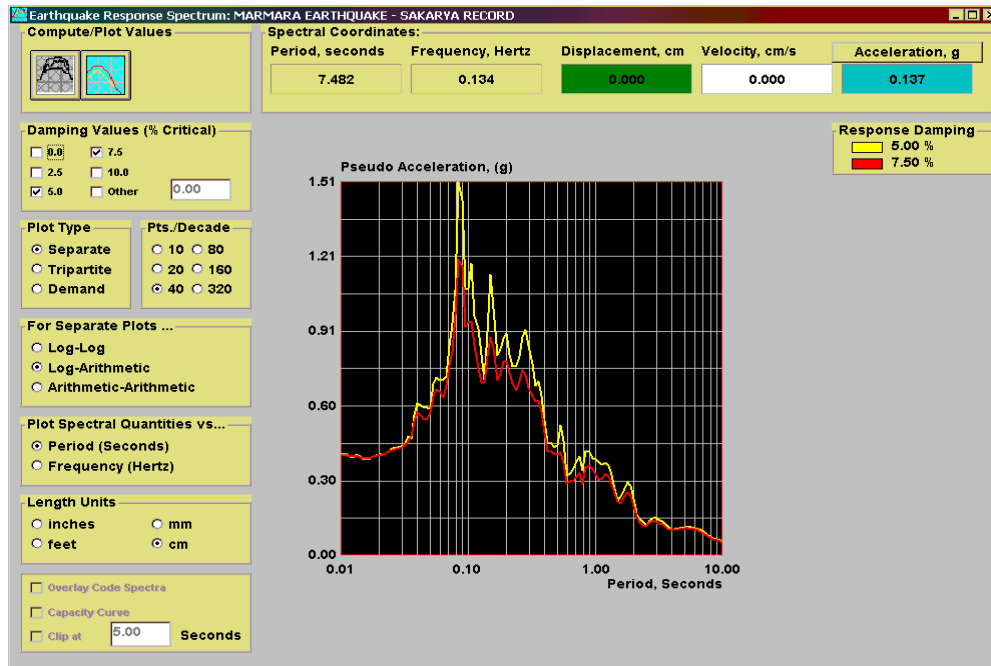


Fig A8 Response Spectrum of the original (Sakarya1999) rock record.

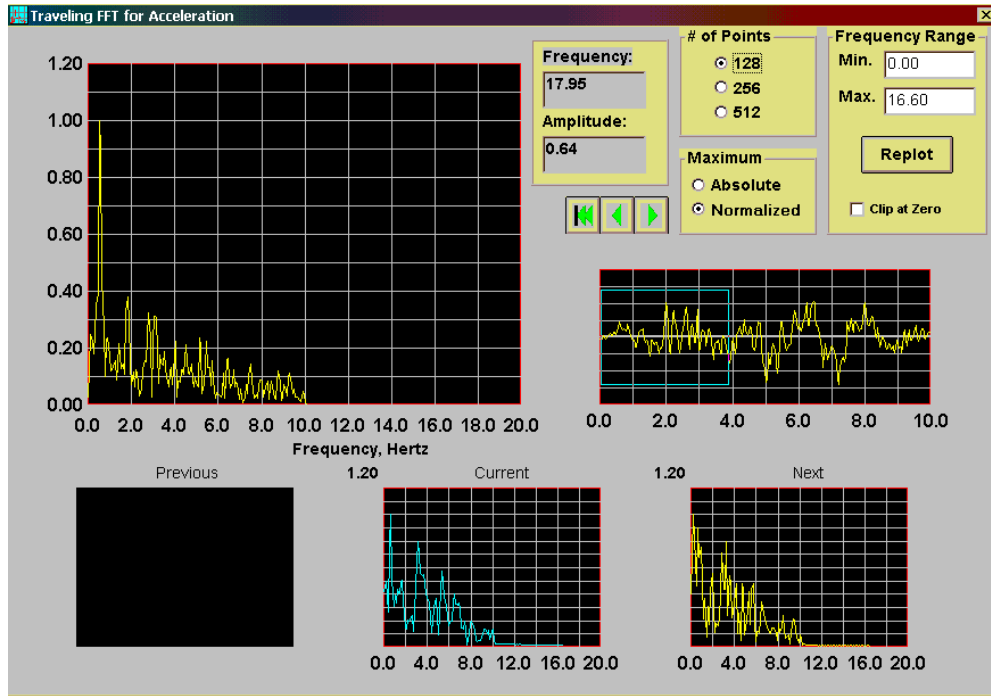


Fig A9 FFT of the Input ground motion used in the analysis.

Appendix B

In this section , the detailed SPT-CPT parameters of the site will be shown briefly. Also the generalized view of the site will be given in more detail to understand the site better.

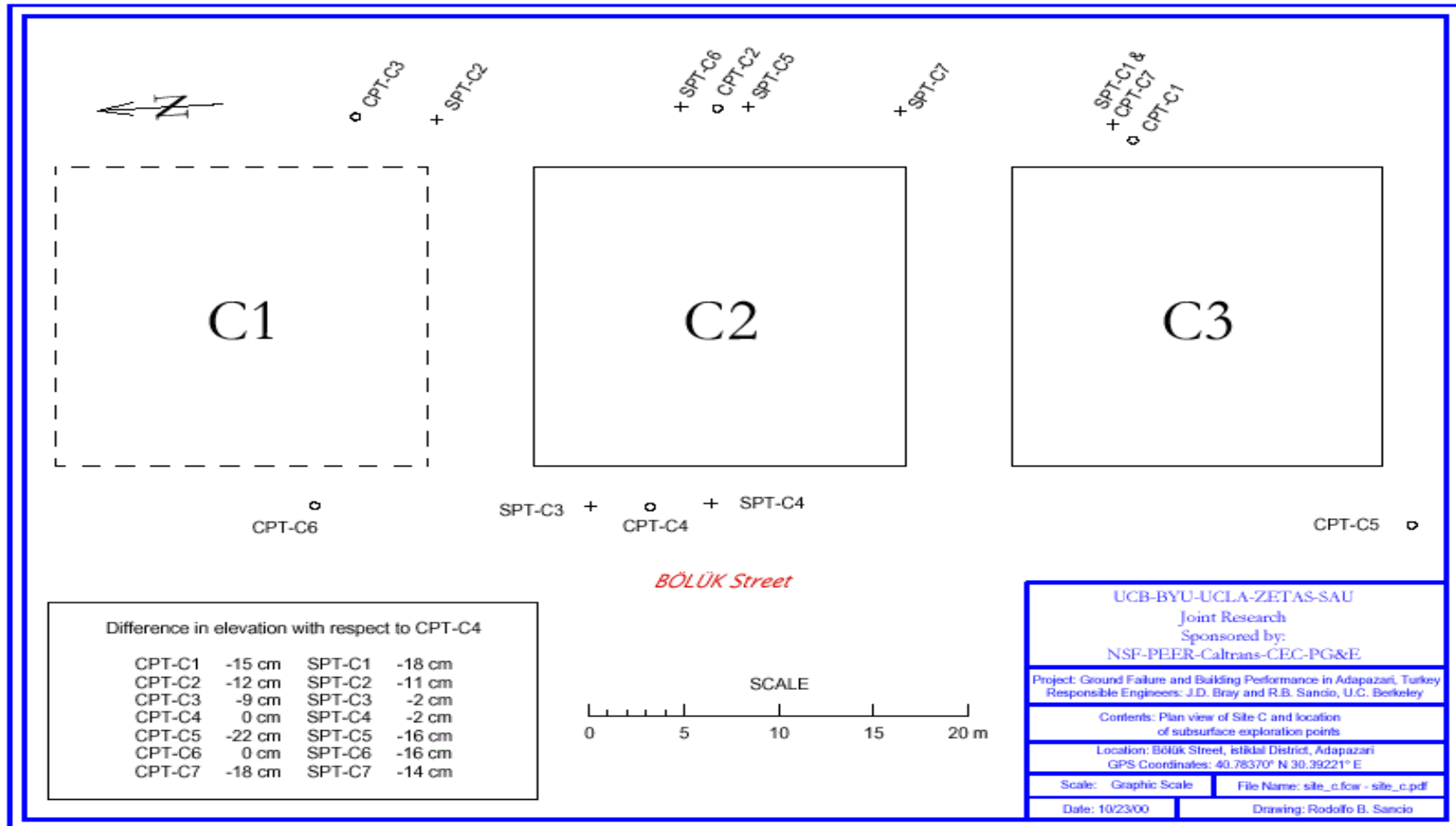


Fig B1 General view of the site in Adapazari

Hogentogler & Co

Operator@: SAKARYA M
 Sounding@: CPT100
 Cone Used@: H464TC

CPT Date/Time@: 02-27-03 11:53
 Location@: CN257
 Job Number@: TEST2

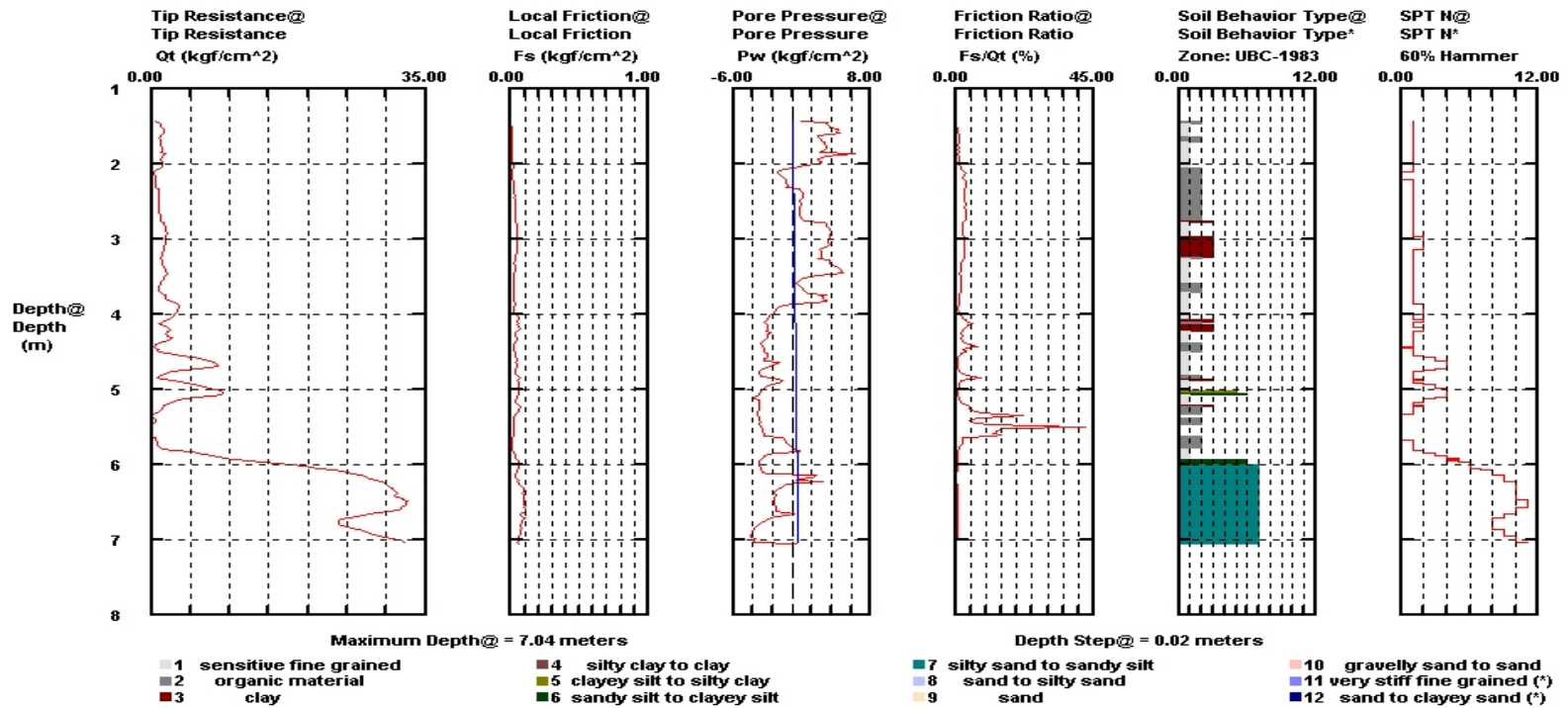


Fig B3 CPT-c1

Hogentogler & Co

Operator@: SAKARYA M
 Sounding@: CPT303
 Cone Used@: H464TC

CPT Date/Time@: 02-27-03 11:53
 Location@: CN257
 Job Number@: TEST2

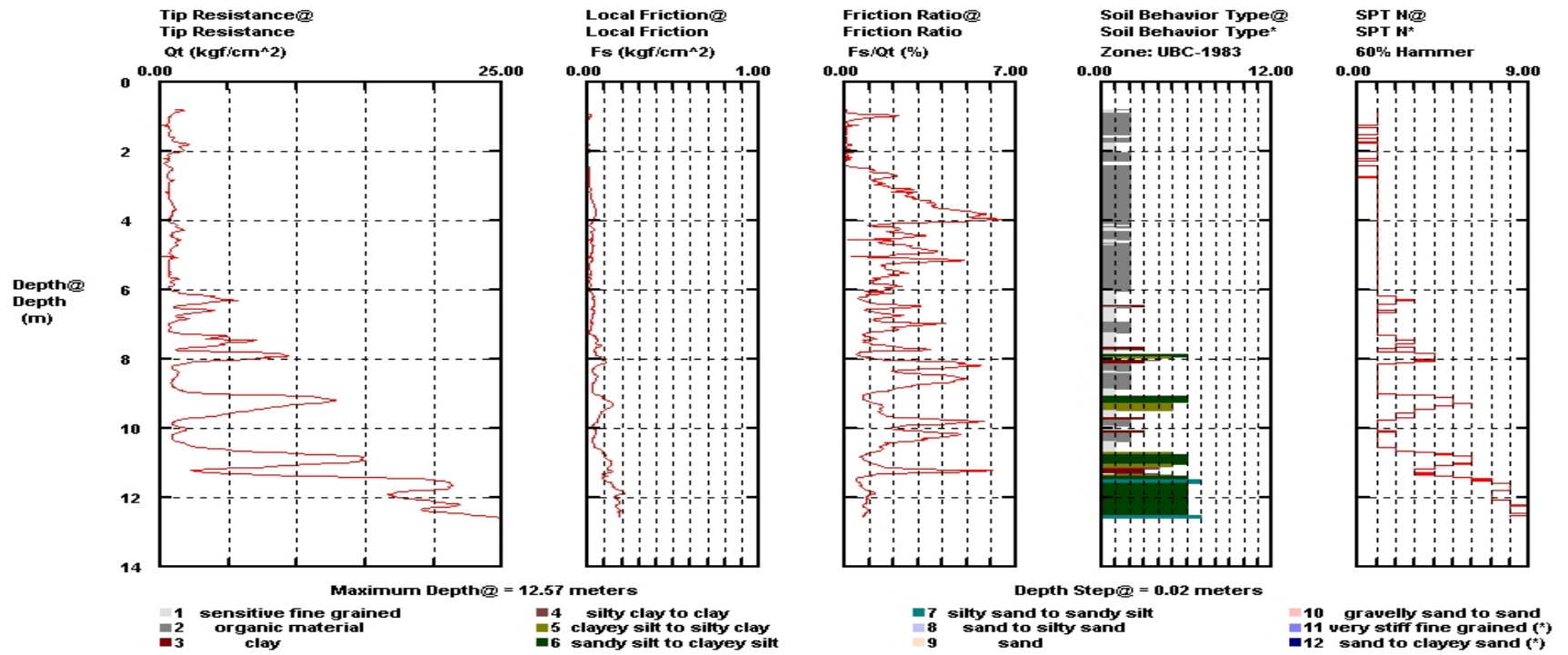


Fig B4 CPT-c3

Hogentogler & Co

Operator@: SAKARYA M
 Sounding@: CPT403
 Cone Used@: H464TC

CPT Date/Time@: 02-27-03 11:53
 Location@: CN257
 Job Number@: TEST2

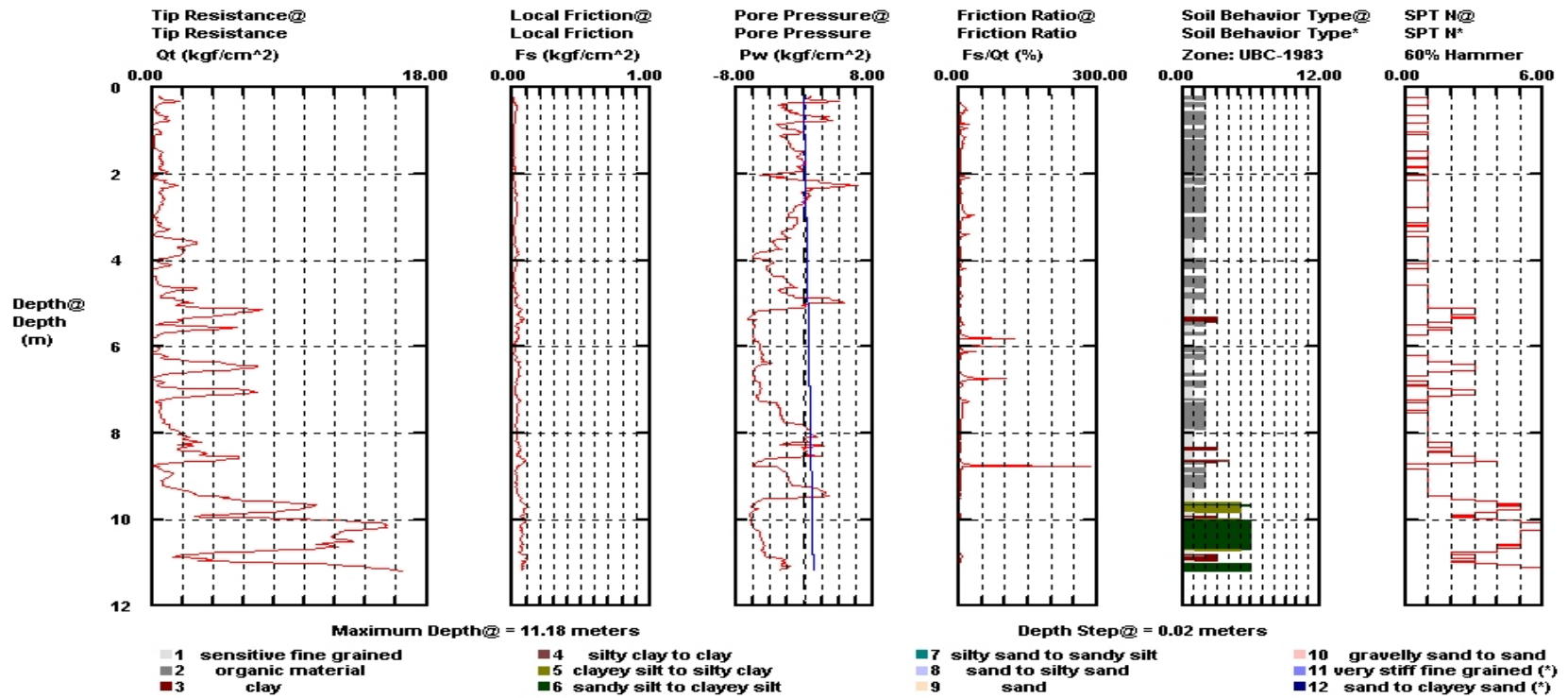


Fig B5 CPT-c4

Hogentogler & Co

Operator@: SAKRYA Me
 Sounding@: CPT503
 Cone Used@: H464TC

CPT Date/Time@: 02-27-03 11:53
 Location@: CN257
 Job Number@: TEST2

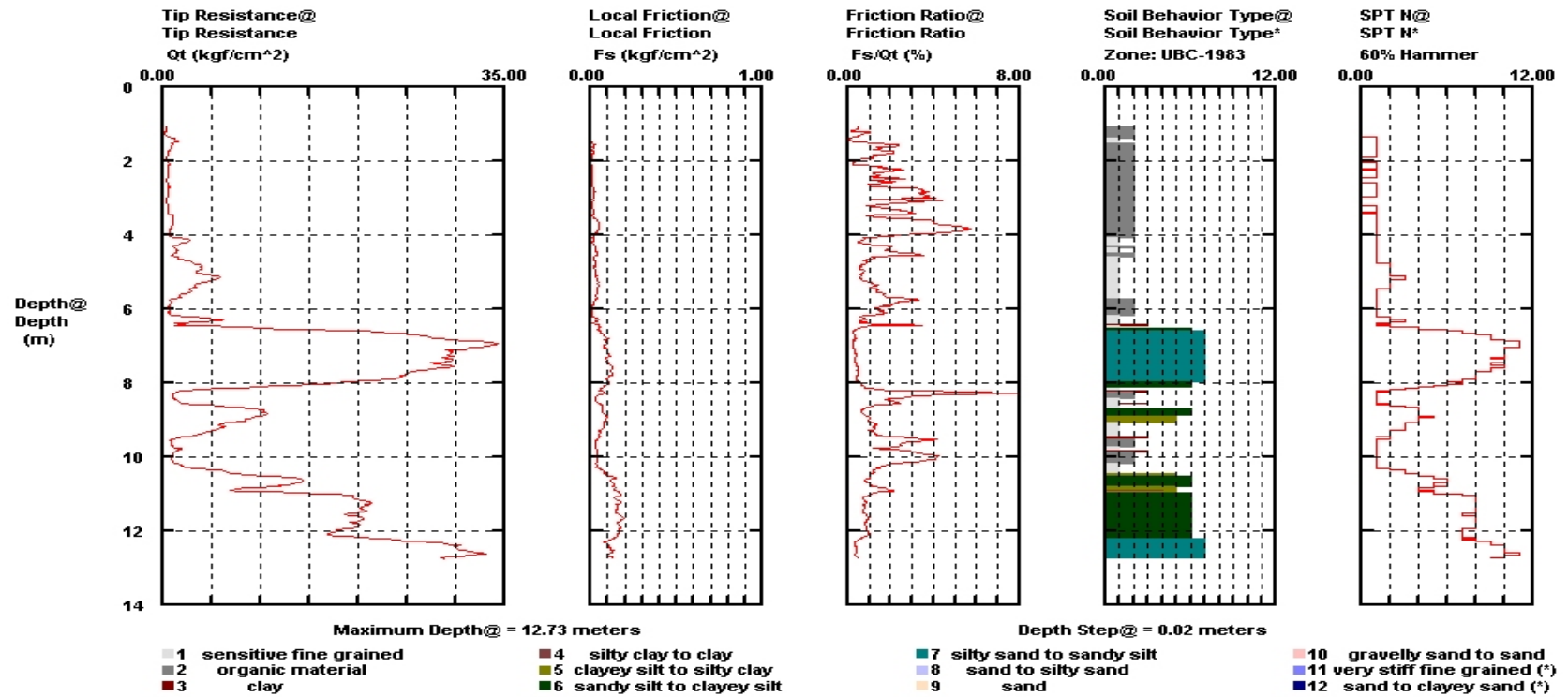


Fig B6 CPT-c5

Hogentogler & Co

Operator@: SAKARYA M
 Sounding@: CPT603
 Cone Used@: H464TC

CPT Date/Time@: 02-27-03 11:53
 Location@: CN257
 Job Number@: TEST2

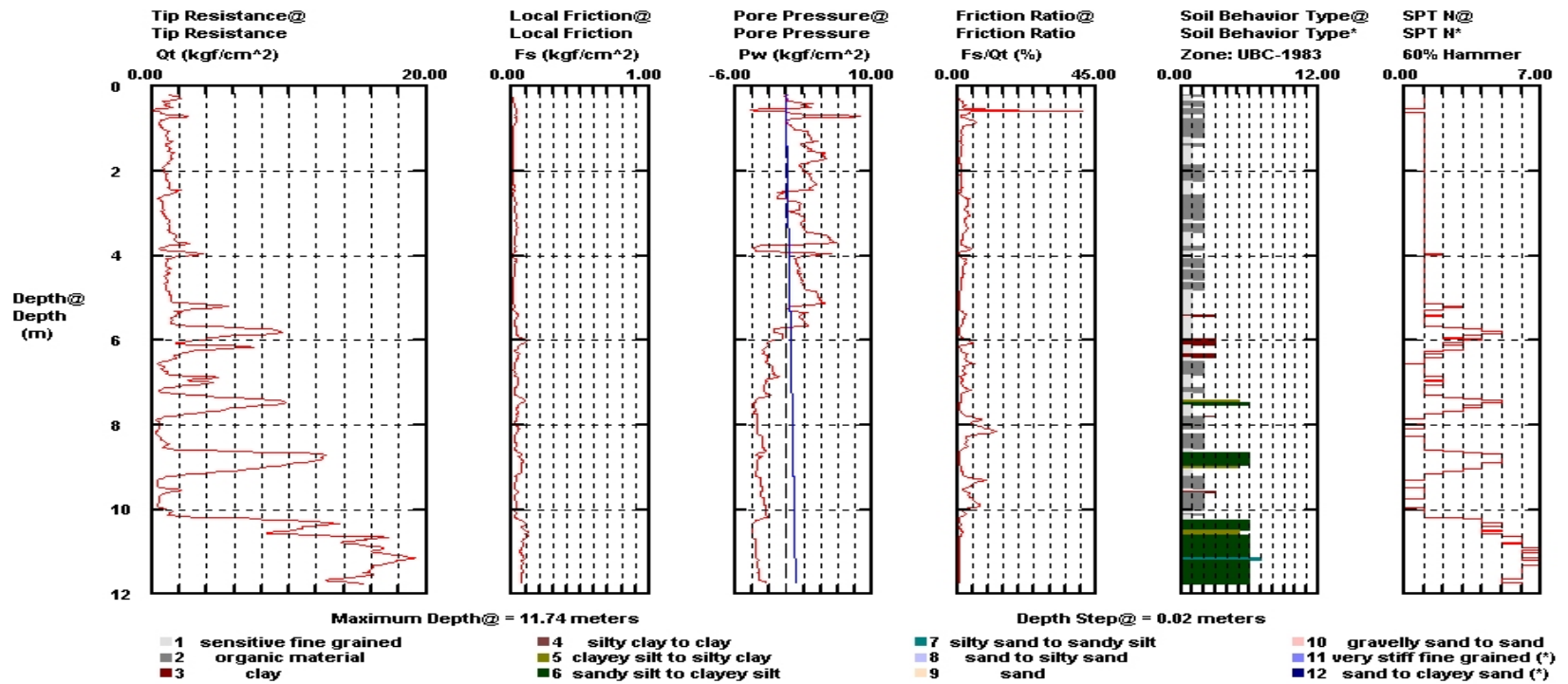


Fig B7 CPT-c6

UCB-BYU-UCLA ZETAS-SaU-METU Joint Research Sponsored by: NSF, Caltrans CEC, PG&E				Project Name: Ground Failure and Building Performance in Adapazari, Turkey Location: Site C - B00k Street, Istiklal District, Adapazari Date: June 26, 2000 Field Log by: Rodolfo B. Sancio Operator: ZETAS (Zemin Teknolojisi, A. S.) Drilling Method: Rotary wash with 9 cm-diameter tricone bit Water Table Elevation: GWL = 1.42 m 06/28, 1.56 m 07/08, 1.53 m 07/19 Notes: Approximately 1.5 m away from CPT-C1				Test ID: SPT-C1 GPS Coordinates: 40.78370°N 30.39221°E Elevation: -18 cm with respect to CPT-C4 Drilling Equipment: Custom made, equivalent to Creallus XC90H Responsible Engineers: J. D. Bray and R. B. Sancio, U. C. Berkeley SPT System: Rope, pulley and cathed method. AWJ rods. Hammer Type: Safety Hammer (per Kovacs et al. 1983)												
Depth Scale (m)	Lithology	USCS	Sample Type and No.	Recovery/Length (cm)	SPT Blows/5 cm	Case Depth (m)	Rod Length (m)	Energy Ratio (%)	Description	f_u Pocket (Pa) (kPa)	f_u Torque (kPa)	Moisture Content (%)	Liquid Limit	Plasticity Index	% fines < 75 μ m	< 5 μ m (%)	< 2 μ m (%)	D ₅₀ (mm)	D ₁₀ (mm)	Remarks
0									Fill: Dark brown clayey fill											
1																				
2		ML/CL	S-C1-1	43/45	1-1-1	-	5.80	-	CLAY: Brown tan silty clay to clayey silt. Red oxidation points in samples indicating oxidation of ferric minerals	30	14	40	44	17	99	-	-	-	-	
3		CH	S-C1-2	35/45	1-2-2	-	5.80	47		120	32	42	64	42	99	84	67	<2 μ m	<2 μ m	
4			SH-C1-3	40/42	-	2.0	-	-		100	24									
5		ML ML	S-C1-4A S-C1-4B	33/45	2-3-5	4.15	7.32	63 63	SANDY SILT: Gray low plasticity sandy silt interbedded with gray silty clay with traces of fine sand. Thin gray clay layer at approximately 5.15 m.	180 130	23 -	35 29	36 30	8 -	98 90	18 -	14 -	0.027 -	<2 μ m	
6		ML SW-SM	S-C1-5 S-C1-6A S-C1-6B	35/45 40/45	2-5-9 5-12-30	5.0 5.95	8.84 8.84	64 59 59		170 - - - - - - -	23 - - - - - - -	28 - - - - - - -	26 - - - - - - -	- - - - - - - -	67 - - - - - - -	- - - - - - - -	- - - - - - - -	- - - - - - - -		
7		SP	S-C1-7	38/45	7-13-7	7.3	10.37	56	SAND: Gray sand to silty sand of variable gradation interspersed with thin layers of silty clay. Variable gravel content in samples S-C1-6B and S-C1-7 (10% - 20%)	-	-	14	-	-	1	-	-	2.8	1	
8																				
9																				
10		ML	S-C1-8	36/45	3-3-8	9.45	11.89	71	ML: Gray low plasticity clayey silt with fine sand	-	30	30	32	-	89	42	32	0.007	<2 μ m	

Fig B8 SPT-c1

UCB-BYU-UCLA ZETAS-SaU-METU Joint Research Sponsored by: NSF, Caltrans CEC, PG&E			Project Name: Ground Failure and Building Performance in Adapazari, Turkey Location: Site C - B00k Street, Istiklal District, Adapazari Date: June 27, 2000 Field Log by: Rodolfo B. Sancio Operator: ZETAS (Zemin Teknolojisi, A. S.) Drilling Method: Rotary wash with 9 cm-diameter tricone bit Water Table Elevation: GWL = 1.45 m 06/28/00, 1.59 m 07/08, 0.98 m 08/03 Notes: Solid flight auger used to a depth of 1.6 m					Test ID: SPT-C2 GPS Coordinates: 40.78370°N 30.39221°E Elevation: -11 cm with respect to CPT-C4 Drilling Equipment: Custom made, equivalent to Creallus XC90H Responsible Engineers: J. D. Bray and R. B. Sancio, U. C. Berkeley SPT System: Rope, pulley and cathead method. AWJ rods. Hammer Type: Safety Hammer (per Kovacs et al. 1983)												
Depth Scale (m)	Lablog	USCS	Sample Type and No.	Recovery/Length (m)	SPT Blows/15 cm	Coreing Depth (m)	Rod Length (m)	Energy Ratio (%)	Description	σ_u Pocket (Pa) (kPa)	σ_u Torque (kPa)	Moisture Content (%)	Liquid Limit	Plasticity Index	% fines < 75 μ m	< 5 μ m (%)	< 2 μ m (%)	D60 (mm)	D10 (mm)	Remarks
0									CLAYEY SILT: Dark brown clayey silt with uniform color. Moist, soft consistency.											Located near the sediment ejecta
1									CLAYEY SILT: Brown clayey silt to high plasticity silty clay. Traces of fine sand											
2		CL/ML	S-C2-1	38/45	1-1-1		4.27	54		50	20	37	40	15	97	-	-	-	-	
3		ML/CL	SH-C2-2	42/42	-	2.4	-	-		80	45	43	42	15	94	22	8	0.013	0.003	
4		CH	S-C2-3	35/45	2-2-4	3.2	7.32	69		170	72	41	74	45	99	-	-	-	-	
5		MH	SH-C2-4	40/42	-	4.05	-	-		85	53	26	73	28	99	60	41	0.003	<2 μ m	
6		ML/CL	S-C2-5	36/45	2-4-3	4.85	8.84	73	CLAYEY SILT: Olive gray clayey silt with fine sand to sandy silt interbedded with clay seams. Very thin lamination at about 5.25 m.	230		33	42	15	87	-	-	-	-	
7		ML SW-SM	S-C2-6A S-C2-6B	38/45	5-15-19	5.65	8.84	70	SW-SM: Well graded gray sand with silt. Approximately 8% gravel content			26 13	27 -	- -	71 5	34 -	24 -	0.014 0.7	<2 μ m 0.15	
8		ML	S-C2-7	36/45	2-5-6	6.45	10.37	75	CLAYEY SILT: Alternating strata of gray silty clay and clayey silt.	300		29	34	-	92	-	-	-	-	Black fibrous wood chip at approx. 6.5 m
9		CL/CH	S-C2-8	35/45	1-3-3	7.5	10.37	65		130		38	49	26	99	48	40	0.006	<2 μ m	
9		ML	S-C2-9	43/45	4-3-4	8.9	13.42	71		280	50	36	37	-	99	60	49	0.002	<2 μ m	

Fig B9 SPT-c2

Depth, Scale (m)	Laboratory	USCS	Sample Type and No.	Recovery/Length (cm)	SPT Blows/15 cm	Casing Depth (m)	Rod Length (m)	Energy Ratio (%)	Description	σ_u Pocket Pen (kPa)	σ_u Torque (kPa)	Moisture Content (%)	Liquid Limit	Plasticity Index	% fines < 75 μ m	< 5 μ m (%)	< 2 μ m (%)	D ₆₀ (mm)	D ₁₀ (mm)	Remarks
0									Fill: The boring was drilled through a thin concrete slab on grade under which lies a gray silty sandy fill											
1																				
2									SILT: Brown silt to clayey silt with traces of fine sand interspersed with strata of brown silty sand to sandy silt											An attempt to obtain a Shelby tube sample at 1.5 m failed
3			SH-C3-1	42/42	-	2.8	-	-												
4	SM		S-C3-2	38/45	3-3-4	3.75	7.32	67		90		27	-	-	28	-	-	0.18	-	
5	CL/ML		S-C3-3	43/45	2-2-1	4.55	8.84	66		130		38	40	15	88	-	-	-	-	Traces of shells in sample S-C3-3
6	CL/ML SM		S-C3-4A S-C3-4B	38/45	3-10-8	5.45	8.84	66		125 250		34 23	45 -	20 -	97 57	- 13	- 10	- 0.09	- 0.001	
7	ML		S-C3-5	36/45	3-4-7	6.65	10.37					31	31	-	63	23	16	0.027	<2 μ m	Traces of wood fragments in sample S-C3-5
8	CH/MH		S-C3-6	35/45	1-3-2	7.65	10.37	62		70	23	42	67	36	98	-	-	-	-	
9									CLAY AND SILT: Gray low plasticity silt with sand interbedded with gray high plasticity clay. Red oxidation zone towards the upper portion of sample S-C3-6. The clay loses strength when remolded											
10	ML		S-C3-7	45/45	2-7-14	9.75	13.42	65		370		25	26	-	75	18	15	0.033	<2 μ m	

Fig B10 SPT-c3

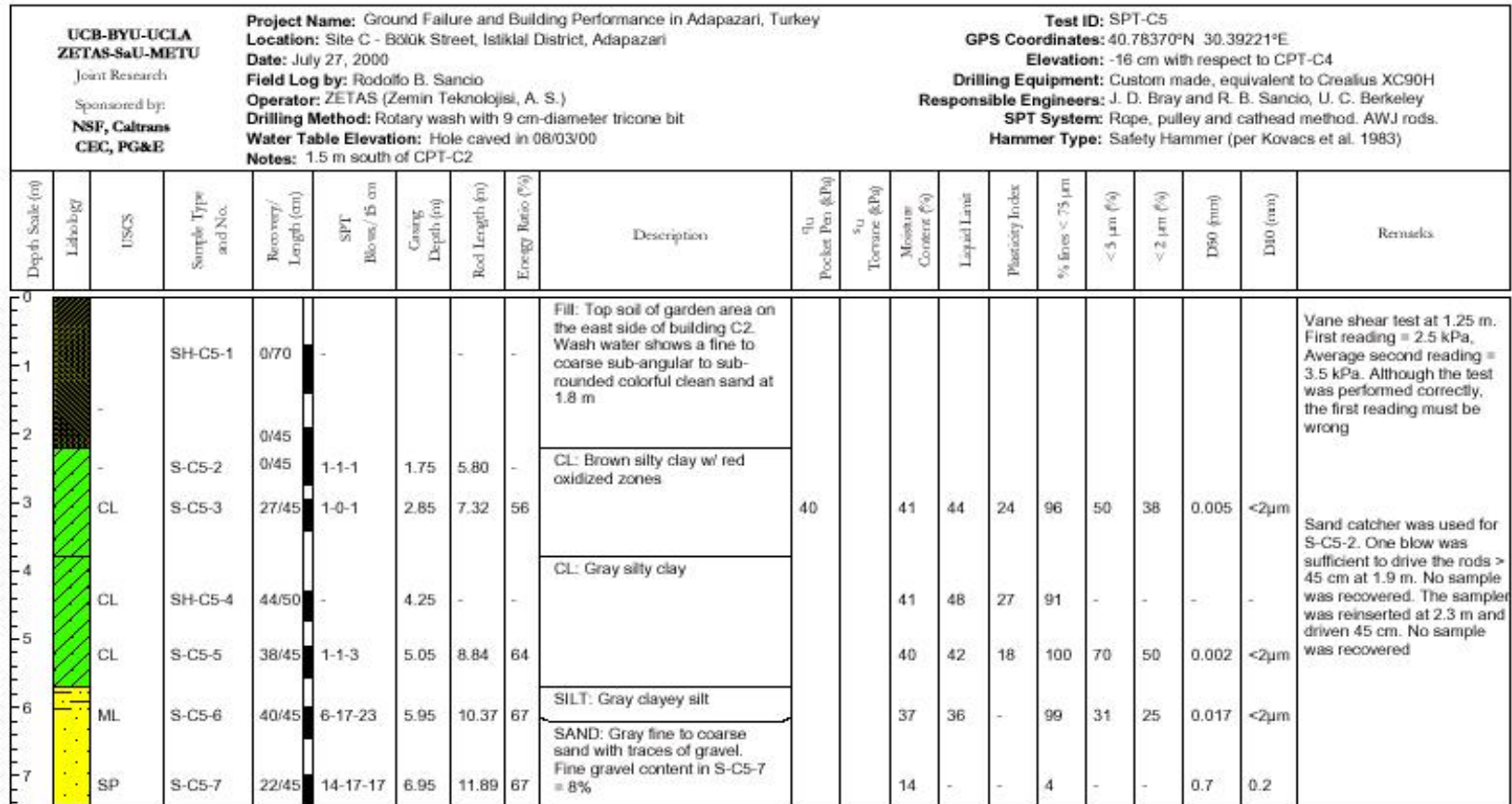


Fig B10 SPT-c

Appendix C

In this section the input of the related Flac3D model and Shake91 can be observed. There are 2 Flac3D inputs which are the Mohr-Coulomb model to evaluate the stress, strain, displacement and the acceleration histories of the site and the the Finn model to evaluate pore pressure.

Analysis using Mohr Model for evaluation of stress, strain, displacement and acceleration

```
conf dyn
set dyn off
;Mesh generation for the building C1
gen zone brick size 20 20 6 p0 0,0,0 p1 40 0 0 p2 0 40 0 p3 0 0 9
gen zone brick size 20 20 6 p0 0,0,9 p1 40 0 9 p2 0 40 9 p3 0 0 15
gen zone brick size 11 11 1 p0 8 8 15 p1 32 8 15 p2 8 32 15 p3 8 8 15.5
attach face range z 14.9 15.1
gen sur brick ver 0,0,0 ver 0,40,0 ver 25,0,0 ver 0,0,9
gen sur brick ver 0,0,9 ver 0,40,9 ver 25,0,9 ver 0,0,15
gen sur brick ver 25,0,0 ver 25,40,0 ver 40,0,0 ver 25,0,9
gen sur xp ver 25,0,8 ver 40,0,8 ver 40,40,5 ver 25,40,8 extrude 0 0 5 cap close
gen sur brick ver 25,0,9 ver 25,40,9 ver 40,0,9 ver 25,0,15
gen sur brick ver 8,8,15 ver 32 8 15 ver 8 32 15 ver 8 8 15.5
group clay2 lblue range vol 1
group clay1 red range vol 2
group clay2 lblue range vol 3
group sand lgreen range vol 4 &
vol 5 not
group clay1 red range vol 5
group stiff yellow range vol 6
;
;
; Mesh generation for the building C2
gen zone brick size 20 20 6 p0 0,0,0 p1 40 0 0 p2 0 40 0 p3 0 0 9
gen zone brick size 20 20 6 p0 0,0,9 p1 40 0 9 p2 0 40 9 p3 0 0 15
gen zone brick size 11 11 1 p0 8 8 15 p1 32 8 15 p2 8 32 15 p3 8 8 15.5
attach face range z 14.9 15.1
gen sur brick ver 0,0,0 ver 0,40,0 ver 15,0,0 ver 0,0,9
gen sur xp ver 0,0,8 ver 15,0,8 ver 15,40,5 ver 0,40,8 extrude 0 0 5 cap close
gen sur brick ver 0,0,9 ver 0,40,9 ver 15,0,9 ver 0,0,15
gen sur brick ver 15,0,0 ver 15,40,0 ver 40,0,0 ver 15,0,9
gen sur xp ver 15,0,8 ver 40,0,6 ver 40,40,5 ver 15,40,5 extrude 0 0 5 cap close
gen sur brick ver 15,0,9 ver 15,40,9 ver 40,0,9 ver 15,0,15
gen sur brick ver 8,8,15 ver 32 8 15 ver 8 32 15 ver 8 8 15.5
group clay2 lblue range vol 1
group sand lgreen range vol 2 &
vol 3 not
group clay1 red range vol 3
group clay2 lblue range vol 4
group sand lgreen range vol 5 &
vol 6 not
group clay1 red range vol 6
group stiff yellow range vol 7
;
;
; Mesh generation for the building C3
gen zone brick size 20 20 6 p0 0,0,0 p1 40 0 0 p2 0 40 0 p3 0 0 9
gen zone brick size 20 20 6 p0 0,0,9 p1 40 0 9 p2 0 40 9 p3 0 0 15
gen zone brick size 11 11 1 p0 8 8 15 p1 32 8 15 p2 8 32 15 p3 8 8 15.5
attach face range z 14.9 15.1
gen sur brick ver 0,0,0 ver 0,40,0 ver 30,0,0 ver 0,0,9
gen sur xp ver 0,0,8 ver 30,0,5 ver 30,40,5 ver 0,40,5 extrude 0 0 6 cap close
gen sur brick ver 0,0,10 ver 0,40,10 ver 30,0,10 ver 0,0,15
gen sur brick ver 30,0,0 ver 30,40,0 ver 40,0,0 ver 30,0,5
gen sur brick ver 30,0,5 ver 30,40,5 ver 40,0,5 ver 30,0,10
gen sur brick ver 30,0,10 ver 30,40,10 ver 40,0,10 ver 30,0,15
gen sur brick ver 8,8,15 ver 32 8 15 ver 8 32 15 ver 8 8 15.5
group clay2 lblue range vol 1
group sand lgreen range vol 2 &
vol 3 not
group clay1 red range vol 3
group clay2 lblue range vol 4
group sand lgreen range vol 5
group clay1 red range vol 6
group stiff yellow range vol 7
;
;
;
mod elas
macro idclay2 'bulk 8e7 shear 4e7'
macro idsand 'bulk 1.2e8 shear 6.5e7'
macro idstiff 'bulk 1e8 shear 1e8'
macro idclay1 'bulk 7e7 shear 2e7'
;
prop idclay1 range group clay1
```

```

prop idclay2 range group clay2
prop idsand range group sand
prop idstiff range group stiff
;
;
;
;
;
;
ini dens=2000
set grav 0,0,-9.81
water density 1000
water table ori 0 0 13.6 normal 0 0 1
apply szz -3e4 range z 14.9 15.1 x 35 40 y 10 30
;
;
;
;
;
sel beam id 1 b (10 10 15.5) e (10 30 15.5)
sel beam id 2 b (10 30 15.5) e (30 30 15.5)
sel beam id 2 b (30 30 15.5) e (30 10 15.5)
sel beam id 1 b (30 10 15.5) e (10 10 15.5)
sel beam id 11 b (10 10 15.5) e (10 10 18)
sel beam id 11 b (30 10 15.5) e (30 10 18)
sel beam id 11 b (30 30 15.5) e (30 30 18)
sel beam id 11 b (10 30 15.5) e (10 30 18)
sel beam id 1 b (10 10 18) e (10 30 18)
sel beam id 2 b (10 30 18) e (30 30 18)
sel beam id 2 b (30 30 18) e (30 10 18)
sel beam id 1 b (30 10 18) e (10 10 18)
sel beam id 11 b (10 10 18) e (10 10 21)
sel beam id 11 b (30 10 18) e (30 10 21)
sel beam id 11 b (30 30 18) e (30 30 21)
sel beam id 11 b (10 30 18) e (10 30 21)
sel beam id 1 b (10 10 21) e (10 30 21)
sel beam id 2 b (10 30 21) e (30 30 21)
sel beam id 2 b (30 30 21) e (30 10 21)
sel beam id 1 b (30 10 21) e (10 10 21)
sel beam id 11 b (10 10 21) e (10 10 24)
sel beam id 11 b (30 10 21) e (30 10 24)
sel beam id 11 b (30 30 21) e (30 30 24)
sel beam id 11 b (10 30 21) e (10 30 24)
sel beam id 1 b (10 10 24) e (10 30 24)
sel beam id 2 b (10 30 24) e (30 30 24)
sel beam id 2 b (30 30 24) e (30 10 24)
sel beam id 1 b (30 10 24) e (10 10 24)
sel beam id 11 b (10 10 24) e (10 10 27)
sel beam id 11 b (30 10 24) e (30 10 27)
sel beam id 11 b (30 30 24) e (30 30 27)
sel beam id 11 b (10 30 24) e (10 30 27)
sel beam id 1 b (10 10 27) e (10 30 27)
sel beam id 2 b (10 30 27) e (30 30 27)
sel beam id 2 b (30 30 27) e (30 10 27)
sel beam id 1 b (30 10 27) e (10 10 27)
sel beam id 1 apply z 30000
sel beam id 2 apply z -30000
sel beam id 1 prop density 2500 emod 25000000 nu 0.3 xcarea 1 xciy 0.083 xciz 0.083 xcj 0.167
sel beam id 2 prop density 2500 emod 25000000 nu 0.3 xcarea 1 xciy 0.083 xciz 0.083 xcj 0.167
sel beam id 11 prop density 2500 emod 25000000 nu 0.3 xcarea 0.36 xciy 0.0108 xciz 0.0108 xcj 0.0216
;
;
;
;
;
;
fix x range x -0.1 0.1
fix x range x 39.9 40.1
fix y range y -0.1 0.1
fix y range y 39.9 40.1
fix z range z -0.1 0.1
;
;
;
step 3000
save d1B1C1st.sav
;
set dyn on
set large
ini xv el 0 yvel 0 zvel 0
ini xdisp 0 ydisp 0 zdisp 0
free x y z

```

```

apply dquiet squiet nquiet plane norm -1,0,0 range x -0.1 0.1 z 0.1 15.1
apply dquiet squiet nquiet plane norm 1,0,0 range x 39.9 40.1 z 0.1 15.1
apply dquiet squiet nquiet plane norm 0,-1,0 range y -0.1 0.1 z 0.1 15.1
apply dquiet squiet nquiet plane norm 0,1,0 range y 39.9 40.1 z 0.1 15.1
fix z range z=-0.1 0.1
;
;
;
prop idclay1 range group clay1 not
prop idclay2 range group clay2 not
prop idsand range group sand not
prop idstiff range group stiff not
mod elas
macro id_clay2 'bulk 8e8 shear 3e7'
macro id_sand 'bulk 3.2e9 shear 6.5e7'
macro id_stiff 'bulk 1e8 shear 1e8'
macro id_clay1 'bulk 1e8 shear 1.4e7 fric 15 coh 5e4 tens 2e4'
;
;
;
mod elas range group clay1 not
mod mohr range group clay1
;
prop id_clay2 range group clay2
prop id_sand range group sand
prop id_stiff range group stiff
prop id_clay1 range group clay1
;
;
;
;
table 1 read 11.eq
apply yvel=1 hist table 1 range z=-0.1 0.1
;
;
;
;
;
;
;1th point
;1
hist gp yacc 10 5 15
hist gp yacc 10 5 14
hist gp yacc 10 5 12
hist gp yacc 10 5 9
hist gp yacc 10 5 6
hist gp yacc 10 5 3
hist gp yacc 10 5 0
;8
hist gp zdisp 10 5 15
hist gp zdisp 10 5 14
hist gp zdisp 10 5 12
hist gp zdisp 10 5 9
hist gp zdisp 10 5 6
hist gp zdisp 10 5 3
hist gp zdisp 10 5 0
;15
hist gp ydisp 10 5 15
hist gp ydisp 10 5 14
hist gp ydisp 10 5 12
hist gp ydisp 10 5 9
hist gp ydisp 10 5 6
hist gp ydisp 10 5 3
hist gp ydisp 10 5 0
;22
hist z syy 10 5 15
hist z syy 10 5 14
hist z syy 10 5 12
hist z syy 10 5 9
hist z syy 10 5 6
hist z syy 10 5 3
hist z syy 10 5 0
;29
hist z szz 10 5 15
hist z szz 10 5 14

```

hist z szz 10 5 12
hist z szz 10 5 9
hist z szz 10 5 6
hist z szz 10 5 3
hist z szz 10 5 0
;36
hist z syz 10 5 15
hist z syz 10 5 14
hist z syz 10 5 12
hist z syz 10 5 9
hist z syz 10 5 6
hist z syz 10 5 3
hist z syz 10 5 0
;43
hist z ssr 10 5 15
hist z ssr 10 5 14
hist z ssr 10 5 12
hist z ssr 10 5 9
hist z ssr 10 5 6
hist z ssr 10 5 3
hist z ssr 10 5 0
;2th point
;50
hist gp yacc 30 5 15
hist gp yacc 30 5 14
hist gp yacc 30 5 12
hist gp yacc 30 5 9
hist gp yacc 30 5 6
hist gp yacc 30 5 3
hist gp yacc 30 5 0
;57
hist gp zdisp 30 5 15
hist gp zdisp 30 5 14
hist gp zdisp 30 5 12
hist gp zdisp 30 5 9
hist gp zdisp 30 5 6
hist gp zdisp 30 5 3
hist gp zdisp 30 5 0
;64
hist gp ydisp 30 5 15
hist gp ydisp 30 5 14
hist gp ydisp 30 5 12
hist gp ydisp 30 5 9
hist gp ydisp 30 5 6
hist gp ydisp 30 5 3
hist gp ydisp 30 5 0
;71
hist z syy 30 5 15
hist z syy 30 5 14
hist z syy 30 5 12
hist z syy 30 5 9
hist z syy 30 5 6
hist z syy 30 5 3
hist z syy 30 5 0
;78
hist z szz 30 5 15
hist z szz 30 5 14
hist z szz 30 5 12
hist z szz 30 5 9
hist z szz 30 5 6
hist z szz 30 5 3
hist z szz 30 5 0
;85
hist z syz 30 5 15
hist z syz 30 5 14
hist z syz 30 5 12
hist z syz 30 5 9
hist z syz 30 5 6
hist z syz 30 5 3
hist z syz 30 5 0
;92
hist z ssr 30 5 15
hist z ssr 30 5 14
hist z ssr 30 5 12
hist z ssr 30 5 9
hist z ssr 30 5 6

```
hist z ssr 30 5 3
hist z ssr 30 5 0
;3th point
;99
hist gp yacc 10 10 15
hist gp yacc 10 10 14
hist gp yacc 10 10 12
hist gp yacc 10 10 9
hist gp yacc 10 10 6
hist gp yacc 10 10 3
hist gp yacc 10 10 0
;106
hist gp zdisp 10 10 15
hist gp zdisp 10 10 14
hist gp zdisp 10 10 12
hist gp zdisp 10 10 9
hist gp zdisp 10 10 6
hist gp zdisp 10 10 3
hist gp zdisp 10 10 0
;113
hist gp ydisp 10 10 15
hist gp ydisp 10 10 14
hist gp ydisp 10 10 12
hist gp ydisp 10 10 9
hist gp ydisp 10 10 6
hist gp ydisp 10 10 3
hist gp ydisp 10 10 0
;120
hist z syy 10 10 15
hist z syy 10 10 14
hist z syy 10 10 12
hist z syy 10 10 9
hist z syy 10 10 6
hist z syy 10 10 3
hist z syy 10 10 0
;127
hist z szz 10 10 15
hist z szz 10 10 14
hist z szz 10 10 12
hist z szz 10 10 9
hist z szz 10 10 6
hist z szz 10 10 3
hist z szz 10 10 0
;134
hist z syz 10 10 15
hist z syz 10 10 14
hist z syz 10 10 12
hist z syz 10 10 9
hist z syz 10 10 6
hist z syz 10 10 3
hist z syz 10 10 0
;141
hist z ssr 10 10 15
hist z ssr 10 10 14
hist z ssr 10 10 12
hist z ssr 10 10 9
hist z ssr 10 10 6
hist z ssr 10 10 3
hist z ssr 10 10 0
;4th point
;148
hist gp yacc 30 10 15
hist gp yacc 30 10 14
hist gp yacc 30 10 12
hist gp yacc 30 10 9
hist gp yacc 30 10 6
hist gp yacc 30 10 3
hist gp yacc 30 10 0
;155
hist gp zdisp 30 10 15
hist gp zdisp 30 10 14
hist gp zdisp 30 10 12
hist gp zdisp 30 10 9
hist gp zdisp 30 10 6
hist gp zdisp 30 10 3
hist gp zdisp 30 10 0
```

;162
hist gp ydisp 30 10 15
hist gp ydisp 30 10 14
hist gp ydisp 30 10 12
hist gp ydisp 30 10 9
hist gp ydisp 30 10 6
hist gp ydisp 30 10 3
hist gp ydisp 30 10 0
;169
hist z syy 30 10 15
hist z syy 30 10 14
hist z syy 30 10 12
hist z syy 30 10 9
hist z syy 30 10 6
hist z syy 30 10 3
hist z syy 30 10 0
;176
hist z szz 30 10 15
hist z szz 30 10 14
hist z szz 30 10 12
hist z szz 30 10 9
hist z szz 30 10 6
hist z szz 30 10 3
hist z szz 30 10 0
;183
hist z syz 30 10 15
hist z syz 30 10 14
hist z syz 30 10 12
hist z syz 30 10 9
hist z syz 30 10 6
hist z syz 30 10 3
hist z syz 30 10 0
;190
hist z ssr 30 10 15
hist z ssr 30 10 14
hist z ssr 30 10 12
hist z ssr 30 10 9
hist z ssr 30 10 6
hist z ssr 30 10 3
hist z ssr 30 10 0
;5th point
;197
hist gp yacc 10 30 15
hist gp yacc 10 30 14
hist gp yacc 10 30 12
hist gp yacc 10 30 9
hist gp yacc 10 30 6
hist gp yacc 10 30 3
hist gp yacc 10 30 0
;204
hist gp zdisp 10 30 15
hist gp zdisp 10 30 14
hist gp zdisp 10 30 12
hist gp zdisp 10 30 9
hist gp zdisp 10 30 6
hist gp zdisp 10 30 3
hist gp zdisp 10 30 0
;211
hist gp ydisp 10 30 15
hist gp ydisp 10 30 14
hist gp ydisp 10 30 12
hist gp ydisp 10 30 9
hist gp ydisp 10 30 6
hist gp ydisp 10 30 3
hist gp ydisp 10 30 0
;218
hist z syy 10 30 15
hist z syy 10 30 14
hist z syy 10 30 12
hist z syy 10 30 9
hist z syy 10 30 6
hist z syy 10 30 3
hist z syy 10 30 0
;225
hist z szz 10 30 15
hist z szz 10 30 14

hist z szz 10 30 12
hist z szz 10 30 9
hist z szz 10 30 6
hist z szz 10 30 3
hist z szz 10 30 0
;232
hist z syz 10 30 15
hist z syz 10 30 14
hist z syz 10 30 12
hist z syz 10 30 9
hist z syz 10 30 6
hist z syz 10 30 3
hist z syz 10 30 0
;239
hist z ssr 10 30 15
hist z ssr 10 30 14
hist z ssr 10 30 12
hist z ssr 10 30 9
hist z ssr 10 30 6
hist z ssr 10 30 3
hist z ssr 10 30 0
;6th point
;246
hist gp yacc 30 30 15
hist gp yacc 30 30 14
hist gp yacc 30 30 12
hist gp yacc 30 30 9
hist gp yacc 30 30 6
hist gp yacc 30 30 3
hist gp yacc 30 30 0
;253
hist gp zdisp 30 30 15
hist gp zdisp 30 30 14
hist gp zdisp 30 30 12
hist gp zdisp 30 30 9
hist gp zdisp 30 30 6
hist gp zdisp 30 30 3
hist gp zdisp 30 30 0
;260
hist gp ydisp 30 30 15
hist gp ydisp 30 30 14
hist gp ydisp 30 30 12
hist gp ydisp 30 30 9
hist gp ydisp 30 30 6
hist gp ydisp 30 30 3
hist gp ydisp 30 30 0
;267
hist z syy 30 30 15
hist z syy 30 30 14
hist z syy 30 30 12
hist z syy 30 30 9
hist z syy 30 30 6
hist z syy 30 30 3
hist z syy 30 30 0
;274
hist z szz 30 30 15
hist z szz 30 30 14
hist z szz 30 30 12
hist z szz 30 30 9
hist z szz 30 30 6
hist z szz 30 30 3
hist z szz 30 30 0
;281
hist z syz 30 30 15
hist z syz 30 30 14
hist z syz 30 30 12
hist z syz 30 30 9
hist z syz 30 30 6
hist z syz 30 30 3
hist z syz 30 30 0
;288
hist z ssr 30 30 15
hist z ssr 30 30 14
hist z ssr 30 30 12
hist z ssr 30 30 9
hist z ssr 30 30 6

hist z ssr 30 30 3
hist z ssr 30 30 0
;7th point
;295
hist gp yacc 10 35 15
hist gp yacc 10 35 14
hist gp yacc 10 35 12
hist gp yacc 10 35 9
hist gp yacc 10 35 6
hist gp yacc 10 35 3
hist gp yacc 10 35 0
;302
hist gp zdisp 10 35 15
hist gp zdisp 10 35 14
hist gp zdisp 10 35 12
hist gp zdisp 10 35 9
hist gp zdisp 10 35 6
hist gp zdisp 10 35 3
hist gp zdisp 10 35 0
;309
hist gp ydisp 10 35 15
hist gp ydisp 10 35 14
hist gp ydisp 10 35 12
hist gp ydisp 10 35 9
hist gp ydisp 10 35 6
hist gp ydisp 10 35 3
hist gp ydisp 10 35 0
;316
hist z syy 10 35 15
hist z syy 10 35 14
hist z syy 10 35 12
hist z syy 10 35 9
hist z syy 10 35 6
hist z syy 10 35 3
hist z syy 10 35 0
;323
hist z szz 10 35 15
hist z szz 10 35 14
hist z szz 10 35 12
hist z szz 10 35 9
hist z szz 10 35 6
hist z szz 10 35 3
hist z szz 10 35 0
;330
hist z syz 10 35 15
hist z syz 10 35 14
hist z syz 10 35 12
hist z syz 10 35 9
hist z syz 10 35 6
hist z syz 10 35 3
hist z syz 10 35 0
;337
hist z ssr 10 35 15
hist z ssr 10 35 14
hist z ssr 10 35 12
hist z ssr 10 35 9
hist z ssr 10 35 6
hist z ssr 10 35 3
hist z ssr 10 35 0
;8th point
;344
hist gp yacc 30 35 15
hist gp yacc 30 35 14
hist gp yacc 30 35 12
hist gp yacc 30 35 9
hist gp yacc 30 35 6
hist gp yacc 30 35 3
hist gp yacc 30 35 0
;351
hist gp zdisp 30 35 15
hist gp zdisp 30 35 14
hist gp zdisp 30 35 12
hist gp zdisp 30 35 9
hist gp zdisp 30 35 6
hist gp zdisp 30 35 3
hist gp zdisp 30 35 0

Analysis using Finn Model for evaluation of the pore pressure

```
conf dyn fluid
set dyn off fluid off
gen zone brick size 5 5 6 p0 0,0,0 p1 40 0 0 p2 0 40 0 p3 0 0 9
gen zone brick size 5 5 6 p0 0,0,9 p1 40 0 9 p2 0 40 9 p3 0 0 15
gen zone brick size 2 2 1 p0 8 8 15 p1 32 8 15 p2 8 32 15 p3 8 8 15.5
attach face range z 14.9 15.1
gen sur brick ver 0,0,0 ver 0,40,0 ver 25,0,0 ver 0,0,9
gen sur brick ver 0,0,9 ver 0,40,9 ver 25,0,9 ver 0,0,15
gen sur brick ver 25,0,0 ver 25,40,0 ver 40,0,0 ver 25,0,9
gen sur xp ver 25,0,8 ver 40,0,8 ver 40,40,5 ver 25,40,8 extrude 0 0 5 cap close
gen sur brick ver 25,0,9 ver 25,40,9 ver 40,0,9 ver 25,0,15
gen sur brick ver 8,8,15 ver 32 8 15 ver 8 32 15 ver 8 8 15.5
group clay2 lblue range vol 1
group clay1 red range vol 2
group clay2 lblue range vol 3
group sand lgreen range vol 4 &
vol 5 not
group clay1 red range vol 5
group stiff yellow range vol 6
;
;
model fl_iso
prop poros=0.5 perm=1e-8
ini fmod=2e9
ini fdens=1000
;
mod elas
prop bulk 7e7 shear 2e7 range group clay1
prop bulk 1.2e8 shear 6.5e7 range group sand
prop bulk 8e7 shear 4e7 range group clay2
prop bulk 1e8 shear 1e8 range group stiff
;
ini dens=2000
set grav 0,0,-9.81
water density 1000
water table ori 0 0 13.6 normal 0 0 1
;
;
;
;
;
sel beam id 1 b (10 10 15.5) e (10 30 15.5)
sel beam id 2 b (10 30 15.5) e (30 30 15.5)
sel beam id 2 b (30 30 15.5) e (30 10 15.5)
sel beam id 1 b (30 10 15.5) e (10 10 15.5)
sel beam id 11 b (10 10 15.5) e (10 10 18)
sel beam id 11 b (30 10 15.5) e (30 10 18)
sel beam id 11 b (30 30 15.5) e (30 30 18)
sel beam id 11 b (10 30 15.5) e (10 30 18)
sel beam id 1 b (10 10 18) e (10 30 18)
sel beam id 2 b (10 30 18) e (30 30 18)
sel beam id 2 b (30 30 18) e (30 10 18)
sel beam id 1 b (30 10 18) e (10 10 18)
sel beam id 11 b (10 10 18) e (10 10 21)
sel beam id 11 b (30 10 18) e (30 10 21)
sel beam id 11 b (30 30 18) e (30 30 21)
sel beam id 11 b (10 30 18) e (10 30 21)
sel beam id 1 b (10 10 21) e (10 30 21)
sel beam id 2 b (10 30 21) e (30 30 21)
sel beam id 2 b (30 30 21) e (30 10 21)
sel beam id 1 b (30 10 21) e (10 10 21)
sel beam id 11 b (10 10 21) e (10 10 24)
sel beam id 11 b (30 10 21) e (30 10 24)
sel beam id 11 b (30 30 21) e (30 30 24)
sel beam id 11 b (10 30 21) e (10 30 24)
sel beam id 1 b (10 10 24) e (10 30 24)
sel beam id 2 b (10 30 24) e (30 30 24)
sel beam id 2 b (30 30 24) e (30 10 24)
sel beam id 1 b (30 10 24) e (10 10 24)
sel beam id 11 b (10 10 24) e (10 10 27)
sel beam id 11 b (30 10 24) e (30 10 27)
sel beam id 11 b (30 30 24) e (30 30 27)
```



```
hist z pp 10 10 11.5
hist z pp 10 10 11
hist z pp 10 10 10.5
hist z pp 10 10 10
;4 pt
;15
hist z pp 30 10 13
hist z pp 30 10 12.5
hist z pp 30 10 12
hist z pp 30 10 11.5
hist z pp 30 10 11
hist z pp 30 10 10.5
hist z pp 30 10 10
;5th point
;22
hist z pp 10 30 13
hist z pp 10 30 12.5
hist z pp 10 30 12
hist z pp 10 30 11.5
hist z pp 10 30 11
hist z pp 10 30 10.5
hist z pp 10 30 10
;6th point
;29
hist z pp 30 30 13
hist z pp 30 30 12.5
hist z pp 30 30 12
hist z pp 30 30 11.5
hist z pp 30 30 11
hist z pp 30 30 10.5
hist z pp 30 30 10
;36
hist gp yacc 20 20 0
hist gp yacc 20 20 14
;
;
;
set dyn multi on
;set dyn damp local 0.06
step 200000
save d1finn.sav
```

Shake analysis to construct the input ground motion

Option 1 - Dynamic Soil Properties Set No. 1

1
6
9 Sand S2 G/Gmax - S2 (SAND CP=1-3 KSC) 3/11 1988
0.0001 0.000316 0.001 0.00316 0.01 0.0316 0.1 0.316
1.
1. 0.985 0.952 0.873 0.724 0.532 0.332 0.2
0.114
9 Sand Damping for SAND, February 1971
0.0001 0.001 0.003 0.01 0.03 0.1 0.3 1.
10.
1. 1.6 3.12 5.8 9.5 15.4 20.9 25.
30.
20 Soil PI=30 G/Gmax - Soil with PI=30, OCR=1-15 (Vucetic & Dobry, J
0.001 0.002 0.003 0.004 0.005 0.006 0.008 0.009
0.01 0.02 0.03 0.04 0.07 0.1 0.2 0.3
0.4 0.6 0.8 1.
1. 0.995 0.985 0.97 0.96 0.95 0.925 0.91
0.9 0.82 0.745 0.7 0.6 0.53 0.42 0.35
0.305 0.24 0.205 0.165
20 Soil PI=30 Damping - Soil with PI=30, OCR=1-8 (Vucetic & Dobry, J
0.002 0.003 0.004 0.005 0.006 0.008 0.01 0.02
0.03 0.04 0.05 0.06 0.08 0.1 0.2 0.3
0.4 0.5 0.7 1.
1.7 2.1 2.5 2.6 2.9 3.3 3.7 5.05
5.7 6.4 6.9 7.3 8.1 8.7 10.8 12.3
13.3 14.1 15.6 16.9
9 Gravel Avg. G/Gmax - GRAVEL, Average (Seed et al. 1986)
0.0001 0.0003 0.001 0.003 0.01 0.03 0.1 0.3
1.
1. 0.97 0.87 0.73 0.55 0.37 0.2 0.1
0.05
9 Gravel Damping for GRAVEL, Average (Seed et al. 1986)
0.0001 0.0003 0.001 0.003 0.01 0.03 0.1 0.3
1.
0.8 1. 1.9 3. 5.4 9.6 15.4 20.8
24.6
20 Soil PI=50 G/Gmax - Soil with PI=50, OCR=1-15 (Vucetic & Dobry, J
0.003 0.004 0.005 0.006 0.007 0.008 0.009 0.01
0.02 0.03 0.04 0.06 0.08 0.1 0.2 0.3
0.5 0.6 0.8 1.
1. 0.99 0.985 0.98 0.97 0.965 0.96 0.955
0.905 0.85 0.815 0.75 0.71 0.67 0.565 0.48
0.385 0.35 0.3 0.25
20 Soil PI=50 Damping - Soil with PI=50, OCR=1-8 (Vucetic & Dobry, J
0.002 0.003 0.004 0.005 0.006 0.008 0.01 0.02
0.03 0.04 0.05 0.06 0.08 0.1 0.2 0.3
0.4 0.5 0.7 1.
1.6 1.8 2.1 2.3 2.4 2.7 3. 3.7
4.2 4.6 5. 5.2 5.7 6.1 8. 9.2
10.1 10.9 12.2 13.5
8 Rock G/Gmax - ROCK (Schnabel 1973)
0.0001 0.0003 0.001 0.003 0.01 0.03 0.1 1.
1. 1. 0.99 0.95 0.9 0.81 0.725 0.55
5 Rock Damping for ROCK (Schnabel 1973)
0.0001 0.001 0.01 0.1 1.
0.4 0.8 1.5 3. 4.6
20 Soil PI=15 G/Gmax - Soil with PI=15, OCR=1-15 (Vucetic & Dobry, J
0.0007 0.0009 0.001 0.002 0.003 0.004 0.006 0.008
0.01 0.02 0.03 0.04 0.08 0.1 0.2 0.3
0.4 0.6 0.8 1.
1. 0.995 0.99 0.97 0.95 0.925 0.875 0.85
0.815 0.72 0.65 0.6 0.455 0.405 0.29 0.22
0.19 0.14 0.11 0.095
20 Soil PI=15 Damping - Soil with PI=15, OCR=1-8 (Vucetic & Dobry, J
0.003 0.004 0.005 0.006 0.008 0.01 0.02 0.03
0.04 0.05 0.07 0.1 0.2 0.3 0.4 0.5
0.6 0.7 0.8 1.
2.5 2.8 3.2 3.5 4.1 4.5 6.4 7.6
8.4 9.2 10.3 11.5 14.3 15.9 17. 17.6
18.3 18.8 19.3 19.9
5 1 2 3 4 5
Option 2 - Soil Profile Set No. 1

2
1 17 Soil Profile No. 1
1 6 15.0 0.05 0.115 300.0
2 1 15.0 0.05 0.115 550.0
3 2 15.0 0.05 0.115 400.0
4 2 50.0 0.05 0.115 600.0
5 2 50.0 0.05 0.115 750.0
6 2 50.0 0.05 0.115 900.0
7 2 50.0 0.05 0.115 1000.0
8 2 50.0 0.05 0.115 1100.0
9 3 10.0 0.05 0.12 1700.0
10 3 20.0 0.05 0.12 2395.0
11 3 20.0 0.05 0.12 2395.0
12 4 20.0 0.05 0.115 1700.0
13 4 30.0 0.05 0.115 1378.0
14 4 50.0 0.05 0.115 1378.0
15 4 30.0 0.05 0.115 1378.0
16 5 16.4 0.05 0.12 2000.0
17 5 0.05 0.125 3000.0
Option 3 - 1999 Sakarya EQ M=7.4 64
3
3533 4096 0.03 sample\sakaryaew.eq (8F10.0)
0.4027 30 3 8
Option 4 - Assignment of Object Motion to a Specific Sublayer Set No. 1
4
17 0
Option 5 - Number of Iterations & Strain Ratio Set No. 1
5
15 0.64
Option 6 - Computation of Acceleration at Specified Sublayers Set No. 1
6
1 4 9 12 16 17
0 1 1 1 1 1
0 1 0 0 0 1
Option 7 - Computation of Shear Stress or Strain Time History Set No. 1
7
1 0 1 2048 Strain History
8 0 1 2048 Strain History
Option 9 - Response Spectrum Set No. 3
9
7 1
1 0 32.2
0.05
Option 10 - Amplification Spectrum Set No. 1
10
1 0 17 1 0.125 Amplification Spectrum
Option 11 - Fourier Spectrum Set No. 1
11
1 0 2 3 150
17 1 2 3 150
Execution will stop when program encounters 0
0

